# Activity-dependent plasticity in the mouse superior paraolivary nucleus

Ezhilarasan Rajaram

Graduate School of
Systemic Neurosciences
LMU Munich


Dissertation der
Graduate School of Systemic Neurosciences der
Ludwig-Maximilians-Universität München

12 November 2020

Supervisor:
PD. Dr. Conny Kopp-Scheinpflug
Ludwig-Maximilians-Universität München
Division of Neurobiology

First Reviewer: PD. Dr. Conny Kopp Scheinpflug
Second Reviewer: Prof. Dr. Benedikt Grothe

Date of defense: 15 March 2021

# Summary

The ability of a neuron to fire an action potential depends on its synaptic inputs and its intrinsic excitability. Excitatory synaptic inputs drive, while inhibitory inputs suppress neuronal firing and the balance between excitation and inhibition is essential in many brain regions. While both excitatory and inhibitory synaptic inputs have been shown to be plastic; inhibitory plasticity is not as well understood as excitatory plasticity. My thesis focuses on introducing the superior paraolivary nucleus (SPN) in the auditory brainstem of mice as an ideal model to study inhibitory plasticity.

We first characterized the excitatory and inhibitory inputs to the SPN and demonstrated that the SPN neurons receive major inhibition from the medial nucleus of the trapezoid body (MNTB) and minor excitation from the octopus cells of the ventral cochlear nucleus (VCN), in accordance with other recent reports. While the hallmark offset response of the SPN neurons could primarily be attributed to the strong inhibition, the functional significance of the excitatory inputs was not clear. Here, we demonstrate that the slow excitation, mediated by NMDA receptors (NMDAR) improves the timing of the post-inhibitory rebound firing. Hodgkin-Huxley modeling suggests that the slow NMDAR-mediated excitation would accelerate the offset-response latency. We found corroborating evidence from *in vitro* and *in vivo* recordings that lack of excitation prolonged offset-response latencies and rendered them more variable to changing sound intensity levels.

This modulatory role of excitation in adapting offset-response latencies called for the question of whether inhibition, as the main driver of SPN responses, would exhibit any plasticity at all. We tested this by investigating developmental and activity-dependent synaptic plasticity of inhibition. We first focused on the maturation of the inhibitory input to the SPN during hearing onset. We demonstrate that the MNTB input to the SPN does not exhibit the pronounced experience-dependent synaptic refinement seen in other collaterals of the MNTB, projecting to the medial and lateral superior olive (MSO and LSO). This emphasizes that the development and plasticity of synapses cannot be inferred from one synaptic target to the next, even if they share the same pre-synaptic neuron. Activity-dependent inhibitory plasticity in the SPN was triggered by acoustic overstimulation. After exposure to acoustic trauma, we observed an increase in the intrinsic excitability of the SPN neurons, which might be facilitating inhibitory synaptogenesis. Understanding the molecular mechanisms that underlie intrinsic excitability and its ability to facilitate inhibitory synaptogenesis could pave the way for novel therapeutic interventions.

# Table of Contents

# List of Figures

Chapter 1

# Introduction

## 1.1 Regulation of neuronal firing

Information is encoded in our brain in the form of a binary code, embodied by the presence or the absence of neuronal action potentials. Synaptic inputs from other neurons either aid the neuron to fire an action potential or restrain it from firing. The nature of these synaptic inputs depend on the neurotransmitters and the difference in the concentration of ions between the neuron and the extracellular medium. Typically, neurotransmitters such as glutamate and acetylcholine, upon binding to their receptors result in the depolarization of the neuronal membrane potential to nudge the cell toward firing an action potential and are classified as excitatory. Other transmitters including glycine and gamma-aminobutyric acid (GABA) upon binding to their receptors lead to hyperpolarization of the cell membrane to restrain the cell from firing and are termed inhibitory transmitters.

Synaptic inputs to neurons have been shown to be malleable, with the strength of synaptic inputs changing with time (Citri and Malenka, 2008; Roelfsema and Holtmaat, 2018). The number of inputs, the size of the synapse and its contents have been shown to change in response to neuronal

activity or through homeostatic mechanisms (Citri and Malenka, 2008; Holtmaat and Svoboda, 2009; Turrigiano, 2012). A wealth of knowledge has been accumulated about synaptic plasticity in excitatory inputs. On the other hand, very little is known about inhibitory synaptic plasticity. The balance between excitation and inhibition plays a crucial role in dictating the physiological function of the neuron, while disturbances in the balance of excitation and inhibition manifest as pathological conditions, such as epileptic seizures (Bonansco and Fuenzalida, 2016). Aside from the excitatory and inhibitory synaptic inputs, neuronal firing can also be regulated by influencing the intrinsic excitability of the neurons (Desai et al., 1999; Nelson et al., 2003). Such changes in the intrinsic excitability have been shown to play an important role in synaptic plasticity (Brager and Johnston, 2007; Jung and Hoffman, 2009). This work introduces the superior paraolivary nucleus (SPN), an auditory brainstem nucleus in the superior olivary complex of rodents as an ideal model to study inhibitory plasticity.

## 1.2 Auditory brainstem

Nestled in the brainstem of mammals is a cluster of nuclei that play a crucial role in auditory processing, including sound localization in the horizontal plane. This cluster of nuclei termed the superior olivary complex (SOC) in rodents is primarily comprised of the medial nucleus of the trapezoid body (MNTB), the medial superior olive (MSO), the lateral superior olive (LSO) and the SPN. Through evolutionary pressures over several epochs, the SOC has evolved to process auditory information with sophistication and high temporal precision (Grothe and Pecka, 2014; Nothwang, 2016).

The auditory information from the cochlea is transmitted through the spiral ganglion neurons to the neurons of the cochlear nucleus, which is divided in two subdivisions: dorsal and ventral cochlear nucleus. The dorsal cochlear nucleus (DCN) has a cytoarchitecture similar to that of the cerebellum and has been known to process multisensory information and complex auditory tasks (Shore, 2005; Wigderson et al., 2016). The ventral cochlear nucleus (VCN) is further subdivided into anterior and posterior ventral cochlear nucleus (AVCN and PVCN, respectively). They both contain globular bushy cells, D- and T-stellate cells (Oliver et al., 2018; Figure 1.1). The AVCN has spherical

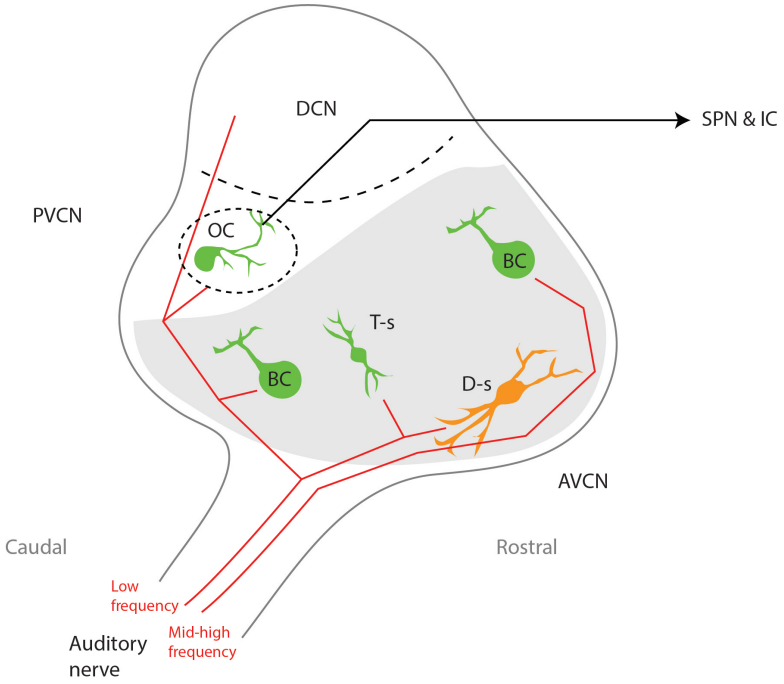


Figure 1.1. Sagittal view of mouse cochlear nucleus schematic showing the different cell types found in the ventral cochlear nucleus (VCN). VCN is divided to posteroventral cochlear nucleus (PVCN) and anteroventral cochlear nucleus (AVCN). Both AVCN and PVCN are populated by bushy cells (BC), D-stellate cells (D-s) and T-stellate cells (T-s). PVCN in addition contains octopus cells (OC), which projects to the superior paraolivary nucleus (SPN) and the inferior colliculus (IC). Excitatory cells and inhibitory cells are labeled in green and orange, respectively.

bushy cells in addition, while the PVCN also contains the octopus cells. Globular bushy cells of the VCN project to the MNTB forming the largest synapse in the mammalian brain, the calyx of Held. This excitatory input is converted to an inhibitory, glycinergic output by the MNTB.

The glycinergic MNTB neurons projects to all the other nuclei of the SOC- MSO, LSO, SPN and to the neurons of the ventral nucleus of the lateral lemniscus (VNLL) (Grothe et al., 1994; Kim and Kandler, 2003; Couchman et al., 2010; Kopp-Scheinpflug et al., 2011). While globular bushy cells project to the contralateral MNTB, the spherical bushy cells provide strong excitatory input to the ipsilateral LSO and bilateral MSO. The octopus cells of the PVCN project contralaterally to the neurons of the contralateral VNLL and the SPN. In addition to the above-mentioned primary nuclei, the mammalian SOC contains other, smaller nuclei. These include the lateral and ventral nuclei of

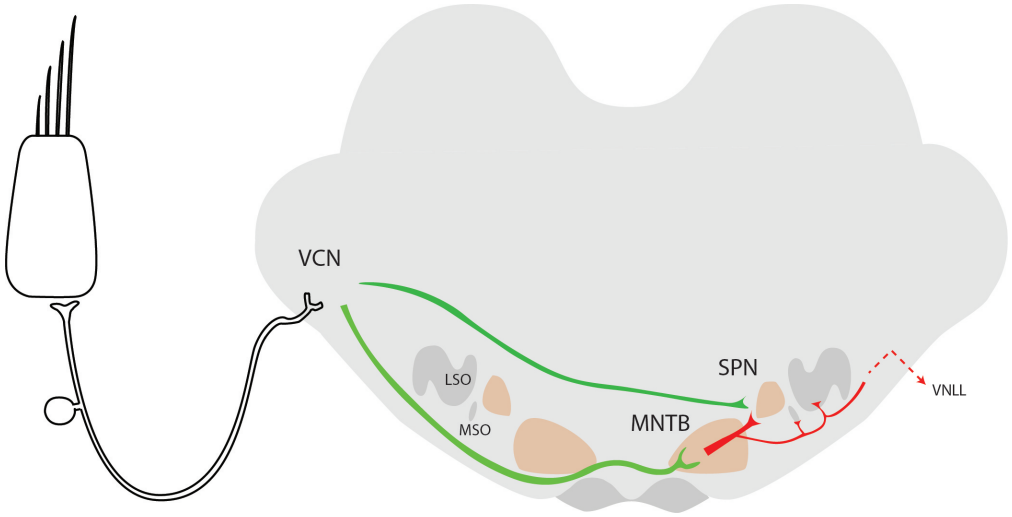


Figure 1.2. Coronal view of the mouse superior olivary complex schematic showing the inputs to the neurons of the superior paraolivary nuleus (SPN). Auditory information from the inner hair cells of the cochlea are relayed via spiral ganglion neurons to the cochlear nucleus. Globular bushy cells of the ventral cochlear nucleus (VCN) project to the contralateral medial nucleus of the trapezoid body (MNTB), which ends as the calyx of Held. The MNTB neurons provide inhibitory inputs to the neurons of the SPN, medial superior olive (MSO), lateral superior olive (LSO) and to the ventral nucleus of the lateral lemniscus (VNLL). Octopus cells of the VCN provide excitatory inputs to the SPN

the trapezoid body and several periolivary nuclei (Olivier et al., 2018).

The prominence of the SOC in auditory processing comes to the fore in two pathways that encode the position of a sound source in the horizontal plane. This has been attributed to the ability of the MSO and LSO to encode interaural time differences (ITDs) and the interaural level differences (ILDs), respectively (Grothe et al., 2010). According to the duplex theory originally proposed in 1907, mammals rely on ITDs for localizing low frequency sounds and on ILDs for localizing high frequency sounds (Rayleigh, 1907). A low frequency sound wave would reach one of the two ears, earlier than the other ear, depending on the location of the sound source respective to the animal and the size of its head. The MSO developed the ability to detect microsecond time differences that arise when the sound wave impinges with a delay between the two ears. Given the smallish head sizes of most mammals, at frequencies higher than 2-4K Hz the ITDs become too short and difficult to detect. Mammals rely on the ILDs for localizing high frequency sounds. Sound waves at higher frequencies

are refracted or shadowed by the head and this gives rise to differences in the sound intensity between the two ears. The sound intensity is higher in the ear closest to the sound source. The LSO has evolved the ability to detect such interaural level differences. The fast glycinergic inhibition from the MNTB is crucial in encoding the ITDs and ILDs. In addition, another major recipient of MNTB inhibition within the SOC is the SPN, which has not been implied to contribute to sound localization.

## 1.3 Superior paraolivary nucleus

The SPN is a part of the SOC in the auditory brainstem of rodents and is located dorsal to the MSO, in between the MNTB and the LSO. The similar region in other mammals including cats and bats has been termed dorso-medial periolivary nucleus (DMPO), a potential homologous nucleus. There are many species-dependent variations in the SPN / DMPO and its anatomical borders are not clearly defined. Studies have described two major cell types in the SPN / DMPO so far. Large multipolar neurons and smaller spindle shaped or elongate cells have been described in cats, bats, guinea pigs, opossums, chinchillas and gerbils (Morest, 1968; Nordeen et al., 1983; Willard and Martin, 1983; Aschoff and Ostwald, 1987; Helfert et al., 1989; Schofield, 1991; Azeredo et al., 1999). However, in the mouse, SPN is reported to consist of mainly large multipolar cells and a small population of less than 5% spindle shaped cells (Willard and Ryugo, 1983). In rats, the SPN cells show their largest cell body profiles in the parasagittal sections and smallest in the coronal sections, they have been described as parasagittaly flattened cell bodies, with their long axis extending in the rostro-caudal direction (Saldaña and Berrebi, 2000).

Early studies, using retrograde tracers injected into the cochlea, found labeled neurons in the SPN / DMPO. Such efferent neurons that provide a projection back into the cochlea are called olivocochlear neurons and have been observed in in the SPN / DMPO of cats, guinea pigs, chinchillas and some bat species (Morest, 1968; Warr, 1975; Aschoff and Ostwald, 1987; Bishop and Henson, 1987; Robertson et al., 1987; Tokunaga, 1988; Winter et al., 1989; Thompson and Thompson, 1991; Azeredo et al., 1999). Olivocochlear neurons are predominantly cholinergic and thus stain positively for acetylcholinesterase (AChE) and choline acetyltransferase (ChAT) (Osen and Roth, 1969; Warr, 1975). A sub-population of neurons in the SPN / DMPO indeed tests positively for the presence of AchE in

cats, guinea pigs, bats, moles and gerbils (Warr, 1975; Nordeen et al., 1983; Aschoff and Ostwald, 1987; Tokunaga, 1988; Kudo et al., 1990; Thompson and Thompson, 1991). However, neurons in the SPN / DMPO of rats and mice stain poorly for AchE (Brown and Howlett, 1972; Osen et al., 1984; Grothe et al., 1994). The presence or absence of cholinergic neurons has been suggested as a way to distinguish between SPN and DMPO, with DMPO classified as containing cholinergic neurons and the SPN as being devoid of cholinergic neurons. It is tempting to assume that the apparent lack of cholinergic neurons in rats and mice correlates with the vast under-representation of the smaller spindle shaped cells. It is, however, the large multipolar cells that tend to be AchE positive and project to the cochlea in cats, guinea pigs and bats. On the other hand, in horseshoe bats, Rhinolophusrouxi, the fusiform cells make up most of the olivocochlear neurons (Aschoff and Ostwald, 1987).

In addition to the species dependent variations in the SPN / DMPO, there have actually been conflicting reports about the nature of cholinergic neurons in guinea pigs. Retrograde tracer injections into the cochlea label large multipolar neurons in the SPN / DMPO in guinea pigs (Tokunaga, 1988; Winter et al., 1989; Thompson and Thompson, 1991). However, these large multipolar SPN neurons have also been labeled by retrograde labeling from the Inferior Colliculus (IC), while the smaller cells project to the cochlear nucleus (Schofield, 1995). Even in rats, which stain poorly for cholinergic markers have been reported to contain some olivocochlear neurons (Osen et al., 1984; Riemann and Reuss, 1998; Reuss et al., 1999). In mice, a cluster of neurons dorsal to the LSO, named dorsal periolivary nucleus (DPO) has been reported to contain olivocochlear projection neurons (Brown, 1993). A similar region in humans also show olivocochlear projections (Moore, 2000). It is not clear if the DPO is part of the DMPO that moved away in some species and it is not clear, where the borders of these periolivary nuclei lie. One way to define these nuclei could be based on their connectivity.

## 1.4 SPN neuronal connectivity

### 1.4.1 Inputs to SPN neurons

The SPN / DMPO (hereafter referred to as SPN) receives a strong inhibitory input from the ipsilateral MNTB in all species tested (Morest, 1968; Banks and Smith, 1992; Kuwabara and Zook, 1992; Sommer et al., 1993). The SPN has also been shown to receive an ipsilateral non-MNTB glycinergic input in young rats (Srinivasan et al., 2004). The study shows that electrical stimulation ventral to the LSO in *in vitro* brain slices evokes glycinergic responses in the SPN. The ipsilateral lateral nucleus of the trapezoid body (LNTB) could represent this source, as these cells have been labeled by retrograde tracers injected in the SPN of rats (Saldaña et al., 2009). In another set of experiments, a transgenic mouse line was created that lack MNTB neurons. Unexpectedly, these mice also showed very strong perisomatic staining for the glycine transporter 2 (GlyT2), which developed with a one week delay compared to the control animals, but were present nonetheless (Jalabi et al., 2013; Altieri et al., 2014). It is believed, that this non-MNTB glycinergic input is not from the SOC, as the labeled fibers seem to cross the midline from the contralateral side (Jalabi et al., 2013). Despite the non-MNTB sources of glycinergic input to the SPN, it has been established that the MNTB input, which in itself receives input from the contralateral VCN through the calyx of Held, represents the predominant input to SPN (Srinivasan et al., 2004; Rajaram et al., 2019). In addition to the inhibitory input, the SPN shows, although much weaker, evidence for excitatory inputs with staining for vesicular Glutamate transporters (vGLUTs) -vGLUT1, vGLUT2 and vGLUT3, and NB-2, a neuronal cell recognition molecule important for the formation of glutamatergic synapses (Blaesse et al., 2005; Toyoshima et al., 2009; Rajaram et al., 2019).

The primary excitatory input to the SPN originates from the contralateral VCN, as demonstrated by anterograde tracers injected in the cochlear nucleus and retrograde tracers injected in the SPN (Robertson and Winter, 1988; Thompson and Thompson, 1991; Schofield, 1995; Felix II et al., 2017). Species dependent variations are manifested in this projection as well. Earlier studies, using extracellular recording from VCN globular bushy cells (GBCs) followed by intracellular labeling, have shown that the globular bushy cells in the cat project to the SPN (Smith et al., 1991). This projection

has also been reported in some bat species and tends to be a collateral from the ipsilateral GBC axon that forms the calyx of Held in the contralateral MNTB (Morest, 1968; Kuwabara et al., 1991). There was very poor or no labelling of GBCs, when retrograde tracers were injected in the SPN of guinea pigs (Schofield, 1995). Some labeled GBCs were seen when retrograde tracers were injected into the SPN of rats (Saldaña et al., 2009). However, such studies cannot ensure that the tracers have not spilled over to the neighbouring nuclei, in this case the MNTB, which receives its prime calyceal input from the GBCs. A more stringent experiment where extracellular recording from the axons of GBCs paired with intracellular labelling has shown that there is not much evidence to support the GBC-SPN projection in rats (Friauf and Ostwald, 1988). A GBC-SPN projection is also absent in the mouse (Felix II et al., 2017). The presence or absence of the GBC-SPN projection has been suggested as another classifier between SPN and DMPO, with cats and bats showing this projection and guinea pigs, rats and mice lacking it (Schofield, 1995).

Despite the fact that the SPN stains weakly for excitatory inputs and the lack of GBC-SPN projection in rodents, all SPN cells seem to receive an excitatory input from the cells of the PVCN. This projection has been conserved in all species tested and represents a defining feature of the SPN, along with the glycinergic input from the MNTB. Studies employing anterograde / retrograde tracers have labeled the multipolar stellate cells and the octopus cells in the PVCN of cats, bats, rats, guinea pigs and mice (Zook and Casseday, 1985; Friauf and Ostwald, 1988; Thompson and Thompson, 1991; Schofield, 1995; Warr, 1995; Saldaña et al., 2009; Felix II et al., 2017). Recent studies have questioned the projection of multipolar stellate cells to the SPN, while confirming the projection of octopus cells to the SPN in mice (Felix II and Magnusson, 2016; Felix II et al., 2017). In some species, the projection from the contralateral side represents the main source of excitatory input, while in other species there is evidence for binaural excitatory input (Behrend et al., 2002; Dehmel et al., 2002). Binaural excitatory inputs to SPN neurons have been described for the guinea pigs (Thompson and Thompson, 1991; Schofield, 1995) and the rat (Saldaña et al., 2009). However, in the latter the ipsilateral projection was reported to be very weak (Srinivasan et al., 2004). A recent study proposes that the inpsilateral excitatory input all together vanishes in the mouse, with no labelling of the ipsilateral VCN following the injection of retrograde tracers in the SPN (Felix II et al., 2017).

An array of other nuclei have also been linked with connections to the SPN. They however, are thought to play a minor role compared to the inputs from the MNTB and the VCN. En passant axonal projections from the MSO of gerbils have been shown to project to the SPN (Kuwabara and Zook, 1999; Stange-Marten et al., 2013). SPN also receives descending input from upstream nuclei in the auditory pathway, like the inferior colliculus (IC), tectal longitudinal column (TLC) and the subparafascicular thalamic nucleus (Yasui et al., 1992; Thompson and Thompson, 1993; Viñuela et al., 2011). SPN cells are also thought to project collaterals to other ipsilateral SPN cells, but this projection has not yet been corroborated physiologically (Kulesza and Berrebi, 2000). There have been some reports that the VNLL and the dorsal nucleus of the lateral lemniscus (DNLL) project to the SPN (Whitley and Henkel, 1984; Bajo et al., 1993). However, in the above-mentioned studies, retrograde tracers were injected in DNLL and VNLL and SPN cell were labeled. One cannot ignore the possibility that the tracers could also label axons that pass through these nuclei, especially since the main afferent axon from the SPN projects to the IC and is passing straight through the nuclei of the lateral lemniscus.

### 1.4.2 Ascending SPN efferents

The IC is the primary target of the SPN projections in all the species tested so far. Majority of the SPN neurons project to the ipsilateral IC (cats: Adams, 1983, rats: Beyerl, 1978; Coleman and Clerici, 1987, mice: Willard and Ryugo, 1983; Frisina et al., 1998, gerbil: Nordeen et al., 1983; Cant and Benson, 2006, ferrets : Moore, 1988, moles: Kudo et al., 1990, chinchillas: Saint Marie and Baker, 1990, bats: Grothe et al., 1994, guinea pigs : Saint Marie and Baker, 1990; Schofield, 1995). While in rats, mice, gerbils and moles this projection is strictly ipsilateral, in guinea pigs, chinchillas and bats a few neurons have been observed to also project to the contralateral IC. The projection to the IC has been shown to innervate the central nucleus, dorsal cortex and the external cortex of the IC (Coleman and Clerici, 1987; González-Hernández et al., 1996). The SPN-IC projection is tonotopically organized in all the model species tested (Kelly et al., 1998; Saldaña and Berrebi, 2000; Saldaña et al., 2009). Studies report that axons that innervate the IC, continue on to project to the TLC, the superior colliculus and the thalamus (Edwards and Stein, 1979; Viñuela et al., 2011; Schofield et al., 2014; Mellott et al., 2018).

### 1.4.3 Descending SPN projections

A descending projection from the SPN to the cochlea, as mentioned earlier is a feature restricted to certain species. Interestingly, a descending projection to the CN has also been reported in some species. In cats and guinea pigs, retrograde tracers in the CN have labeled SPN neurons (Adams, 1983; Spangler et al., 1987; Winter et al., 1989; Benson and Potashner, 1990; Shore et al., 1991). These descending projections the CN could be collaterals of the olivocochlear neurons that project to the cochlea. In the guinea pig, however, the projection to the cochlea has been controversial and the projection to the CN was suggested to represent a different subset of the SPN neurons. Some cells in the SPN of guinea pigs are positive for AChE, qualifying them as the alleged olivocochlear neurons (Thompson and Thompson, 1991). It is questionable- if the SPN to CN projection is cholinergic, as injection of radioactive 3H glycine in the CN labels SPN cells, suggesting the SPN to CN projection to be glycinergic (Benson and Potashner, 1990).

### 1.4.4 Neurotransmitters of SPN neurons

The uptake of radioactive 3H glycine and the labelling of SPN cells might lead one to believe that the SPN is composed of glycinergic neurons and in addition cholinergic neurons in the species that contain olivocochlear neurons in the SPN. However, evidence about the neurochemical nature of SPN neurons is weak and so the content of their neurotransmitter remains uncertain. Many studies using immunohistochemistry or retrograde transport of radioactive 3H glycine, in guinea pigs, have shown that at least some SPN neurons are glycinergic (Wenthold et al., 1987; Helfert et al., 1989; Benson and Potashner, 1990; Saint Marie and Baker, 1990). Early studies with anti-serum raised against GABA or glutamic acid decarboxylase (GAD) have shown contrasting results. Some studies in rats show that at SPN cell bodies stain lightly from GABA/GAD or show no staining at all (Kumoi et al., 1987, 1993; Moore and Moore, 1987). The study showing light staining in SPN in rats and other similar studies reporting moderate GABA/GAD staining in SPN in gerbils and guinea pigs, also show GABAergic cells in the LSO (Moore and Moore, 1987; Roberts and Ribak, 1987; Helfert et al., 1989). However, recent studies have established the LSO to contain primarily glutamatergic and glycinergic

neurons and thus, questioning the specificity of the antibodies (Altschuler and Shore, 2010; Friauf et al., 2019).

A couple of more recent studies have shown that at least in rats, a substantial portion of SPN is composed of GABAergic neurons. Gonzalez et al., used retrograde tracer HRP and GABA immunohistochemistry to show that a part of SPN is GABAergic (González-Hernández et al., 1996). Kulesza et al., used antibodies against GAD 65 and GAD 67, the two isoforms of GAD to show that more than 90% of SPN is GABAergic (Kulesza and Berrebi, 2000). Given the fact that there is plenty of species specific diversity in cell morphology, the nature of the SPN cell projection could also differ between species and thus warranting a more systematic approach like RNA-sequencing to better understand structure-function relationship in the SPN. Although such species differences seem to complicate things initially, they will also help to gain a better understanding of the physiological function of the SPN, which is not well understood.

## 1.5 SPN neuronal physiology

The hallmark of SPN neurons is the firing of OFF responses at the end of the sound stimulus. An early study using *in vivo* recording in the SOC of cats have reported offset or off responses as a sharp peak in the PSTH after the end of the acoustic stimulation (Guinan et al., 1972a, 1972b). Subsequent studies have seen OFF responses in the SOC of bats, rabbits, gerbils, rats and mice (Grothe et al., 1994; Kuwada and Batra, 1999; Behrend et al., 2002; Dehmel et al., 2002; Kulesza et al., 2003; Felix II et al., 2011; Kopp-Scheinpflug et al., 2011). *In vitro* studies revealed a number of adaptations that allow SPN neurons to reliably fire at stimulus offset (Felix II et al., 2011; Kopp-Scheinpflug et al., 2011). Firstly, the strong hyperpolarizing glycinergic input to the SPN and the primary-like firing pattern of the MNTB *in vivo*, where discharges are sustained and last for the whole stimulus duration, is believed to hyperpolarize the SPN cell during the entire stimulus. This inhibitory power is further increased by the fact that the driving force of chloride ions, which mediates the glycinergic current, is very strong in the SPN, due to high expression and activity of the Chloride Potassium cotransporter 2 (KCC2), which extrudes chloride out of the cells to maintain low chloride concentrations within the cell (Löhrke et al., 2005). Thirdly, the inhibition activates hyperpolarisation-

activated cyclic nucleotide gated channels (HCN) which gives rise to a non-specific cation current (IH) which depolarizes the cell and accelerates the membrane time constant. The strong inhibition also removes steady-state inactivation from voltage-gated calcium and sodium channels. Finally, the de-inactivated voltage gated T-type calcium channels open when the inhibition ends and the cell quickly depolarizes, aided by the depolarising IH current to help fire a burst of action potentials at the end of the inhibition/ sound stimulus (Kopp-Scheinpflug 2011). These four factors play a vital role in defining the ability of SPN neurons to fire OFF responses.

Though the OFF responses are a characteristic SPN feature, the proportion of neurons with OFF responses varies between species and studies. While one study in gerbils reports only few OFF responses in the SPN (Behrend et al., 2002), a subsequent study found a considerable number of OFF responses in the SPN (Dehmel et al., 2002). Differences in the anesthesia are too small to give rise to such discrepancies. A study in unanesthetized rabbit however, did find OFF responses in the rabbit model (Kuwada and Batra, 1999). Thus, variability between regions of recording within the SPN might be a more likely explanation. The pattern of OFF response also varies between different species. In gerbils, cats and rabbits many neurons have been described with an offset-chopper with equally spaced spikes in response to offset of pure tones, off-sustained or an offset response pattern with two peaks and a pause in between responses. In rats and mice, offset-chopper and offset with two peaks response patterns were recorded only from a minority of neurons and the vast majority of neurons exhibit off-sustained response properties. It is noteworthy that in the gerbil model, a significant proportion of SPN responds to binaural stimulation, while it is predominantly monaural in rats and mice (Behrend et al., 2002; Dehmel et al., 2002; Kulesza et al., 2003; Kopp-Scheinpflug et al., 2011; Felix II and Magnusson, 2016). A majority of SPN neurons are sensitive to slow sinusoidally amplitude-modulated (SAM) tone stimuli across species and show phase locking to the sound envelope (Kuwada and Batra, 1999; Behrend et al., 2002; Kadner and Berrebi, 2008; Felix II et al., 2011). This sensitivity of the SPN neurons to the envelope rather than the temporal fine structure of auditory stimuli is beneficial for gap detection and speech processing.

The MNTB-SPN circuit has the ability to detect brief gaps in ongoing acoustic stimuli, with

gap durations in the range of 1-2 ms (Kadner and Berrebi, 2008). This ability to detect gaps in acoustic stimuli, or in other words to encode the end of one sound before the next one starts, is destined to play a role in encoding sound duration (Kadner et al., 2006). Neurons tuned to sound duration have been described in the IC of bats (Casseday et al., 1994, 2000; Ehrlich et al., 1997; Faure et al., 2003) and in rodents (Brand et al., 2000; Pérez-González et al., 2006). Intriguingly, blocking GABAergic inhibition in the IC has been shown to reduce or abolish duration tuning in the IC (Jen and Wu, 2006; Yin et al., 2008; reviewed in: Sayegh et al., 2011). Selective inactivation of SPN has been shown to reduce entrainment of IC neurons to SAM stimuli and increase the thresholds for gap detection (Felix II et al., 2015). It is believed that duration tuning is not inherited in the IC, but rather computed de novo. An underlying neural mechanism for duration tuning has been suggested for the rather short (3-50ms) echolocation calls of bats (Sayegh et al., 2011). A short-pass model, a band-pass model and a long-pass model are suggested to encode tones of different (shortish) durations. All three models rely on the coincidence of delayed onset responses with fast offset responses. However, since onset responses can only be delayed by a couple-tens of milliseconds, the neural mechanism for encoding the durations of longer vocalisation calls (hundreds of ms) remains elusive. The role of sound offsets in speech processing, signaling temporal edges for perceptual grouping and helping consonant discrimination (reviewed in: Kopp-Scheinpflug et al., 2018) is only beginning to be uncovered. Thus, the SPN remains a rather mysterious nucleus, which plays a vital role in auditory processing.

## 1.6 Developmental inhibitory plasiticity

SOC neurons show remarkable plasticity in the first few postnatal weeks, and like other sensory systems, they experience fine-tuning in morphology and physiology. Cellular properties like membrane time constant and input resistance, which dictate the voltage kinetics of the membrane, decrease in SOC neurons with postnatal age. This paves the way for faster kinetics in all the SOC nuclei, including the SPN (Magnusson et al., 2005; Chirila et al., 2007; Walcher et al., 2011; Felix II et al., 2013; Fischl et al., 2016). The kinetics of the glycinergic input from the MNTB has been shown to become faster in the SOC over the course of the first few weeks after birth (Smith et al., 2000; Magnusson et al., 2005). Interestingly, the development of the inhibitory input from the MNTB, which

is shared among the MSO, LSO and the SPN takes different form in the MSO and the LSO.

Many SOC nuclei receive shared MNTB inputs (Kuwabara and Zook, 1991; Banks and Smith, 1992; Sommer et al., 1993). A subtype of MNTB projection that projects exclusively to one of the target nuclei in low-frequency specialists like gerbils cannot be ruled out, but it has not yet been shown. The shared MNTB input exhibits morphological and physiological differences between MSO and LSO, while the nature of its development in the SPN has not yet been studied. However, it has been shown that the MNTB-SPN projection is already established during embryonic days 17-18 (Lohrke et al., 2005; Altieri et al., 2014). The expression of axon guidance signals lays the foundation for the topographic arrangement of inputs, which would preserve the tonotopy later on.

In the MNTB-LSO projection, the initial axon collaterals are more diffused and extend across a large target area. With increasing postnatal age, the length of the collaterals reduces and the projections become more specific (Sanes and Siverls, 1991a; Sanes and Friauf, 2000). Synaptic pruning and strengthening of the remaining synapses by increasing the quantal content is thought to underlie this change (Kim and Kandler, 2003, 2010; Kandler and Gillespie, 2005; Sonntag et al., 2009; Clause et al., 2014). Studies from the Kandler lab have shown that this process begins before hearing onset and that glutamate co-release from the MNTB axons plays an important role in this process (Noh et al. 2010; Clause et al. 2014).

The MNTB-MSO synapse shows plasticity of a different kind. Early in development, the inhibitory synapses could be found on both the dendrites and the soma of the MSO cells. After hearing onset, inhibitory synapses are mainly observed on the cell body. Intriguingly, this phenomenon is specific to animals that have specialized low-frequency hearing (Kapfer et al., 2002). In addition to the synaptic elimination from the dendrites, axonal pruning has also been observed in the MNTB-MSO synapse of gerbils with a reduction in the axonal branching and end segments (Werthat et al., 2008). Interestingly, this refinement of the MNTB axonal input is altered in the face of a loss in activity by cochlear ablation or an increase in activity through omnidirectional noise rearing (Seidl and Grothe, 2005; Werthat et al., 2008) ). It is not yet known what form of developmental plasticity of

the inhibitory inputs occurs in the SPN. It will be interesting to know, to what extent the synaptic mechanisms dictating this activity-dependent refinement are shared among the different collaterals and are thus determined by the presynaptic terminal or alternatively, how the postsynaptic target regions contributes.

## 1.7 Activity dependent inhibitory plasticity

Plasticity in the auditory brainstem has been studied from all the three main perspectives – no activity, moderate activity and very high activity. Cochlear ablation, congenitally deaf animals and other methods have been deployed to decrease or eliminate activity (Sanes and Siverls, 1991b; Kitzes et al., 1995; Gabriele et al., 2000; Vale and Sanes, 2002; Vale et al., 2003; Shibata et al., 2004; Leao et al., 2006) . Auditory enrichment and rearing animals in noise elicit moderate levels of activity that do not result in pathological conditions (Brand et al., 2002; Kapfer et al., 2002; Chang, 2003; Magnusson et al., 2005; Seidl and Grothe, 2005; Pecka et al., 2008). And, exposure to an acoustic stimulus at very high sound intensity levels that lead to manifestation of pathological conditions have also been studied (Brozoski et al., 2002; Bauer et al., 2008; Middleton et al., 2011; Vogler et al., 2011; Li et al., 2013; Pilati et al., 2016) . Noise trauma resulting in hearing loss, can be hidden or lead to debilitating conditions such as hyperacusis or tinnitus. Here, we focus on the implications of noise-induced plasticity.

Tinnitus and hyperacusis (increased sensitivity to certain frequencies or volume range of sound) have both been associated with hyperactive areas and increased spontaneous firing rates in the auditory pathway (Melcher et al., 2000; Brozoski et al., 2002; Seki and Eggermont, 2003; Ma et al., 2006; Vogler et al., 2011), with the dorsal cochlear nucleus in particular being strongly associated with tinnitus. Noise trauma has been shown to increase the intrinsic excitability of the DCN neurons as well as to reduce synaptic inhibition (Wang et al., 2009; Middleton et al., 2011; Li et al., 2013, 2015; Pilati et al., 2012). After noise trauma, only mice that later develop tinnitus, show an increase in intrinsic excitability that is dependent on reduced potassium channel (Kv7.2/3) activity in the DCN (Li et al., 2013). In the resilient mice that do not develop tinnitus, reduced Kv7.2/3 activity appears to be compensated along with a reduction in the activity of hyperpolarization-activated cyclic nucleotide gated channel (HCN) activity (Li et al., 2015). These changes in intrinsic properties

were observed a week after noise exposure and might not catch adaptive synaptic changes. In rats, the animals with evidence of tinnitus showed decreased expression of glycine receptors' mRNAs and proteins, 4 months after noise exposure (Wang et al., 2009). Another study in mice, showed a decrease in GABAergic inhibition in the DCN 2-9 weeks post noise exposure. The neurons of the VCN have also been implied in tinnitus (Vogler et al., 2011; Gu et al., 2012). The above-mentioned studies use very different parameters to study noise plasticity, with different duration of the noise stimulus, sound intensity levels, frequency bands and time between exposure and testing. It is important to keep these factors in mind when considering the nature and type of noise-induced plasticity.

In the SOC, noise trauma has been shown to slow down the kinetics of excitatory currents in the LSO (Pilati et al., 2016). The decay kinetics of the excitatory and inhibitory currents have been shown to match each other in the LSO at the end of posthearing development, which has been implied to play a role in maintaining precision in ILD detection and sound localization. One week after exposure to noise trauma however, the excitatory post-synaptic currents (EPSCs) decay slower than in control animals. This has been attributed to changes in the composition of AMPA receptor subunits, with increased GluA1 and decreasing GluA4 mRNA. Computational modelling hints that the increased EPSC duration can shift the ILD function and compensate for the noise induced hearing loss (Pilati et al., 2016). The implications of such changes are not well understood. Indeed, the inferior colliculus that receives strong inputs from the LSO, MSO and the SPN shows significant changes after auditory trauma (Sturm et al., 2017).

Sturm et al., 2017 found that noise trauma induces gap detection deficits, which are correlated with changes in the balance of excitation and inhibition in the IC. Glutamate uncaging and laser-scanning photostimulation were used to study the synaptic changes in the local IC circuitry. It was revealed that in mice with gap detection deficits, the glutamatergic neurons of the IC show a significant change in the balance of excitation and inhibition, resulting in a dominant excitation. The glutamatergic neurons show reduced inhibitory synaptic maps and increased frequencies of spontaneous EPSCs, demonstrating changes in both the inhibitory and excitatory circuits. The impact of noise trauma in the IC is unclear, with studies reporting large variations (reviewed in: Shore and Wu,

2019). Some studies have reported increased spontaneous firing rates (Bauer et al., 2008; Longenecker and Galazyuk, 2011, 2016; Berger et al., 2014); while others have failed to reproduce this (Heeringa and van Dijk, 2014; Shaheen and Liberman, 2018). It thus necessitates a better understanding of the noise induced changes in all the regions that provide inputs to the IC. The changes induced by noise trauma in the SPN are a missing link in the projections to the IC and the assessment of mechanistic changes underlying hyperacusis and tinnitus will be addressed in this thesis.

## 1.8 Measuring synaptic parameters

In this thesis, synaptic parameters and synaptic plasticity were studied through *in vitro* electrophysiological and immunocytochemical techniques. On the presynaptic axon side, synaptic vesicles, that typically release their contents following an action potential, can sometimes also release their contents stochastically. This leads to currents measured in the postsynaptic neuron, termed as miniature synaptic currents or minis. The minis are typically measured in the presence of tetrodoxin (TTX) that block action potentials. The minis reveal a lot of information about synapses, with the frequency and the amplitude of the minis being the most widely studied parameters. Changes in the amplitude of the minis are related to the postsynaptic neurotransmitter sensitivity, determined by the postsynaptic receptor numbers and their conductance (Graziane and Dong, 2016). The changes in the frequency of minis are primarily related to presynaptic changes in release probability and / or changes in the number of synapses (Graziane and Dong, 2016). Immunocytochemical techniques can be used to study changes in the expression levels of postsynaptic receptors and the number of synapses. There are numerous approaches to study the factors determining the presynaptic release probability.

Release probability (Pr) and the number of vesicles that are docked near the synaptic membrane, termed the readily-releasable pool (RRP) can be investigated using presynaptic voltage steps or photolytic calcium release or application of hypertonic sucrose to release all the presynaptic vesicles and postsynaptic capacitance or voltage clamp recordings (Thanawala and Regehr, 2016). Another approach to measure Pr and RRP, is through high frequency synaptic stimulation, which is more akin to physiological conditions and can be applied to many types synapses. Two other

parameters describe synaptic transmission: quantal size (Q) - the postsynaptic response to the release of a single vesicles' content, and the number of independent release sites (n). When using the high-frequency stimulation method, there are multiple ways to determine the release probability, such as the Schneggenburger (SMN) method, Thanawala and Regehr (TR) method and Elmqvist and Quastel (EQ) method (reviewed in Neher, 2015 and Thanawala and Regehr, 2016). The three methods use different sets of assumptions and can be broadly classified in two approaches - using backward extrapolation of vesicular recycling and forward extrapolation of pool depletion. While SMN and TR use the former approach, EQ methods uses the latter (Neher, 2015). In this thesis, both SMN and EQ methods were used to investigate synaptic properties.

Chapter 2

# Slow NMDA-Mediated Excitation Accelerates Offset-Response Latencies Generated via a Post-Inhibitory Rebound Mechanism

## 2.1 Author contributions

*Rajaram E, Kaltenbach C, Fischl MJ, Mrowka L, Alexandrova O, Grothe B, Hennig MH, Kopp-Scheinpflug C (2019) Slow NMDA-Mediated Excitation Accelerates Offset-Response Latencies Generated via a Post-Inhibitory Rebound Mechanism. Eneuro 6:ENEURO.0106-19.2019.*

The contributions of the authors Ezhilarasan Rajaram (ER), Carina Kaltenbach (CK), Matthew J. Fischl (MJF), Leander Mrowka (LM), Olga Alexandrova (OA), Benedikt Grothe (BG), Matthias H. Henning (MHH) and Conny Kopp-Scheinpflug (CKS) are as follows: ER, CK, MJF, LM, OA, and CKS performed research; ER, CK, MJF, OA, and CKS analyzed data and interpreted the results of experiments; ER, BG, MHH, and CKS wrote the paper; MHH and CKS designed research. ER contributed Figures 1, 5, 6 and 7 and also assisted the experiments resulting in figures 2 and 3.

eNeuro

New Research

Sensory and Motor Systems

# Slow NMDA-Mediated Excitation Accelerates Offset-Response Latencies Generated via a Post-Inhibitory Rebound Mechanism

**Ezhilarasan Rajaram,[1,2] Carina Kaltenbach,[3] Matthew J. Fischl,[1,*] Leander Mrowka,[1] Olga Alexandrova,[1] Benedikt Grothe,[1] Matthias H. Hennig,[3] and Conny Kopp-Scheinpflug[1]**

https://doi.org/10.1523/ENEURO.0106-19.2019

[1]Division of Neurobiology, Department Biology II, Ludwig-Maximilians-University Munich, Planegg-Martinsried 82152, Germany, [2]Graduate School of Systemic Neurosciences, Ludwig-Maximilians-University Munich, Planegg-Martinsried 82152, Germany, and [3]Institute for Adaptive and Neural Computation, School of Informatics, University of Edinburgh, Edinburgh EH8 9AB, United Kingdom

## Abstract

In neural circuits, action potentials (spikes) are conventionally caused by excitatory inputs whereas inhibitory inputs reduce or modulate neuronal excitability. We previously showed that neurons in the superior paraolivary nucleus (SPN) require solely synaptic inhibition to generate their hallmark offset response, a burst of spikes at the end of a sound stimulus, via a post-inhibitory rebound mechanism. In addition SPN neurons receive excitatory inputs, but their functional significance is not yet known. Here we used mice of both sexes to demonstrate that in SPN neurons, the classical roles for excitation and inhibition are switched, with inhibitory inputs driving spike firing and excitatory inputs modulating this response. Hodgkin–Huxley modeling suggests that a slow, NMDA receptor (NMDAR)-mediated excitation would accelerate the offset response. We find corroborating evidence from *in vitro* and *in vivo* recordings that lack of excitation prolonged offset-response latencies and rendered them more variable to changing sound intensity levels. Our results reveal an unsuspected function for slow excitation in improving the timing of post-inhibitory rebound firing even when the firing itself does not depend on excitation. This shows the auditory system employs highly specialized mechanisms to encode timing-sensitive features of sound offsets which are crucial for sound-duration encoding and have profound biological importance for encoding the temporal structure of speech.

*Key words:* auditory development; duration encoding; gap-detection; level-tolerance; sound-offset encoding; superior paraolivary nucleus

**Significance Statement**

Temporal features like sound-onset and sound-offset responses are crucial for acoustic pattern recognition and vocal communication. In contrast to onset responses, offset responses can be generated solely from inhibition via post-inhibitory rebounds. Here, we demonstrate that excitatory inputs are nevertheless present at offset-encoding neurons of the auditory brainstem where they serve to shorten the response latency of the offset response and stabilize the offset latency against changes in stimulus level.

## Introduction

The relative strength and temporal interaction of excitatory and inhibitory synaptic inputs determine neuronal temporal firing patterns in many parts of the brain including the auditory pathway (Wehr and Zador, 2003; Sun et al., 2010; Denève and Machens, 2016). Acoustic pat-

Received March 20, 2019; accepted May 2, 2019; First published May 31, 2019.
The authors declare no competing financial interests.

Author contributions: E.R., C.K., M.J.F., L.M., O.A., and C.K.-S. performed research; E.R., C.K., M.J.F., O.A., and C.K.-S. analyzed data; E.R., B.G., M.H.H., and C.K.-S. wrote the paper; M.H.H. and C.K.-S. designed research.

tern recognition and vocal communication require precise processing of the temporal structure of sounds, such as the distinct detection of onsets and offsets, which are encoded by two dissociable channels in the auditory pathway (Anderson and Linden, 2016; Gómez-Álvarez et al., 2018; Kopp-Scheinpflug et al., 2018).

In previous studies of the central auditory system, sound-offset responses were often ignored (Kopp-Scheinpflug et al., 2018). While sound offsets are typically less abrupt (Cavaco and Lewicki, 2007) and more easily obscured by reverberation than onsets, and perceptually less prominent than onsets (Phillips et al., 2002; Deneux et al., 2016; Sohoglu and Chait, 2016), this view is changing with the discovery of neurons dedicated to detecting offsets. Recent studies suggest that neural representations of sound transients, such as offsets, are important for speech perception (Eggermont, 2015), are implicated in auditory dysfunction in brain disorders (Felix et al., 2018) and appear to be involved in short-term memory formation during auditory task performance (Elgueda et al., 2019). A previous study showed that neurons responding to sounds in a sustained fashion do not encode the end of a stimulus as reliably as those which respond specifically to the offset (Kopp-Scheinpflug et al., 2011). Detection of the end of a sound stimulus using the last sound-evoked spike in a neuron with a sustained response is highly variable, mainly due to cellular and synaptic properties changing during stimulus time. At stimulus onset, a neuron is in resting conditions and typically highly excitable, which allows fast and precise spiking. After a period of tonic activity, synaptic depression and activation of voltage-gated conductances reduce excitability, leading to less precise responses (cf. Kopp-Scheinpflug et al., 2011, their Fig. 7). Thus, a careful examination of auditory offset responses will aid in understanding their underlying coding mechanisms, both of which are prerequisites to study their behavioral relevance.

Sound-evoked offset responses have been reported in all processing stages of the ascending auditory pathway from brainstem to cortex (Kopp-Scheinpflug et al., 2018). Offset responses in higher areas such as the auditory cortex seem to be largely inherited from subcortical structures via nonoverlapping sets of excitatory inputs (Scholl et al., 2010). The de-novo generation of sound-offset responses has so far been best described for neurons in the superior olivary complex (SOC) of the mammalian auditory brainstem which exhibit acoustically-evoked offset firing at the end of a sound stimulus (Grothe, 1994; Kuwada and Batra, 1999; Behrend et al., 2002; Dehmel et al., 2002; Kulesza et al., 2003; Kulesza, 2008). These offsets can be generated via a post-inhibitory rebound mechanism that is initiated by strong glycinergic inputs and aided by the activation of hyperpolarization-activated cyclic nucleotide-modulated currents ($I_H$) and T-type calcium currents (Felix et al., 2011; Kopp-Scheinpflug et al., 2011). The main source of the glycinergic input triggering these offset responses is the medial nucleus of the trapezoid body (MNTB; Grothe, 1994; Kulesza et al., 2007), which on stimulation evokes IPSCs (Kopp-Scheinpflug et al., 2011) reversing at voltages around −100 mV, well below the neurons' resting membrane potential (Löhrke et al., 2005; Yassin et al., 2014).

It has been shown in *in vivo* measurements that this strong inhibition is essential for generating short-latency offset responses in a substantial population of SOC neurons (cat: Guinan et al., 1972; bat: Grothe, 1994; rabbit: Kuwada and Batra, 1999; gerbil: Behrend et al., 2002; Dehmel et al., 2002; rat: Kulesza et al., 2003; mouse: Kopp-Scheinpflug et al., 2011; Felix et al., 2013), but the anatomic location and number of SOC neurons with offset responses varies across mammalian species and experimental approaches. In rodents, neurons with offset responses are concentrated in the superior paraolivary nucleus (SPN) where current-clamp recordings *in vitro* show offset firing in nearly 100% of neurons (Kopp-Scheinpflug et al., 2011; Felix et al., 2013), while SPN recordings *in vivo* revealed more differential response types (Behrend et al., 2002; Dehmel et al., 2002; Kopp-Scheinpflug et al., 2011; Felix et al., 2013). These discrepancies in observing different response types between *in vivo* and *in vitro* data suggest that so far, *in vitro* experiments have missed factors that might modulate offset responses and generate more diverse response types.

Excitatory responses of SPN neurons *in vivo* have been reported either as increased sound-evoked firing rates without obvious inhibition (Behrend et al., 2002; Dehmel et al., 2002) or as responses masked by inhibition, only to be revealed after pharmacological blockade of glycinergic inputs (Kulesza et al., 2007; Jalabi et al., 2013). However, the relevance of excitatory inputs to these predominantly offset-responding neurons for auditory processing is unknown. Octopus cells of the ventral cochlear nucleus have been suggested as one source of SPN excitation based on the contralateral origin of the sound-evoked excitation, its broad frequency tuning (Dehmel et al., 2002) and anatomic tracing experiments (Thompson and Thompson, 1991; Schofield, 1995; Saldaña et al., 2009; Felix et al., 2017). An *in vitro* study also reports the presence of AMPA receptor (AMPAR)-mediated responses in the mouse SPN (Felix and Magnusson, 2016), but their function and mechanism of action are still unknown.

To gain better insight into the functional relevance of excitatory inputs during sound-offset encoding we performed immunocytochemistry, single-cell recording *in vivo*, computational modeling, and patch-clamp recordings *in vitro*. We demonstrate that the time course of slow

This work was supported by German Research Council (DFG) Grants KO2207/3-1, SFB870-A10, and GS-82 Graduate School of Systemic Neurosciences GSN$^{LMU}$.

*M. J. Fischl's present address: National Institutes of Health, Section on Neuronal Circuitry, Bethesda, MD 20814.

Acknowledgements: We thank Dr. Jennifer Linden and Dr. James Sinclair for helpful discussions and invaluable experimental support.

Correspondence should be addressed to Conny Kopp-Scheinpflug at cks@bio.lmu.de.

https://doi.org/10.1523/ENEURO.0106-19.2019

**Table 1. Primary and secondary antibodies used for immunocytochemistry**

| Primary antibody | Antigene | Supplier | Catalog number | Host | Dilution |
|---|---|---|---|---|---|
| GlyT2 | Synthetic from the C terminus as predicted from the cloned rat GLYT2 | Millipore | AB1773 | Guinea pig | 1:1000 |
| GlyT2 | Recombinant protein (aa1–229 of rat GlyT2) | SySy | 272003 | Rabbit | 1:1000 |
| NMDA- R2c | Fusion protein from the NR2C subunit of the NMDAR | R&D Systems | PPS033 | Rabbit | 1:500 |
| MAP2 | Purified MAP2 isolated from bovine brain | Acris | TA336617 | Chicken | 1:500 |
| VGLUT1 | Purified recombinant protein of rat VGLUT 1 (aa456–560) | SySy | 135304 | Guinea pig | 1:2000 |
| VGLUT2 | Strep-Tag fusion protein of rat VGLUT 2 (aa510–582) | SySy | 135402 | Rabbit | 1:1000 |
| *VGLUT3* | Peptide (C)ELNHEAFVSPRKK, corresponding to amino acid residues 533–545 of rat VGLUT3 (accession Q7TSF2); cytoplasmic, C terminus | Alomone Labs | AGC-037 | Rabbit | 1:300 |
| Secondary antibody | Host species | Supplier | Catalog number | Conjugated | Dilution |
| Rabbit | Donkey | Dianova | 711-165-152 | Cy3 | 1:300 |
| Rabbit | Donkey | Dianova | 711-586-152 | Alexa Fluor 594 | 1:200 |
| Guinea pig | Donkey | Dianova | 706-546-148 | Alexa Fluor 488 | 1:200 |
| Guinea pig | Donkey | Dianova | 706-166-148 | Cy3 | 1:300 |
| Chicken | Donkey | Dianova | 703-156-155 | AMCA | 1:100 |

NMDA receptor (NMDAR)-mediated excitation extends into the temporal window of post-inhibitory rebound firing. Simultaneous activation of excitation and inhibition accelerates post-inhibitory rebound responses and makes them more tolerant against changes in sound intensity *in vivo*, which is a prerequisite for sound-duration tuning and level-independent gap detection (Forrest and Green, 1987).

## Materials and Methods

All experimental procedures were reviewed and approved by the Bavarian district government (TVV AZ: 55.2-1-54-2532-38-13) and were done according to the European Communities Council Directive (2010/63/EU). C57Bl6J mice were housed in a vivarium with a normal light dark cycle (12/12 h light/dark) and food and water *ad libitum*. Mice of both sexes were used for the physiologic and anatomic experiments.

### Immunohistochemistry

Mice (P21–P35) were anesthetized with an overdose of pentobarbital and perfusion-fixed with 4% paraformaldehyde (PFA) intracardially. Following overnight postfixation in 4% PFA, coronal brainstem sections including the cochlear nucleus and the SOC of 50-$\mu$m thickness were taken using a vibrating microtome (Leica Biosystems, VT1200S). After 3 $\times$ 10-min washes in PBS, sections were transferred to a blocking solution containing 1% bovine serum albumin, 0.5% Triton X-100, and 0.1% saponin in PBS. For NMDAR staining, proteinase K treatment (1:1000 in PBS) for 20 min at 37°C was included before transferring the sections into blocking solution. Tissue was incubated for 48 h at 4°C with primary antibodies (Table 1) diluted in blocking solution. Biocytin was labeled with streptavidin conjugated to Cy3 (1:500 in blocking solution). Tissue was then washed 3 $\times$ 10 min in PBS at room temperature, before incubation for 24 h at 4°C with secondary antibodies diluted in blocking solution. Then sections were rinsed 3 $\times$ 10 min in PBS, and coverslipped with Vectashield mounting medium.

### Confocal microscopy

Confocal optical sections were acquired with a confocal laser-scanning microscope equipped with HCX PL APO CS 20X/NA0.7 and HCX PL APO Lambda Blue 63$\times$/NA1.4 immersion oil objectives (Leica). Fluorochromes were visualized with excitation wavelengths of 405 nm (emission filter 410–430 nm) for amino-methylcoumarin (AMCA), 488 nm (emission filter 510–540 nm) for Alexa Fluor 488, 561 nm (emission filter 565–585 nm) for Cy3, and 594 nm (emission filter 605–625 nm) for Alexa Fluor 594. For each optical section, the images were collected sequentially for the different fluorochromes. Stacks of 8-bit grayscale images were obtained with axial distances of 290 nm between optical sections and pixel sizes of 120–1520 nm depending on the selected zoom factor and objective. To improve the signal-to-noise ratio, images were averaged from three successive scans. RGB stacks, montages of RGB optical sections and maximum-intensity projections were assembled using the ImageJ 1.37k plugins and Adobe Photoshop 8.0.1 software.

### *In vivo* physiology

Young adult (6–16 weeks) mice of either sex ($n$ = 9) were anesthetized with a subcutaneous injection of 0.01 ml/g MMF (0.5 mg/kg body weight medetomidine, 5.0 mg/kg body weight midazolam, and 0.05 mg/kg body weight fentanyl) and were placed on a temperature-controlled heating pad (WPI: ATC 1000) in a soundproof chamber (Industrial Acoustics). Depth of anesthesia was measured using the toe pinch reflex and animals responding were given supplemental MMF at 1/3 the initial dose. The mice were then stabilized in a custom stereotaxic device. An incision was made at the top of the skull, and a head post was fixed to the skull using dental cement. A craniotomy was performed above the cerebellum to ac-

cess the auditory brainstem. A ground electrode was placed in the muscle at the base of the neck. Glass microelectrodes were pulled from glass capillaries so that the resistance was 5–20 MΩ when filled with 3 M KCl solution or 2 M potassium acetate with 2.5% biocytin. Signals were amplified (AM Systems, Neuroprobe 1600), filtered (300–3000 Hz; Tucker-Davis-Technologies PC1), and recorded (~50 kHz sampling rate) with an RZ6 processor (Tucker-Davis Technologies). Python-based SPIKE software (Brandon Warren, V.M. Bloedel Hearing Research Center, University of Washington) was used to calibrate the multi-field magnetic speakers, generate stimuli and record action potentials. Stimuli consisted of pure tones (50- to 100-ms duration, 5-ms rise/fall time) at varying intensity (0- to 90-dB SPL) and were presented through hollow ear bars connected to the speakers with Tygon tubing. PSTHs were assessed at characteristic frequency (CF) and 80-dB SPL. Spike sorting and data analysis were performed offline using custom MATLAB programs. At the end of the experiment, biocytin (2.5%) was deposited at the final penetration using the current injection mode of the amplifier (+0.5 μA, 1–2 min). Thirty minutes were allowed for cellular uptake before the animal was perfused, and the tissue was processed for biocytin fluorescence as described above. Recording sites were determined using the biocytin deposition as a reference for stereotaxic reconstruction.

### *In vitro* electrophysiology

Mice of either sex P15–P22 were briefly anaesthetized with isoflurane and rapidly decapitated. Coronal brainstem sections (150–200 μm thick) containing the SOC were cut in an ice-cold high-sucrose, low-sodium artificial CSF (ACSF). Brainstem slices were maintained after slicing in normal ACSF at 37°C for 30–45 min, after which they were stored in a slice-maintenance chamber at room temperature (~22°C). Composition of the normal ACSF: 125 mM NaCl, 2.5 mM KCl, 26 mM $NaHCO_3$, 10 mM glucose, 1.25 mM $NaH_2PO_4$, 2 mM sodium pyruvate, 3 mM myo-inositol, 2 mM $CaCl_2$, 1 mM $MgCl_2$, and 0.5 mM ascorbic acid, pH 7.4, bubbled with 95% $O_2$, 5% $CO_2$. For the low-sodium ACSF $CaCl_2$ and $MgCl_2$ concentrations were 0.1 and 4 mM, respectively, and NaCl was replaced by 200 mM sucrose. Experiments were conducted at 36 ± 1°C, maintained by an inline feedback temperature controller and heated stage (Warner Instruments) with the recording chamber being continuously perfused with ACSF at a rate of 1–2 ml $min^{-1}$. Whole-cell patch-clamp recordings were made from visually identified SPN neurons using an EPC10/2HEKA amplifier (HEKA Electronik), sampling at 50 kHz and filtering between 2.9 and 10 kHz. Patch pipettes were pulled from borosilicate glass capillaries (Warner Instruments) using a DMZ Universal electrode puller (Zeitz-Instuments Vertriebs GmbH), filled with a patch solution containing: 126 mM K-gluconate, 4 mM KCl, 40 mM HEPES, EGTA 5 mM HEPES, 1 mM $MgCl_2$, 5 mM $Na_2$phosphocreatine, 0.2% biocytin, 292 mOsm, pH was adjusted to 7.2 with KOH. For recordings of EPSCs the internal solution contained: 135 mM Cs-gluconate, 10 mM HEPES, 1 mM EGTA, 3.3 mM $MgCl_2$, 3 mM $Na_2$phosphocreatine, 2 mM NaATP, 20 mM TEA-Cl, 0.2% biocytin, 300 mOsm. pH was adjusted to 7.2 with CsOH. Data were corrected for liquid junction potentials of –13.8 and –13.7 mV for the potassium-based and the cesium-based internal solutions, respectively. Electrode resistance was between 2.4 and 6 MΩ. Synaptic responses were evoked by afferent fiber stimulation with either concentric or bipolar (FHC) electrodes. Voltage pulses were generated by the HEKA amplifier and post-amplified by an isolated pulse stimulator (AM Systems). Synaptic conductances were calculated from the synaptic currents: $G = PSC/(V_m - E_{PSC})$, with PSC being the postsynaptic current, $V_m$ being the holding potential (–60 mV for inhibition; 40 mV for excitation), $E_{PSC}$ being the reversal potential of the postsynaptic current ($E_{EPSC}$: 0 mV; $E_{IPSC}$: –100 mV).

### Computational model

Two simple, single-compartment models of a SPN neuron were simulated using NEURON (version 7.5; Hines and Carnevale, 2001). In both models, the basic set-up of the neuron, including the membrane properties and the ionic channels, is identical to the model developed by Kopp-Scheinpflug et al. (2011), available on ModelDB (https://senselab.med.yale.edu/modeldb/ShowModel.asp?model=139657), accession number 139657. In the two current models, the excitatory noise was removed, and four excitatory synapses were added in addition to the inhibitory synapses already present. The synapses are modeled using the NEURON built-in function Exp2Syn. In both models, the excitatory and inhibitory stimuli consist of 10 such spikes with 10-ms gaps, resulting in a total stimulus duration of 100 ms. The excitatory and inhibitory conductances and the respective time constants used in the model are provided by the patch-clamp experiments performed for this paper. In the first model (including AMPA currents), all four excitatory synapses are simulating AMPA synapses, with a reversal potential $E_{rev\_AMPA} = 0$ mV, a rise time constant of $\tau_1 = 0.1$ ms and a decay time constant of $\tau_2 = 0.9$ ms. In the second model (including AMPA and NMDA currents), only two excitatory synapses are simulating AMPA synapses, with the same parameters as in the first model; while the two other excitatory synapses are simulating simplified NMDA synapses, with reversal potential $E_{rev\_NMDA} = 0$ mV, a rise time constant of $\tau_1 = 3$ ms, and a decay time constant of $\tau_2 = 9$ ms. The conductances of the excitatory synapses were varied in both models. Both models included 14 inhibitory synapses with reversal potential $E_{rev\_inh} = -100$ mV, a rise time constant $\tau_1 = 0.1$ ms, a decay time constant $\tau_2 = 2$ ms and a peak conductance of 82 ns and 41 nS. A simplified depression of the input synapses was modeled using the steady-state depression values collected for this paper.

### Experimental design and statistical analysis

In the text data are presented in parenthesis as (median; 25/75 quartiles or as mean ± SEM; test: *p* value) unless indicated otherwise. In the figures, data are presented as medians (lines in boxes); 25/75 quartiles (boxes); and 10th/90th percentiles (whiskers) in addition to individual data points. Statistical analyses of the data

were performed with SigmaStat/SigmaPlot. Normality was tested by the Shapiro–Wilk test. Comparisons between different data sets were made depending on the distribution of the data using parametric tests for normally distributed data (two-tailed Student's *t* test for comparing two groups and ANOVA for comparing three or more groups). When the normality assumption was violated, nonparametric tests (Mann–Whitney rank-sum test for comparing two groups and Kruskal–Wallis ANOVA on ranks for comparing three or more groups) were used. Paired *t* tests or Wilcoxon signed rank tests were used when two data sets were recorded from individual neurons under different conditions. Differences were considered statistically significant at $p \leq 0.05$ and presented in the figures as n.s. for nonsignificant differences and as $*p \leq 0.05$, $**p \leq 0.01$, and $***p \leq 0.001$ for significant differences. Intrinsic properties as well as postsynaptic current amplitudes and kinetics were analyzed using Stimfit software (Guzman et al., 2014). For data acquired with *in vivo* single-unit recording or patch-clamp recording; *n* is the number of neurons, with two to three brain slices per animal and at least three animals per group.

## Results

### SPN neurons receive glycinergic and glutamatergic synaptic input

We previously showed that only inhibitory synaptic input is required to generate offset responses in the SPN (Kopp-Scheinpflug et al., 2011). Here, this was corroborated by immunocytochemistry showing strong expression of the neuronal glycine transporter type 2 (GlyT2), which labels glycinergic synaptic terminals around the soma of SPN neurons (Fig. 1, green boutons). However, the additional presence of excitatory synapses was confirmed by labeling for the vesicular glutamate transporter (VGLUT) types 1–3 (Fig. 1*A*,D,*G*). While VGLUT1 and VGLUT2 positively labeled presynaptic terminals in SPN (Fig. 1*B*,*C*,*E*,*F*), the signal strength for VGLUT3 was quite low and somatic rather than in the presynaptic boutons (Fig. 1*H*,*I*).

### SPN neurons with sound-offset responses can exhibit moderate excitatory responses during contralateral sound stimulation

To explore the contribution of excitatory inputs to signal processing in neurons with sound-offset responses, spikes were recorded from single SPN neurons in anesthetized mice *in vivo*, during (peristimulus) and after (poststimulus) the presentation of sound (Fig. 2*A*). The sample of 20 SPN neurons had CFs ranging from 9.25 to 50.4 kHz (Fig. 2*B*); 85% (17/20) of these neurons showed a burst of increased firing at the end of contralateral sound stimulation (offset responses) and little or no firing during sound presentation (Fig. 2*C*,*D*), consistent with a prevalent inhibitory input and the dominance of offset responses reported in previous studies (Dehmel et al., 2002; Kulesza et al., 2003; Felix et al., 2013). Only 3/20 SPN neurons did not exhibit offset firing, but responded with an onset, primary-like or sustained firing pattern during sound stimulation (Fig. 2*E*). These neurons that fired spikes only during but not after the stimulus were not included in further analyses. Of SPN neurons with offset responses, 53% (9/17) additionally showed excitatory responses during sound stimulation that exceeded 5% of the respective neurons' overall firing rate (Fig. 2*F*). These neurons will be further referred to as ON-OFF type neurons (Fig. 2*F*,*G*, gray) and will be contrasted against neurons that exhibit offset responses without peristimulus excitation (OFF-only type; Fig. 2*F*, blue). Average temporal response patterns show ON-OFF type neurons with either an onset or a primary-like temporal response pattern during sound followed by a poststimulus offset response (Fig. 2*G*, gray histogram). Onset or primary-like temporal response patterns are associated with octopus cells in the ventral cochlear nucleus (Rhode et al., 1983) which are one source of excitatory input to the SPN (Thompson and Thompson, 1991; Schofield, 1995; Saldaña et al., 2009; Felix et al., 2017). The average response of the OFF-only type neurons is characterized by only little spontaneous firing during sound followed by a slightly delayed poststimulus offset response (Fig. 2*G*, blue histogram). The ratio of peristimulus to poststimulus rate is significantly larger in the ON-OFF type neurons (ON-OFF type: 0.22; 0.12/1.39; $n = 9$; OFF-only type: 0; 0/0.09; $n = 8$; Mann–Whitney rank-sum test: $p = 0.002$; Fig. 2*H*).

### SPN neurons that exhibit additional excitation have accelerated and level-independent offset-response latencies

The average temporal response pattern in Figure 2*G* suggests that offset-response latencies are shorter in ON-OFF type neurons compared to OFF-only type neurons. To investigate potential differences in latency in more detail, offset responses were recorded at CF for increasing sound intensities (Fig. 3*A*,*B*). Indeed, offset-response latencies were significantly faster for ON-OFF type neurons (5.55 ms, 3.80/6.97 ms, $n = 8$) than for OFF-only type neurons (8.84 ms, 6.38/16.75 ms, $n = 9$; Mann–Whitney rank-sum test: $p = 0.018$; Fig. 3*C*). However, no difference was observed for the variability of the offset-response latency (jitter) between *ON-OFF* and OFF-only type neurons ($jitter_{ON\text{-}OFF}$: 1.23 ms; 0.62/2.54 ms, $n = 8$; $jitter_{OFF\text{-}only}$: 1.11 ms; 0.45/5.23 ms; $n = 9$; Mann–Whitney rank-sum test: $p = 0.665$; Fig. 3*D*), suggesting that the intrinsic properties of the cells that regulate precise spike firing are not the reason for the difference in latencies.

A common feature in stimulus encoding across different sensory modalities is that response latencies decrease with increasing stimulus intensity (auditory: Kitzes et al., 1978; Klug et al., 2000; somatosensory: Mountcastle et al., 1957; visual: Morgan and Thompson, 1975). In contrast, offset-response latencies of both ON-OFF type (Fig. 3*A*) and OFF-only type (Fig. 3*B*) SPN neurons did not show a strong dependency on stimulus intensity but remained rather constant over a large sound intensity range or even showed a trend of increasing latencies with increasing intensities (single cell examples shown in Fig. 3*A*,*B*). On average, there were no significant changes in

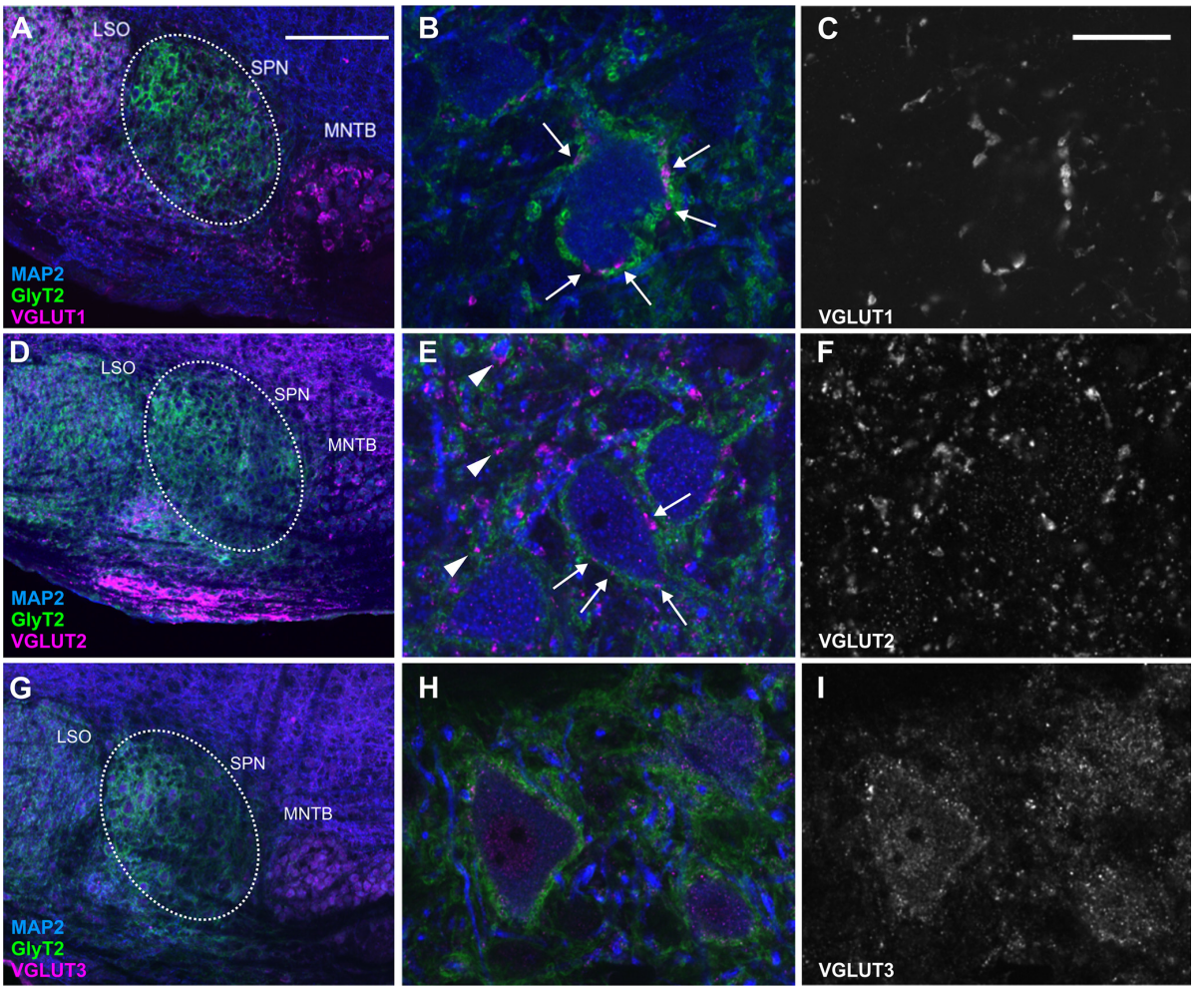


**Figure 1.** Histochemical profile of excitatory and inhibitory inputs to the SPN. ***A***, ***B***, ***D***, ***E***, ***G***, ***H***, Glycinergic input forms the most prominent input to SPN (white dotted circle in ***A***, ***D***, ***G***) and is depicted by neuronal GlyT2 (green) labeling. Immunolabeling for microtubule associated protein 2 (MAP2, blue) is used as a neuronal marker in all images. Glutamatergic inputs are shown by labeling for the VGLUTs (magenta): VGLUT1 (***A–C***), VGLUT2 (***D–F***), VGLUT3 (***G–I***). ***A–F***, While both VGLUT1 (***B***, white arrows) and VGLUT2 (***E***, white arrows) positive synaptic boutons are present at the soma, VGLUT2 boutons are also seen in the neuropil (***E***, white arrowheads). ***G–I***, VGLUT3 shows only weak somatic but no presynaptic bouton labeling. Scale bars = 200 $\mu$m (left images) and 20 $\mu$m (middle and right images).

latency per decibel sound intensity for the ON-OFF type neurons (–9.83 $\mu$s/dB; –19.46/5.11 $\mu$s/dB; $n = 6$; Fig. 3*E*), while changes in latencies per decibel for the OFF-only type neurons were significantly larger (–47.79 $\mu$s/dB; –67.37/–13.87 $\mu$s/dB; $n = 6$, Kruskal–Wallis ANOVA on ranks followed by Dunn's multiple comparisons versus a zero change control: $p = 0.032$).

If the neurons firing either ON-OFF or OFF-only responses represent two distinct populations, they may inhabit different locations in the SPN. This was tested by testing whether ON-OFF or OFF-only responding neurons have similar or different CFs. The CFs of the offset response for ON-OFF type neurons (15.1 kHz; 12.0/21.8 kHz; $n = 8$) were compared with those for OFF-only type neurons (18.5 kHz; 12.3/22.3 kHz; $n = 9$) but no significant difference was found (Mann–Whitney rank-sum test: $p = 1.000$; Fig. 3*F*). Tonotopically organized glycinergic projections from MNTB into SPN suggest that neurons tuned to high frequencies are located more medially and neurons tuned to low frequencies are located more laterally (Banks and Smith, 1992). As a result, neurons with different CFs should inhabit separate anatomic locations within the tonotopic axis of the SPN, which was not observed in the present sample of ON-OFF and OFF-only type neurons and suggests, that neurons having ON-OFF or OFF-only responses are part of a continuum with the only difference being differently balanced excitation and inhibition. Response thresholds of offset responses were also not significantly different between ON-OFF type (32-dB SPL; 16.3/48.8-dB SPL; $n = 8$) and OFF-only type neu-

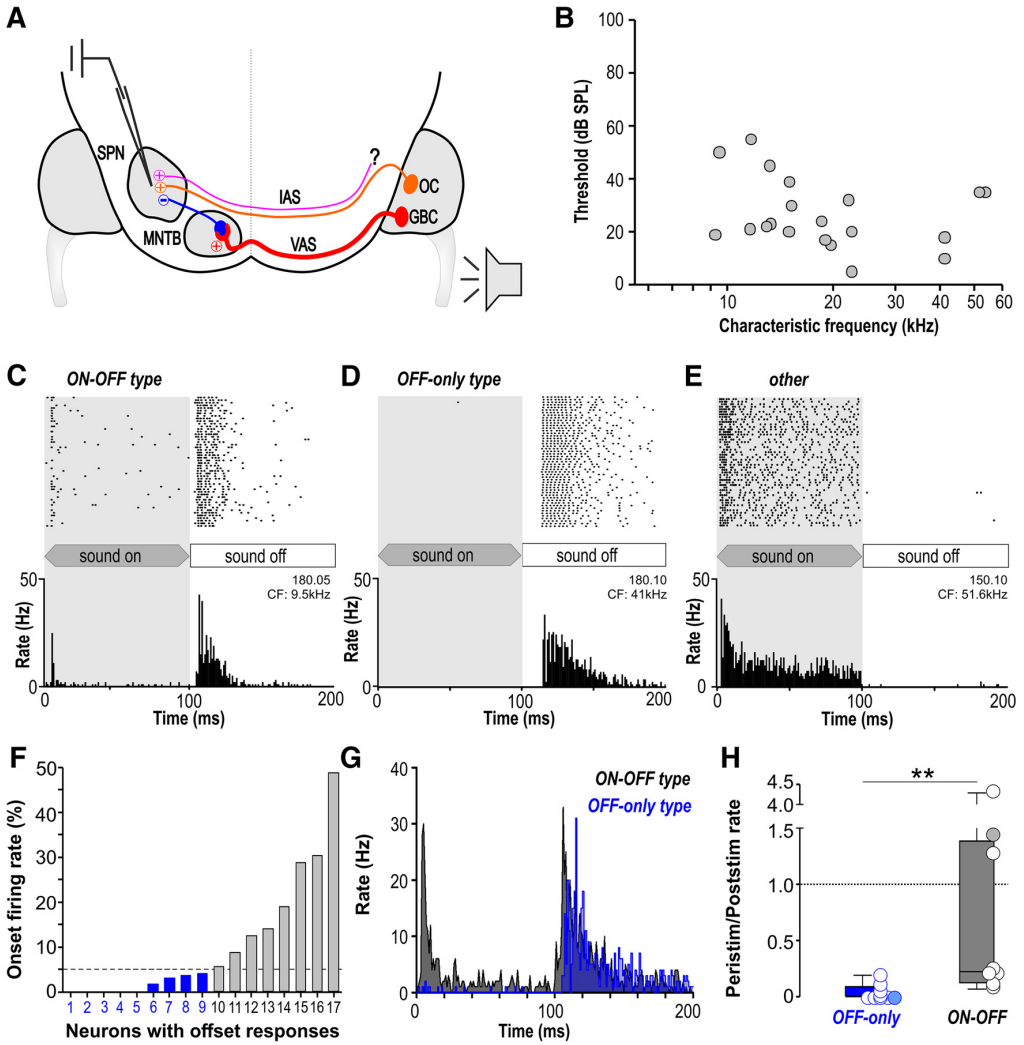


**Figure 2.** SPN neurons with post-inhibitory rebound responses at sound offset can also show excitatory responses during sound. ***A***, Schematic of a sound-offset encoding circuit in the mammalian brainstem. Globular bushy cell (GBC) axons project via the ventral acoustic stria (VAS) to the contralateral MNTB to form one-to-one connections via the giant calyx of Held synapses. MNTB neurons then project to neurons of the SPN. SPN cells also receive excitatory input from octopus cells (OCs) and possibly other, yet unknown sources (?) in the contralateral ventral cochlear nucleus via the IAS. ***B***, Plot of CFs and auditory thresholds of all SPN neurons recorded in this sample. ***C–E***, Raster plots and PSTHs (at CF, 80-dB SPL, 50 trials) shown for three individual SPN neurons with different response patterns. ***C***, ON-OFF type, showing a peristimulus response related to sound onset followed by a response related to sound offset. ***D***, OFF-only type, showing responses related to sound offset, but no peristimulus firing. ***E***, Response type showing only peristimulus firing but no poststimulus response at sound offset. ***F***, Distribution of neurons with offset responses depending on how much of their overall firing activity during the combined 200-ms peristimulus and poststimulus period was present within the first 20 ms of the response. The dashed line represents the 5% criterion we used to classify the neurons into either OFF-only type neurons (blue: 1–9) or ON-OFF type neurons (gray: 10–17). ***G***, Average temporal response patterns for OFF-only type neurons (blue) and ON-OFF type neurons (gray). ***H***, Peristimulus-to-poststimulus ratio for OFF-only type neurons (blue) and ON-OFF type neurons (gray). Firing rates were averaged over the whole peristimulus time window and divided by the average of the whole poststimulus time window. Equal firing rates in both time windows result in a ratio of zero (dotted line). Filled circles represent the ratios for the example cells shown in ***C***, ***D***. Note that OFF-only neurons with ratios larger than zero exhibit spontaneous APs which also appear during the peristimulus time window but not concentrated within the first 20 ms to form an onset response. $**p \leq 0.01$.

rons (21-dB SPL; 18.5/28-dB SPL; $n = 9$; Mann–Whitney rank-sum test: $p = 0.386$; Fig. 3*G*).

The occurrence of excitatory responses in some but not all neurons of a nucleus with generally dominant inhibition could also be attributed to a reduced inhibitory constraint in ON-OFF type neurons, resulting in higher spontaneous firing rates compared to OFF-only type neurons. Inhibition in SPN neurons is provided by

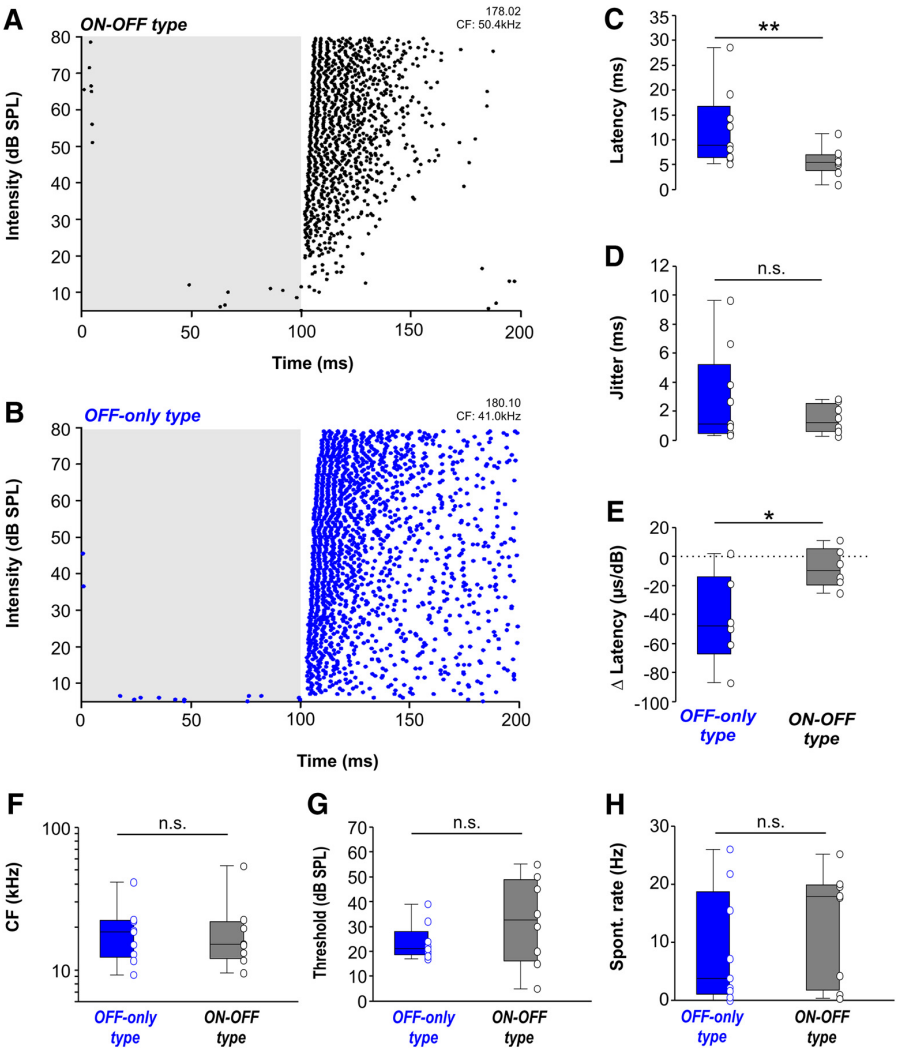


**Figure 3.** ON-OFF type SPN neurons have shorter offset-response latencies and less level dependence than OFF-only type neurons. ***A***, ***B***, Raster plot at CF and changing intensity levels for representative (***A***) ON-OFF type and (***B***) OFF-only type neurons. Each dot represents an action potential. Gray-shaded area indicates sound duration. ***C***, ***D***, Distribution of (***C***) offset latencies and (***D***) jitter for OFF-only type (blue) and ON-OFF type (gray) neurons at CF/80-dB SPL. Statistical assessment in ***C***, ***D*** was unaltered if the two extreme values were removed. ***E***, Average change of offset-response latency per dB intensity change for OFF-only type (blue) and ON-OFF type (gray) SPN neurons. OFF-only type neurons (blue) showed a significantly larger variability of offset-response latency with changes in intensity. Latency change/dB was not significantly different from zero (dotted line) for ON-OFF type neurons (=level invariant). ***F–H***, Between SPN neurons of either OFF-only type or ON-OFF type, physiologic parameters like (***F***) CFs, (***G***) thresholds, and (***H***) spontaneous firing rates are not significantly different. $*p \leq 0.05$, $**p \leq 0.01$, n.s. = non-significant.

strong glycinergic input from MNTB neurons. Despite high firing rates during sound stimulation, MNTB neurons are spontaneously active with an average rate of 20–30 Hz (Kopp-Scheinpflug et al., 2008) which tonically suppresses SPN activity. Spontaneous firing rates in SPN were not significantly different between ON-OFF type neurons (13.25 ± 3.5 Hz) compared to OFF-only type neurons (8.73 ± 3.7 Hz; two-tailed $t$ test: $p = 0.359$; $t = 0.946$; df = 15; Fig. 3*H*), implying a similar strength of inhibitory innervation across neurons. Across the population of cells tested, ON-OFF type and OFF-only type neurons do not exhibit differences in location or general physiologic properties suggesting them to belong to one cell population with differing strength of excitatory input.

### Offset-response thresholds are more sensitive than peristimulus-response thresholds

Comparing the peristimulus and poststimulus excitatory responses within each ON-OFF type SPN neuron revealed that their spectral tuning largely overlapped (Fig. 4*A*,*B*), which is in contrast to results from auditory cortex

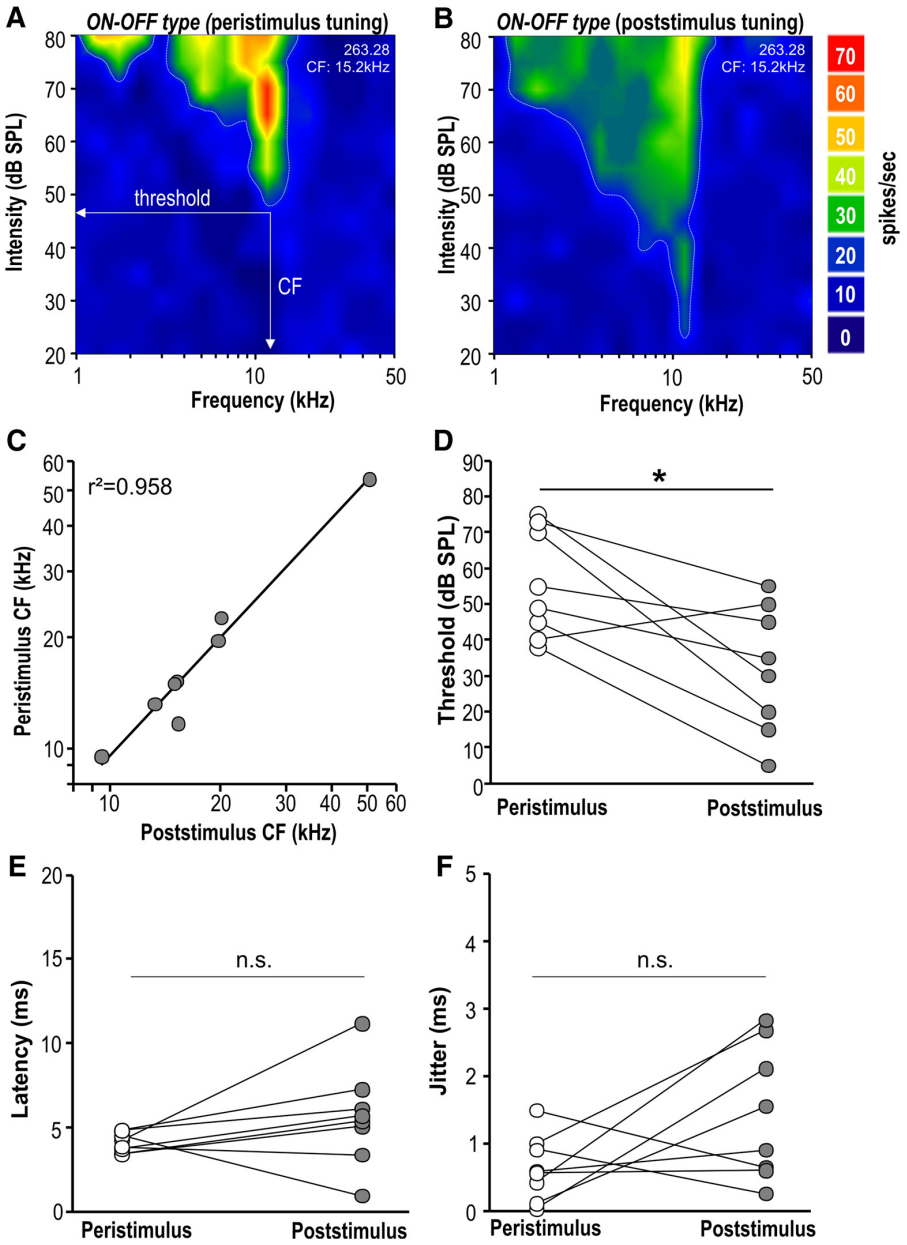


**Figure 4.** Within ON-OFF type SPN neurons, peristimulus responses have similar tuning, but elevated threshold compared to their poststimulus offset-responses. ***A***, ***B***, Frequency-intensity response maps for an individual ON-OFF type SPN neuron plotted for the peristimulus response (***A***) and for the poststimulus response after sound cessation (***B***). ***C***, Linear correlation between peristimulus and poststimulus CFs for individual ON-OFF type SPN neurons. ***D***, Thresholds for the responses during sound (peristimulus, white circles) are higher than thresholds for responses after sound termination (poststimulus, gray circles). ***E***, ***F***, Latencies and jitter were not significantly different between peristimulus and poststimulus response of individual ON-OFF type SPN neurons. $*p \leq 0.05$, n.s. = non-significant.

(Scholl et al., 2010; Sollini et al., 2018) and will be discussed later. There was no significant difference between the peristimulus and poststimulus CFs for ON-OFF type neurons ($CF_{peristim}$: 19.8 ± 4.5 kHz; $n = 8$; $CF_{poststim}$: 20.0 ± 4.9 kHz; $n = 8$; two-tailed paired $t$ test: $p = 0.74$; $t = -0.345$; df = 7; Fig. 4*C*). Thresholds were significantly lower for poststimulus offset responses (32 ± 6-dB SPL) compared to excitatory peristimulus responses (56 ± 5-dB SPL; $n = 8$; two-tailed paired $t$ test: $p = 0.011$; $t = 3.407$; df = 7; Fig. 4*D*). For each ON-OFF type neuron first-spike latencies for the excitatory peristimulus response (4.12 ± 0.2 ms) were barely faster than those of

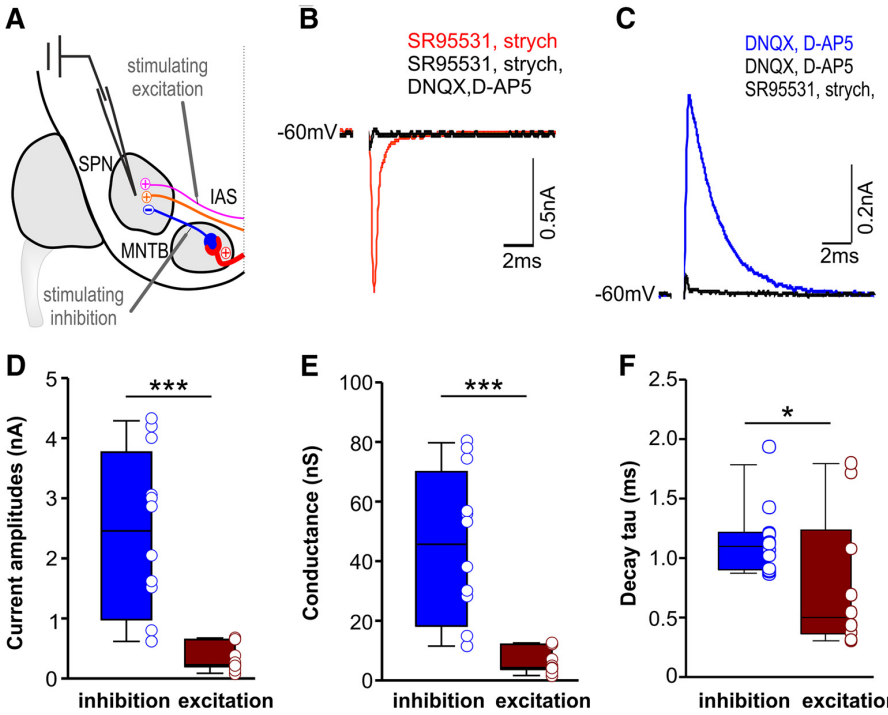


**Figure 5.** Comparison of synaptic strength between EPSCs and IPSCs in SPN neurons. ***A***, Schematic of the sound-offset encoding circuit depicting the positions of the stimulating electrodes for eliciting either excitation or inhibition. ***B***, ***C***, Voltage-clamp traces of pharmacologically isolated EPSCs (***B***) evoked by stimulating IAS and IPSCs (***C***) evoked by stimulating MNTB (average of 10 traces). Black traces indicate the blockade of (***B***) EPSCs or (***C***) IPSCs. ***D***, Average IPSC (blue) and EPSC (red) amplitudes measured in response to maximum stimulation. ***E***, EPSCs and IPSCs expressed as conductance reveals that mean IPSG values are more than five times larger than EPSGs. ***F***, Average decay time constants ($\tau$) of EPSCs and IPSCs. $Tau_{IPSC}$ is significantly slower than $Tau_{EPSC}$. ***$p \leq 0.001$.

the offset response following sound cessation (5.64 ± 1.0 ms; two-tailed paired *t* test: $p = 0.188$; $t = 1.458$; df = 7; Fig. 4*E*), indicating a high speed in generating offset responses despite the additional synaptic delay arising during the sign conversion in the MNTB. Jitter as a measure of the temporal precision of the first spike in the response was also not significantly different between the peristimulus (0.64 ± 0.17 ms) and the poststimulus (1.45 ± 0.35 ms) response (two-tailed paired *t* test: $p = 0.111$; $t = 1.822$; df = 7; Fig. 4*F*). The mean latency of ~4 ms for the peristimulus response is similar to that of other SOC neurons in mouse (Kopp-Scheinpflug et al., 2008). Although the average temporal response pattern of the ON-OFF type neurons shows a primary-like pattern (Fig. 2*G*), 5/8 ON-OFF type neurons show onset firing patterns. To investigate whether primary-like or onset-responses can influence the offset response, *in vivo* recordings of spikes do not provide sufficient information about possible subthreshold activity that lasts throughout the stimulation, which will more appropriately be measured by whole-cell patch-clamp recordings *in vitro*.

### Strength of inhibition outweighs excitation in SPN neurons

Whole-cell patch-clamp recordings *in vitro* were made of SPN neurons. Neurons had resting membrane potentials of −61.74 ± 0.79 mV, an average input resistance of 74.39 ± 10.94 MΩ and an average membrane capacitance of 65.63 ± 7.78 pF ($n = 23$). Glutamatergic EPSCs were regularly activated in neurons throughout the SPN. For electrical stimulation, a concentric stimulating electrode was placed on the intermediate acoustic stria (IAS) medial to the SPN and just dorsal to the MNTB (Fig. 5*A*). EPSCs were pharmacologically isolated by adding the $GABA_A$ receptor blocker SR95531 (20 μM) and the glycine receptor blocker strychnine (1 μM) to the bath solution (Fig. 5*B*). Glycinergic IPSCs were evoked by direct electrical stimulation of the ipsilateral MNTB using a concentric stimulating electrode and were pharmacologically isolated by adding the AMPAR blocker 6,7-dinitroquinoxaline-2,3-dione (DNQX; 10 μM) and the NMDAR blocker D-2-amino-5-phosphonopentanoic acid (D-AP5; 50 μM) to the bath solution (Fig. 5*C*). At physiologic holding voltages near the neurons resting membrane potential (−60 mV), IPSC amplitudes were significantly larger than EPSCs (IPSC: 2.46; 0.98/3.77; $n = 12$; EPSC: 0.23; 0.20/0.65; $n = 11$; Mann–Whitney rank-sum test: $p \leq 0.001$; Fig. 5*D*). The considerable difference between the strength of excitation and that of inhibition was even more obvious when both were expressed as conductances (IPSG: 45.65; 18.22/70.02; $n = 12$; EPSG: 4.26; 3.72/12.08; $n = 11$; Mann–Whitney rank-sum test: $p \leq 0.001$; Fig. 5*E*). The decay time constants of IPSCs were significantly slower than that of EPSCs ($Tau_{IPSC}$: 1.09; 0.90/

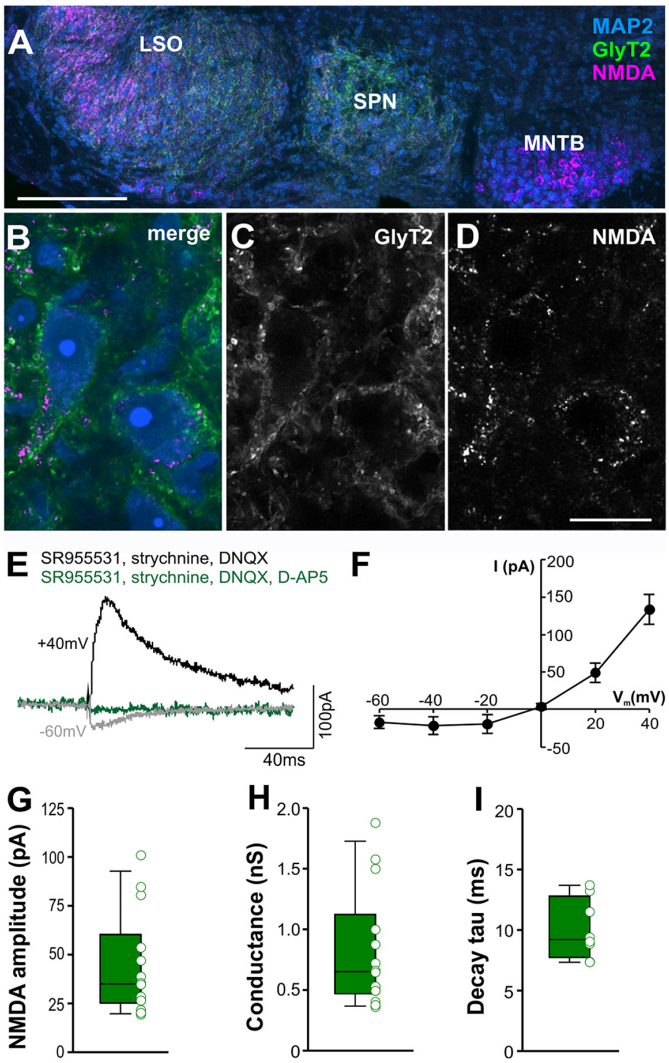


**Figure 6.** SPN neurons express NMDARs which mediate moderate EPSCs at depolarized voltages. ***A***, Low-power image of SOC showing NMDA immunoreactivity (magenta), which was strong in the MNTB and the lateral superior olive (LSO), and to a lesser degree present in the SPN. GlyT2 labeling (green) identifies the outline of the SPN. MAP2 (blue) was used as a neuronal marker. ***B–D***, Higher magnification images show that NMDARs are present in SPN neurons. ***E***, Voltage-clamp traces of pharmacologically isolated NMDA currents at −60 mV (gray) and at +40 mV (black). Currents were blocked by D-AP5 (green). ***F***, Average NMDA currents show the typical nonlinearity due to the $Mg^{2+}$ block at hyperpolarized membrane voltages. ***G***, Amplitude of NMDA currents at +40 mV. ***H***, NMDA conductance. ***I***, Decay time constants ($\tau$) of NMDA currents at +40 mV. Scale bars = 200 $\mu$m (***A***) and 20 $\mu$m (***B–D***).

1.21; $n$ = 12; $Tau_{EPSC}$: 0.49; 0.36/1.24; $n$ = 11; Mann–Whitney rank-sum test: $p$ = 0.038; Fig. 5*F*).

### NMDAR-mediated currents are present in SPN neurons

Glutamate released from excitatory synaptic inputs typically activates AMPAR and/or NMDAR with fast and slow kinetics, respectively. Current-clamp recordings of SPN neurons near the neuronal resting potential suggested that excitatory responses are primarily mediated by AMPARs (Felix and Magnusson, 2016). Here, we used immunocytochemistry to probe for the presence of NMDARs and performed voltage-clamp recordings to assess the strength of NMDAR-mediated currents at different membrane potentials. NMDAR expression is evident in mature SPN neurons, although weaker compared to neurons in the MNTB or LSO (Fig. 6*A–D*). Electrophysiological measurement of NMDA currents in whole-cell voltage-clamp mode revealed the characteristic voltage dependence causing larger currents once the membrane voltage reaches depolarized values (Fig. 6*E*,*F*) and showed that they were sensitive to the NMDAR antagonist D-AP5 (Fig. 6*E*). NMDA currents in SPN neurons (35.0pA; 25.2/60.3pA; $n$ = 14; Fig. 6*G*) were smaller than in MNTB

(Steinert et al., 2010), but similar to LSO (Alamilla and Gillespie, 2011; Pilati et al., 2016) and MSO (Smith et al., 2000; Couchman et al., 2012). NMDA conductances calculated from these currents ranged from 0.36 to 1.88 nS (0.65; 0.47/1.12 nS; $n = 14$). The small, yet prevalent NMDA currents resemble the general decline of NMDA currents in the auditory brainstem following hearing onset. However, as Steinert and colleagues have shown for neurons in the neighboring MNTB, after the initial reduction in amplitudes, NMDA currents reach a steady state with no signs of further decline after about two weeks of age (Steinert et al., 2010), corroborating the presence of NMDA current in the SPN for ages of 15 d and older. Decay time constants of the NMDAR-mediated EPSCs ranged from 7.34 to 13.69 ms (9.21 ms; 7.74/12.79 ms; $n = 8$; Fig. 5*H*). In later experiments AMPAR and NMDAR responses will be activated and blocked in unison by a cocktail of DNQX/D-AP5 and together will be contrasted against glycinergic inhibition to reveal the contribution of excitation to ON-OFF type SPN neurons.

### Differential short-term plasticity between excitatory and inhibitory SPN synapses

To test for a balance between excitatory and inhibitory inputs in an adapted, more physiologic state, pharmacologically or electrically isolated inhibitory, excitatory and NMDAR-mediated synaptic currents were evoked in SPN neurons by applying 50-pulse fiber stimulation trains at 100 Hz (Fig. 7*A*). Since NMDAR-mediated currents can only be activated at depolarizing potentials positive to the EPSC reversal potential, they are shown as outward currents in the green trace in Figure 7*A*. For better visualization NMDA currents are flipped in the superimposed enlargement of all three current types for the first 100 ms of the response (Fig. 7*B*). Both fast inhibitory and excitatory currents showed pronounced short-term depression, calculated from a train of IPSCs and EPSCs, respectively, and normalized to the first peak (Fig. 7*C*,*D*). In contrast NMDAR-mediated currents showed very little depression (Fig. 7*C*,*D*). The time constant of depression was fastest for EPSCs (1.92 ms; 1.41/2.39 ms; $n = 9$), a little slower in IPSCs (2.88 ms; 2.53/3.23 ms; $n = 17$) and very slow in NMDAR-mediated currents (10.31 ms; 4.01/16.45 ms; $n = 5$; Kruskal–Wallis ANOVA on ranks followed by Dunn's multiple comparisons; $p \leq 0.001$; Fig. 7*E*). The average level of steady state depression was similar between EPSCs and IPCSs, but significantly lower in in NMDAR-mediated currents (inhibition: 66.70%; 62.57/72.05%; $n = 17$; excitation: 74.03%; 71.54/81.42%; $n = 9$; NMDA: 42.36%; 25.87/55.40%; $n = 5$; Kruskal–Wallis ANOVA on ranks followed by Dunn's multiple comparisons; $p \leq 0.001$; Fig. 7*F*).

Across the SPN, IPSCs were always larger than EPSCs. The position of each recorded neuron within the SPN was logged by taking a picture of the electrode position in 4× magnification. The SPN was then divided into 4 quadrants, which were correlated to the size of the currents. No correlation was found, suggesting a homogeneous distribution of excitatory inputs across the SPN with no distinct, spatially segregated subpopulations. The moderate, excitatory inputs to SPN neurons become visible as patterns of increased firing activity during sound presentation in about half of the offset-responding SPN neurons. The fact that these neurons have peristimulus as well as poststimulus responses raises new questions: do glutamatergic inputs, that drive peristimulus excitatory responses, interact with peristimulus inhibitory inputs that drive the poststimulus offset response, and if so, what is their impact on the offset response? To specifically address the role of NMDAR-mediated currents, compared to AMPAR-mediated currents, we fed the data acquired by voltage-clamp recording into a computational model to simulate both types of excitatory synapses and the inhibitory inputs to an SPN neuron.

### Computational modeling suggests that moderate and slow excitation affects offset-response latency

A basic Hodgkin–Huxley model of SPN neuron firing was developed to test the effect of excitatory inputs of variable strength that are present in addition to inhibitory inputs. All synaptic conductances used for the following simulations were taken from the results presented in Figures 5–7. Conductance evoked by a single pulse, the synaptic depression during trains of synaptic stimulation and the duration of the stimulus train were taken into consideration while determining the range of conductances to be used in the model. Inhibitory conductances, recorded *in vitro* after a single pulse ranged from 11.5 to 80.5 nS with a median of 45 nS. We estimated the synaptic depression during a 100-Hz stimulation for 100 ms to be around 50%, resulting in a conductance of 41 nS (50% of 80.5 nS). For longer stimulation of 500 ms, a steady state depression estimated at 64%, results in minimal possible conductance values of 3.9 nS (64% of 11.5 nS). This is approximately the value where the inhibition becomes strong enough to generate a rebound spike in the model depicted in Figure 8*E*. Excitatory conductances were subjected to a similar approach, with minimum experimentally acquired excitatory conductances of 0.4 nS (minimal measured value with maximum depression) to 12.6 nS (maximal measured value with no depression). For NMDA currents, the range between the minimal measured value with maximum depression and maximum measured value with no depression was 0.3–1.9 nS. However, since NMDA currents depress only little and even initially facilitate (Fig. 7*C*,*D*), an average of 11% facilitation was added to the maximum measured value, providing an NMDA conductance of 2.1 nS. The values from *in vitro* experiments might be underestimating the synaptic conductances, as axons will be cut during the slicing procedure. To account for this caveat, we take advantage of the model to simulate a broader range of conductances. These physiologically feasible core conductances for inhibition, excitation and NMDA are covered in the matrices in Figure 8*E*,*F*. When using an inhibition-only model (Kopp-Scheinpflug et al., 2011) with adapting inputs, SPN neurons reliably fired a burst of offset responses following a 100-ms train of IPSCs presented at 100 Hz (Fig. 8*A*). The original model was amended in the full model by adding adapting AMPAR-mediated and NMDAR-mediated currents (Fig. 8*B*). This

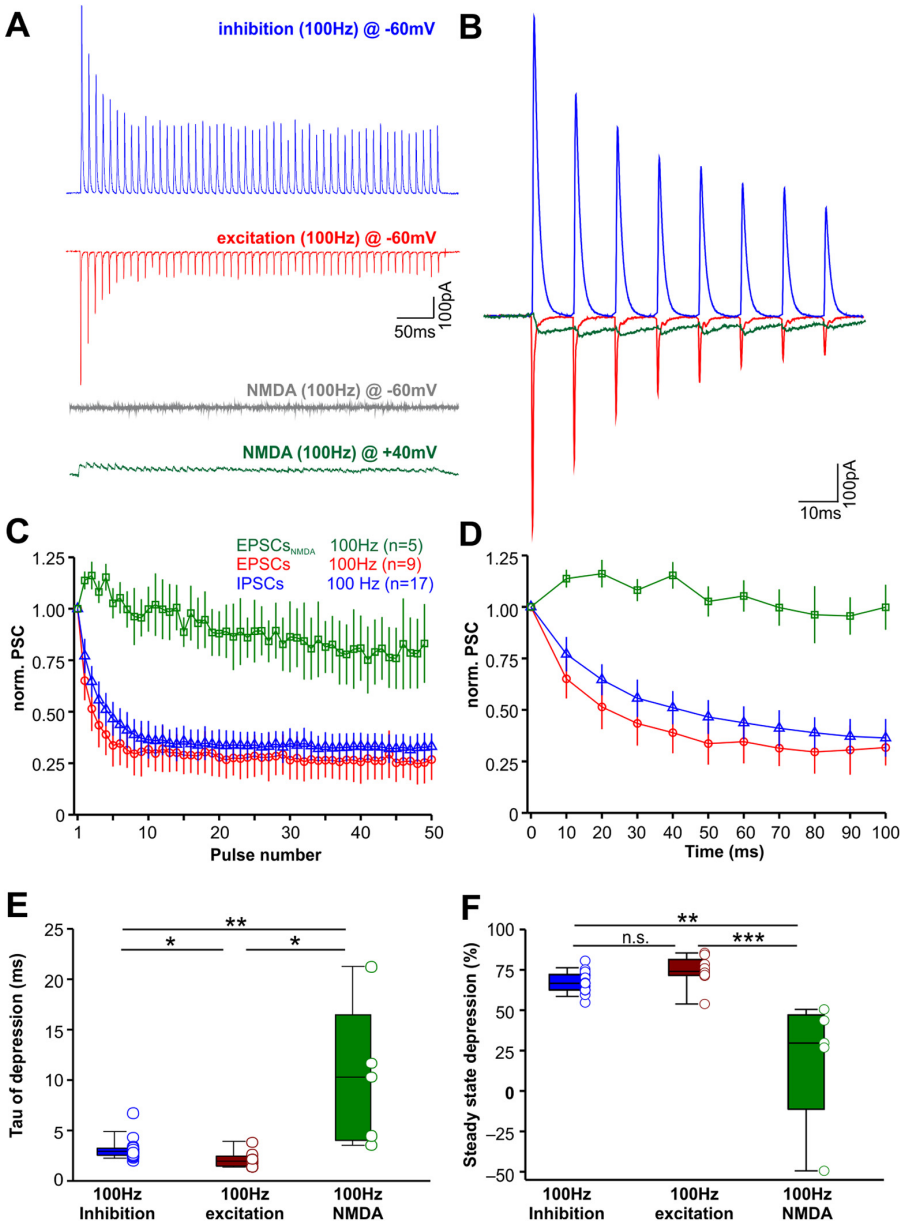


**Figure 7.** Short-term plasticity of excitatory and inhibitory inputs to SPN neurons. ***A***, Examples of inhibitory (blue), excitatory (red), and NMDAR (green)-mediated responses to 50 stimulations at 100 Hz (averages of 10 repetitions). Gray trace depicts the lacking NMDAR mediated response at −60 mV. ***B***, Overlaid and magnified first responses of the examples shown in ***A***. The NMDA trace (green) has been flipped to symbolize its excitatory nature. ***C***, Normalized and averaged current amplitudes to each of the 50 pulses of the 100-Hz train for NMDA currents (green), EPSCs (red), and IPSCs (blue). ***D***, First 100 ms of the plots shown in ***C***. ***E***, Time constant ($\tau$) of the rate of depression acquired from fitting exponential decay functions to the functions shown in ***C***. ***F***, Summary of synaptic currents steady-state depression: 100% − (average current amplitudes in response to the last five pulses ∗ 100). $*p \leq 0.05$, $**p \leq 0.01$, $***p \leq 0.001$, n.s. = non-significant.

model, now including inhibition and excitation, caused neurons to fire spikes not only at the end of the stimulus train but also at the onset of stimulation (Fig. 8*B*). Comparing the offset responses elicited by either model revealed that the model incorporating excitation (Fig. 8*C*, full model) generated shorter offset-response latencies. Adding stochastic noise to either model introduced a jitter to the offset-response latencies (Fig. 8*D*). However, the average latencies for the full model (7.55 ± 0.36 ms) were still shorter compared to the inhibition only model (9.12 ± 0.33 ms) by 1.57 ms (two-tailed *t* test: $p = 0.0012$; $t = 3.245$; *DF*: 998; Fig. 8*D*, red and blue vertical lines).

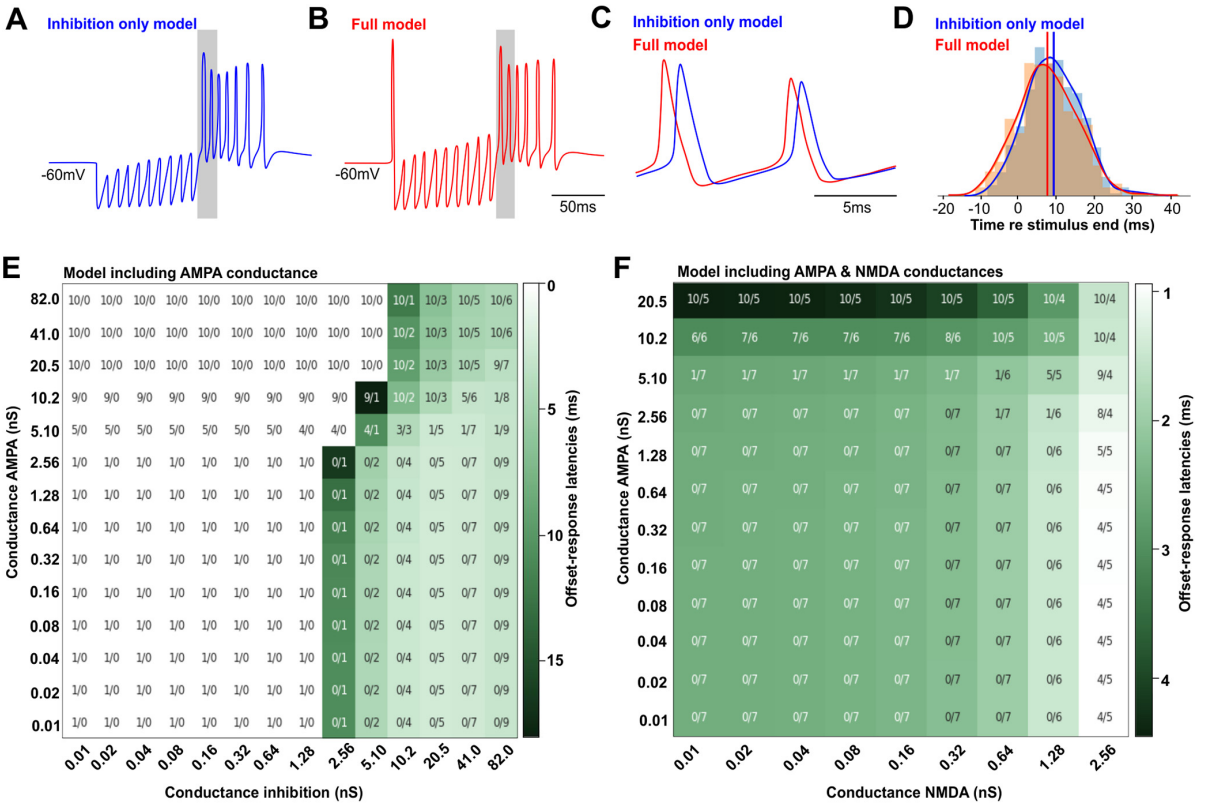


**Figure 8.** Excitatory input modulates offset-response timing in a computational model of SPN neurons. ***A***, Voltage trace of a SPN neuron's response to a train of 10 stimuli using an inhibition only model shows 10 IPSPs followed by a burst of spikes at stimulus offset. ***B***, Voltage trace of a SPN neuron's response to a train of 10 stimuli using the amended "full" model including AMPAR-mediated and NMDAR-mediated excitation shows a spike at stimulus onset followed by 10 IPSPs and then by a burst of spikes at stimulus offset. ***C***, Larger temporal resolution of the first two action potentials of the offset response (gray shaded area in ***A***, ***B***). ***D***, Distributions of offset-response latencies for the inhibition only model (blue) and the full model (red) for 500 repetitions when stochastic noise was added. The red and blue solid lines represent the mean offset latencies for the full and inhibition only model, respectively. ***E***, Heat map showing changes in offset-response latencies in relation to the strength of inhibition (*x*-axis) and AMPAR-mediated excitation (*y*-axis). The first number for each stimulus combination depicts the number of peristimulus spikes followed by the number of poststimulus spikes in the offset response. Darker green stands for longer latencies and lighter green for shorter latencies. ***F***, Heat map showing changes in offset-response latencies in relation to the strength of AMPAR-mediated responses (*y*-axis) and NMDAR-mediated responses (*x*-axis). Numbers and color code are the same as in ***E***. White areas in ***E*** specify stimulus combinations that do not generate offset responses.

To assess how the balance between excitation and inhibition affects offset-response latencies, both conductances were independently varied in strength and the corresponding changes in latencies shown in a heat map (Fig. 8*E*; model including AMPA currents). Specific combinations elicited both onset and offset responses and were thus most comparable to the ON-OFF type neuronal responses *in vivo*, while in most cases no onset response was generated. Comparing the offset-response latencies for vertical columns of a specific inhibitory conductance (e.g., 41 nS in Fig. 8*E*) and increasing AMPA conductances revealed that varying the AMPA conductance alone mediates the spike at stimulus onset, but did not significantly shorten the latencies of spikes in the offset-response (Fig. 8*E*). On the contrary, increasing the AMPA response beyond the physiologic estimates will prolong the offset-response latencies due to the occurrence of peristimulus spikes that interfere with the refractory period of the offset-response spikes. The shortest offset-response latencies were obtained with a combination of strong inhibition (41 nS) coupled with both AMPA and NMDA conductances (Fig. 8*F*). In the latter condition, varying the AMPA conductance between 0 and 2.56 nS (*y*-axis) did not change the offset-response latency. However, increasing the NMDA conductance (*x*-axis) for any of these AMPA conductances increasingly shortened the offset-response latency. Increasing the AMPA conductance further (≥5.1 nS), caused continuous peristimulus spike firing which then prolonged offset-response latencies due to refractory interactions. A combination of inhibition and NMDA conductance alone did not have an effect on offset-response latencies (data not shown).

These simulations suggest that although offset responses can be generated by exclusively activating the chloride conductance, the slow NMDA conductance that accompanies fast AMPA-mediated responses serve to

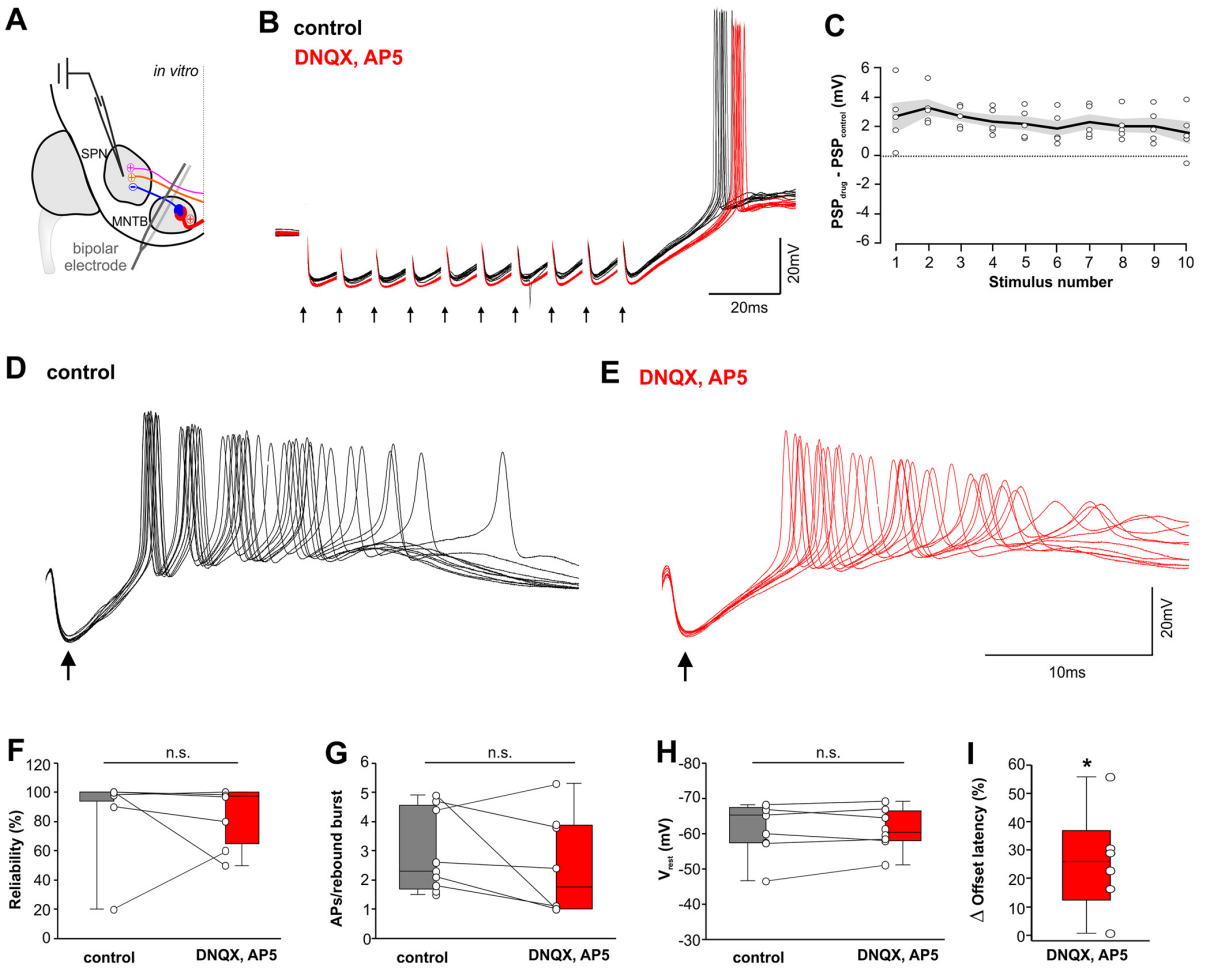


**Figure 9.** Excitation improves offset-response timing. ***A***, Schematic sound-offset circuit depicting the position of the fork-electrode for simultaneously stimulating excitation and inhibition. ***B***, 100-Hz synaptic stimulation (black arrows) elicited an offset response in control (black) and during blockade of excitation (red). Stimulus artifacts are removed for clarity. Postsynaptic potentials were more depolarized in control (black). ***C***, Average difference in amplitudes of PSPs (not spikes) between blockade of excitation and control was plotted against stimulus number within each train (circles are averages of 10 trials/cell; $n = 5$ cells). Black line and gray-shaded area represent mean ± SEM. ***D***, ***E***, Higher temporal resolution of the offset responses of the cell shown before (***D***) and after (***E***) the blockade of excitation. ***F***, Reliability of offset responses in 10 consecutive traces (as shown in ***D***, ***E***; 100%: at least one rebound spike/trace); $n = 9$. ***G***, Average number of rebound spikes (10 trials; $n = 9$). ***H***, Resting membrane potential averaged over 10 ms before the start of synaptic stimulations ($n = 9$). ***I***, Normalized increase in offset-response latencies after blocking excitation ($n = 6$). $*p \leq 0.05$, n.s. = non-significant.

accelerate the offset response. Overall, a longer EPSC decay time results in a shorter latency, as the effect of the excitation is carried forward into the rebound, providing additional excitatory drive. We found that the shortest offset-response latency was generated with simulated EPSC decay time constants of 30 ms, but even EPSC decay times of 10 ms accelerate the offset response.

### Simultaneous activation of excitation and inhibition *in vitro* results in a reduced net hyperpolarization of PSPs and shorter offset-response latencies

Excitatory inputs to SPN neurons are not a prerequisite for generating offset responses (Kopp-Scheinpflug et al., 2011). However, computational modeling (Fig. 8) suggests that excitation might shape the temporal precision of the offset responses. Here we compared synaptically evoked offset responses in SPN neurons in control condition and during blockade of excitatory inputs by simultaneously stimulating both the MNTB and IAS using a fork-like bipolar stimulating electrode (Fig. 9*A*). At the end of a 100 ms, 100-Hz train of stimuli, SPN neurons reliably generated an offset response consisting of a burst of spikes (Fig. 9*B*). The blockade of glutamatergic transmission during 100-Hz stimulation for 100 ms (Fig. 9*B*, red trace) caused a hyperpolarizing drop in the net amplitude of the evoked PSPs (Fig. 9*B*). In control condition, the stimulation of synaptic input triggered a combined response of excitation and inhibition resulting in a net hy-

perpolarization of −80.9 ± 0.3 mV ($n$ = 5) averaged over the stimulus train. However, blocking excitation caused the PSPs to drop by 2.6 ± 0.1 mV ($n$ = 5) toward more hyperpolarizing voltages (Fig. 9*B*,*C*). The voltage difference between drug and control condition revealed a small, yet sustained depolarizing drive over the whole stimulus time (Fig. 9*C*), consistent with our simulations which predicted the presence of a small, slow excitatory conductance which extends into the temporal window of the offset response.

Blockade of excitatory inputs (only the last IPSPs of the trains shown in Fig. 9*D*,*E*) did not significantly change the reliability of generating an offset response: in 10 consecutive input trains, offset bursts were generated in 90 ± 9% of trains in controls and 86 ± 7% of trains during blockade of excitation (Mann–Whitney rank-sum test: $p$ = 0.551; Fig. 9*F*). The number of spikes within each burst of the offset response was also not significantly different between the control condition (2.30; 1.7/4.6; $n$ = 9) and following the blockade of excitation (1.75; 1.0/3.8; $n$ = 8; Mann–Whitney rank-sum test: $p$ = 0.359; Fig. 9*G*). To probe whether tonically active excitation is present in the SPN, we compared the resting membrane potential in absence of synaptic stimulation before and during blockade of excitation, but no significant difference was found ($V_{rest}$control: −61.8 ± 2.4 mV; $V_{rest}$drug: −61.1 ± 2.0 mV; two-tailed $t$ test: $p$ = 0.832; $t$ = 0.215; df = 15; Fig. 9*H*). Functionally, the blockade of excitation caused longer offset-response latencies. Depending on the exact positioning of the stimulating electrode and patch pipette in each *in vitro* preparation, the latencies of synaptically-evoked offset-responses varied between cells from 5.6 to 68.5 ms (control) and from 7.2 to 84.2 ms (DNQX/AP5). However, each paired recording showed an increase in latency during blockade of excitation and resulted in a significant increase of 30.68 ± 6.71% in offset-response latency when excitation was blocked (two-tailed paired $t$ test: $p$ = 0.01; $t$ = −4.571; df = 4; Fig. 9*I*).

In conclusion, our data show that the right balance of moderate, slow excitation and strong inhibition will accelerate acoustically-evoked offset responses. Besides this faster offset firing, the presence of additional excitation also significantly reduces intensity-dependent changes in response latency. Based on the distributions of synaptic inputs within the SPN, similar CFs, thresholds and spontaneous rates between neurons with ON-OFF type and OFF-only type responses, we conclude that the different response patterns are not arising from two different types of neurons but rather reflect differences in the balance of excitation and inhibition.

## Discussion

SPN neurons are reliable detectors of sound offsets and respond with a burst of spikes time-locked to the end of the stimulus. The latencies of these offset responses are short and level-invariant over a large range of suprathreshold sound intensities, which are prerequisites for sound-duration encoding and gap-detection (Forrest and Green, 1987; Brand et al., 2000; Faure et al., 2003; Pérez-González et al., 2006). For half of the neurons with offset responses, additional excitatory inputs were observed in *in vivo* recordings. These neurons exhibited even shorter offset-response latencies and stronger level invariance of less than 10 μs/dB. Pharmacological manipulation and computational modeling showed that while inhibition alone can reliably trigger a post-inhibitory rebound response at stimulus offset; excitation alone will not generate an offset response. However, the presence of slow, NMDAR-mediated excitation facilitates the rebound depolarization and speeds up the latencies of offset responses.

### Why don't all SPN offset cells show peristimulus excitation?

Shorter latencies and greater resistance to level dependent latency shifts due to additional excitation provide advantages for computation of sound duration and for detection of silent gaps in noise. So why do not all SPN neurons with offset responses benefit from this advantage? Our immunocytochemical data (Fig. 1) show uniform distributions of excitatory and inhibitory inputs throughout the SPN, suggesting that the observed differences in the strength of excitation and inhibition between ON-OFF type and OFF-only type neurons may not manifest in different synaptic input patterns. This is in agreement with the lack of differences in CFs, spontaneous rates or thresholds between ON-OFF type and OFF-only type neurons. Whether or not neurons in the SPN could be classified into distinct subpopulation has been discussed for 40 years. Ollo and Schwartz (1979) used Golgi impregnations to assess the morphology of mouse SPN neurons. They described slight morphologic differences such as triangular, elongated or polygonal shapes, but stated that these were "not sufficiently distinct to warrant division into different cell types." More complex approaches combined the morphologic description with either immunostaining for the neurotransmitter used by SPN neurons (Helfert et al., 1989) or with neural tracing experiments (Schofield, 1991). As a result five SPN cell types that project to the ipsilateral inferior colliculus (IC) were described: (1) large round glycinergic neurons, (2) large round GABAergic neurons, (3) small, round, projecting bilaterally to IC glycine-negative neurons, (4) small neurons with only ipsilateral IC projections, (5) small neurons with ipsilateral IC and contralateral cochlear nucleus projections (Helfert et al., 1989; Schofield, 1991). Another approach to classify SPN neurons was taken by Felix and co-authors, who reported only subtle differences in the intrinsic properties of SPN neurons and suggested that these might be caused by gradients of potassium currents (Felix et al., 2013). Whether or not the bursting cells in the dorsolateral SPN region can form a particular subtype or are still subject to developmental change is not yet clear. In conclusion, the occurrence of ON-OFF type responses in a subset of SPN offset cells could be the result of differences in the balance of existing excitatory and inhibitory inputs. Previous studies have shown that the assessment of the excitatory-inhibitory balance might be confounded through the use of anesthetics which either block NMDA currents (ketamine-based anesthesia) or alter inhibition

(barbiturate based anesthesia) (Steinert et al., 2008; Felix et al., 2012). Here, we used a fentanyl-based anesthesia, which binds $\mu$-opioid receptors and therefore should not directly interfere with either excitation or inhibition in the auditory brainstem.

We conclude that the occurrence of ON-OFF type and OFF-only type neurons in SPN is neither a developmental nor an experimental (anesthesia-based) effect. Instead, ON-OFF or OFF-only responses in SPN neurons are likely caused by differences in the strength of excitation and inhibition whose activity- or context-dependent control will have to be investigated to further our knowledge on encoding sound offsets.

### Facilitating the post-inhibitory rebound

The excitatory input alone does not generate offset action potentials, yet it is sufficient to modify the offset responses generated via a post-inhibitory rebound mechanism (Felix et al., 2011; Kopp-Scheinpflug et al., 2011). A subthreshold inhibitory input aiding a subthreshold excitatory input to increase temporal precision is generally referred to as post-inhibitory facilitation and has been shown in other SOC neuron types (Dodla et al., 2006; Beiderbeck et al., 2018). This is not the case in our present SPN data, since here the inhibitory input on its own is sufficient to generate offset spikes. However, the slower time course of the additional excitation mediated via NMDARs allows it to extend its depolarization into the temporal window of the post-inhibitory rebound just enough to accelerate the offset response. Such an extension of excitation into the post-inhibitory rebound would require sustained excitatory responses throughout the duration of the stimulus. The fact that the peristimulus excitatory responses observed in the ON-OFF type neurons *in vivo* occur as either sustained (38%) or onset (62%) responses is likely due to most of the excitatory inputs being subthreshold caused by dominant inhibition during sound presentation, rendering subthreshold EPSPs invisible to our single cell extracellular assessment of spiking. Such subthreshold, peristimulus excitation was demonstrated by pharmacological blockade of inhibition *in vivo* (Kulesza et al., 2007). Based on these previous findings and our present results, it seems likely that, at least part of the peristimulus excitatory inputs are subthreshold and may serve modulatory functions rather than to form a reliable representation of sound onset. This would be in agreement with the suggestion that sound onsets and offsets are encoded in segregated pathways within the auditory brain (Scholl et al., 2010; Anderson and Linden, 2016; Kopp-Scheinpflug et al., 2018; Sollini et al., 2018). While the SPN strongly qualifies for encoding offsets, sound onset information is likely provided by different neuronal pathways such as for example the ventral nucleus of the lateral lemniscus.

The behaviorally relevant readout in the present data set is the reduction in offset-response latencies, which can decrease gap-detection thresholds (Yassin et al., 2014). The slow, lasting excitation responsible for the faster offsets, could represent the underlying cellular equivalent to adding background noise in a behavioral gap detection task, where gap detection thresholds have been significantly decreased (better), compared with a condition when no background noise was provided (Horwitz et al., 2011).

However, faster is not always better, especially when temporal precision (as measured by jitter) is equally good. An alternative interpretation is that the modulation of offset-response latencies might present a tool to accelerate or delay the time point of the offset response depending on the balance between excitation and inhibition. Such a shift in latency could present a homeostatic adaptation to a changing balance between excitation and inhibition as might occur during aging or following acoustic trauma.

### Reducing the level dependency of the offset response

The offset-response latency depends on sufficient hyperpolarization and acceleration of the membrane time constant via recruiting additional ionic conductances such as $I_H$ (Kopp-Scheinpflug et al., 2011). Hyperpolarization of the membrane activates $I_H$, which accelerates of the membrane time constant and shortens the offset-response latency. If, however, $I_H$ is already maximally activated by hyperpolarization of the membrane, any further hyperpolarization might prolong the offset-response latency as it takes the membrane longer to move from –100 mV (SPN IPSP reversal potential) to + 40 mV (sodium channel activation voltage) than for example from –80 to +40 mV. This is likely what happens with the trend of increasing offset-response latencies with increasing intensity seen in Figure 3*A*,*B*. At higher sound intensities, multiple MNTB axons will be recruited and due to input summation, the net-depression of inhibitory inputs in SPN neurons will be reduced, resulting in strong hyperpolarization of the membrane voltage even at the end of the stimulus train. The recruitment of additional excitatory conductances as observed in the present study only at higher stimulus intensities is likely to have a similar effect as $I_H$, in shunting the inhibition, providing a depolarizing drive and shortening the offset-response latencies.

In contrast, at lower sound intensities only few MNTB axons might be recruited to inhibit SPN neurons. These inhibitory inputs will depress over time as shown for the SPN in this study or for the LSO and MSO in other studies (Couchman et al., 2010; Walcher et al., 2011; Roberts et al., 2014) and an offset response is generated at the time point when the intrinsic depolarizing drive dominates the hyperpolarization. In the experimental *in vitro* condition, especially for long stimulations of several hundred milliseconds, this can lead to rebound responses even before the end of the stimulus train (unpublished observations). *In vivo*, such rebound response before the end of a sound was never observed, suggesting that *in vivo* the depression of collective inhibitory inputs is low and the hyperpolarization at the stimulus end is strong.

### Implications of level-invariant offset responses for gap-detection and sound-duration encoding

The threshold for detecting brief silent gaps in noise provides a valuable analytical tool to measure temporal

resolution in auditory processing (Moore, 1997). Gaps as short as 2–3 ms can be detected by humans (Penner, 1977) and rodents (Ison, 1982) and it has been suggested that to detect a 3-ms gap, auditory neurons need to encode onsets and offsets of sounds with a temporal acuity of ~1 ms (Oertel et al., 2017). Gap-in-noise stimuli have also proven very helpful in determining the ability of the auditory system to encode sound offsets as a parameter independent of sound onsets (Pratt et al., 2005).

Behaviorally, sound offsets are an important cue for sound-duration encoding. Neurons in the auditory midbrain that are sensitive to sound duration act as coincidence detectors that only fire action potentials if excitatory postsynaptic responses evoked by the onset of sound temporally coincide with excitatory postsynaptic responses evoked by the offset of sound (Casseday et al., 1994; Aubie et al., 2009, 2012, 2014; Sayegh et al., 2011; ). Duration sensitive neurons have been classified according to their ability to preferably encode sounds of different durations and are referred to as short-pass, bandpass and long-pass duration tuned neurons. According to the current models of sound-duration encoding, offset excitation is needed in the coincidence detection bandpass mechanism but not in the anti-coincidence detection short-pass mechanism (Aubie et al., 2012). This is in agreement with previous results showing that temporally precise SPN offset responses vary with stimulus duration and provide an inhibitory projection to the auditory midbrain (Kadner et al., 2006; Kopp-Scheinpflug et al., 2011) where they are suggested to generate a post-inhibitory rebound excitation (Pollak et al., 2011). Interestingly, both the detection of gaps (Moore, 1997) and the discrimination of different sound durations (Klink and Klump, 2004) are relatively independent of changes in suprathreshold sound level. Especially the duration discrimination of longer sounds (>50 ms) has been reported to not show an intensity effect (Henry, 1948). The level-independence and short latency of SPN offset responses over an extremely large range of intensities as shown in the present study provide a perfect function for the ON-OFF type SPN neurons in the encoding of longer sound durations. Deficits in SPN offset encoding might therefore result in difficulties in processing sound offsets in downstream auditory areas like the IC or the MGB (Anderson and Linden, 2016).

## References


Alamilla J, Gillespie DC (2011) Glutamatergic inputs and glutamate-releasing immature inhibitory inputs activate a shared postsynaptic receptor population in lateral superior olive. Neuroscience 196: 285–296.

Anderson LA, Linden JF (2016) Mind the gap: two dissociable mechanisms of temporal processing in the auditory system. J Neurosci 36:1977–1995.

Aubie B, Becker S, Faure PA (2009) Computational models of millisecond level duration tuning in neural circuits. J Neurosci 29: 9255–9270.

Aubie B, Sayegh R, Faure PA (2012) Duration tuning across vertebrates. J Neurosci 32:6373–6390.

Aubie B, Sayegh R, Fremouw T, Covey E, Faure PA (2014) Decoding stimulus duration from neural responses in the auditory midbrain. J Neurophysiol 112:2432–2445.

Banks MI, Smith PH (1992) Intracellular recordings from neurobiotin-labeled cells in brain slices of the rat medial nucleus of the trapezoid body. J Neurosci 12:2819–2837.

Behrend O, Brand A, Kapfer C, Grothe B (2002) Auditory response properties in the superior paraolivary nucleus of the gerbil. J Neurophysiol 87:2915–2928.

Beiderbeck B, Myoga MH, Müller NIC, Callan AR, Friauf E, Grothe B, Pecka M (2018) Precisely timed inhibition facilitates action potential firing for spatial coding in the auditory brainstem. Nat Commun 9:1771.

Brand A, Urban R, Grothe B (2000) Duration tuning in the mouse auditory midbrain. J Neurophysiol 84:1790–1799.

Casseday JH, Ehrlich D, Covey E (1994) Neural tuning for sound duration: role of inhibitory mechanisms in the inferior colliculus. Science 264:847–850.

Cavaco S, Lewicki MS (2007) Statistical modeling of intrinsic structures in impacts sounds. J Acoust Soc Am 121:3558–3568.

Couchman K, Grothe B, Felmy F (2010) Medial superior olivary neurons receive surprisingly few excitatory and inhibitory inputs with balanced strength and short-term dynamics. J Neurosci 30: 17111–17121.

Couchman K, Grothe B, Felmy F (2012) Functional localization of neurotransmitter receptors and synaptic inputs to mature neurons of the medial superior olive. J Neurophysiol 107:1186–1198.

Dehmel S, Kopp-Scheinpflug C, Dörrscheidt GJ, Rübsamen R (2002) Electrophysiological characterization of the superior paraolivary nucleus in the Mongolian gerbil. Hear Res 172:18–36.

Deneux T, Kempf A, Daret A, Ponsot E, Bathellier B (2016) Temporal asymmetries in auditory coding and perception reflect multi-layered nonlinearities. Nat Commun 7:12682.

Denève S, Machens CK (2016) Efficient codes and balanced networks. Nat Neurosci 19:375–382.

Dodla R, Svirskis G, Rinzel J (2006) Well-timed, brief inhibition can promote spiking: postinhibitory facilitation. J Neurophysiol 95: 2664–2677.

Eggermont JJ (2015) Auditory temporal processing and its disorders. New York: Oxford University Press.

Elgueda D, Duque D, Radtke-Schuller S, Yin P, David SV, Shamma SA, Fritz JB (2019) State-dependent encoding of sound and behavioral meaning in a tertiary region of the ferret auditory cortex. Nat Neurosci 22:447–459.

Faure PA, Fremouw T, Casseday JH, Covey E (2003) Temporal masking reveals properties of sound-evoked inhibition in duration-tuned neurons of the inferior colliculus. J Neurosci 23:3052–3065.

Felix RA 2nd, Fridberger A, Leijon S, Berrebi AS, Magnusson AK (2011) Sound rhythms are encoded by postinhibitory rebound spiking in the superior paraolivary nucleus. J Neurosci 31:12566–12578.

Felix RA 2nd, Kadner A, Berrebi AS (2012) Effects of ketamine on response properties of neurons in the superior paraolivary nucleus of the mouse. Neuroscience 201:307–319.

Felix RA 2nd, Vonderschen K, Berrebi AS, Magnusson AK (2013) Development of on-off spiking in superior paraolivary nucleus neurons of the mouse. J Neurophysiol 109:2691–2704.

Felix RA 2nd, Magnusson AK (2016) Development of excitatory synaptic transmission to the superior paraolivary and lateral superior olivary nuclei optimizes differential decoding strategies. Neuroscience 334:1–12.

Felix RA 2nd, Gourévitch B, Gómez-Álvarez M, Leijon SCM, Saldaña E, Magnusson AK (2017) Octopus cells in the posteroventral cochlear nucleus provide the main excitatory input to the superior paraolivary Nucleus. Front Neural Circuits 11:37.

Felix RA 2nd, Gourévitch B, Portfors CV (2018) Subcortical pathways: towards a better understanding of auditory disorders. Hear Res 362:48–60.

Forrest TG, Green DM (1987) Detection of partially filled gaps in noise and the temporal modulation transfer function. J Acoust Soc Am 82:1933–1943.

Gómez-Álvarez M, Gourévitch B, Felix RA 2nd, Nyberg T, Hernández-Montiel HL, Magnusson AK (2018) Temporal informa-

tion in tones, broadband noise, and natural vocalizations is conveyed by differential spiking responses in the superior paraolivary nucleus. Eur J Neurosci 48:2030–2049.
Grothe B (1994) Interaction of excitation and inhibition in processing of pure tone and amplitude-modulated stimuli in the medial superior olive of the mustached bat. J Neurophysiol 71:706–721.
Guinan JJ Jr, Guinan SS, Norris BE (1972) Single auditory units in the superior olivary complex I: responses to sounds and classifications based on physiological properties. Int J Neurosci 4:101–120.
Guzman SJ, Schlögl A, Schmidt-Hieber C (2014) Stimfit: quantifying electrophysiological data with Python. Front Neuroinform 8:16.
Helfert RH, Bonneau JM, Wenthold RJ, Altschuler RA (1989) GABA and glycine immunoreactivity in the guinea pig superior olivary complex. Brain Res 501:269–286.
Henry FM (1948) Discrimination of the duration of a sound. J Exp Psychol 38:734–743.
Hines ML, Carnevale NT (2001) NEURON: a tool for neuroscientists. Neuroscientist 7:123–135.
Horwitz AR, Ahlstrom JB, Dubno JR (2011) Level-dependent changes in detection of temporal gaps in noise markers by adults with normal and impaired hearing. J Acoust Soc Am 130:2928–2938.
Ison JR (1982) Temporal acuity in auditory function in the rat: reflex inhibition by brief gaps in noise. J Comp Physiol Psychol 96:945–954.
Jalabi W, Kopp-Scheinpflug C, Allen PD, Schiavon E, DiGiacomo RR, Forsythe ID, Maricich SM (2013) Sound localization ability and glycinergic innervation of the superior olivary complex persist after genetic deletion of the medial nucleus of the trapezoid body. J Neurosci 33:15044–15049.
Kadner A, Kulesza RJ Jr, Berrebi AS (2006) Neurons in the medial nucleus of the trapezoid body and superior paraolivary nucleus of the rat may play a role in sound duration coding. J Neurophysiol 95:1499–1508.
Kitzes LM, Gibson MM, Rose JE, Hind JE (1978) Initial discharge latency and threshold considerations for some neurons in cochlear nuclear complex of the cat. J Neurophysiol 41:1165–1182.
Klink KB, Klump GM (2004) Duration discrimination in the mouse (*Mus musculus*). J Comp Physiol A Neuroethol Sens Neural Behav Physiol 190:1039–1046.
Klug A, Khan A, Burger RM, Bauer EE, Hurley LM, Yang L, Grothe B, Halvorsen MB, Park TJ (2000) Latency as a function of intensity in auditory neurons: influences of central processing. Hear Res 148:107–123.
Kopp-Scheinpflug C, Tolnai S, Malmierca MS, Rübsamen R (2008) The medial nucleus of the trapezoid body: comparative physiology. Neuroscience 154:160–170.
Kopp-Scheinpflug C, Tozer AJ, Robinson SW, Tempel BL, Hennig MH, Forsythe ID (2011) The sound of silence: ionic mechanisms encoding sound termination. Neuron 71:911–925.
Kopp-Scheinpflug C, Sinclair JL, Linden JF (2018) When sound stops: offset responses in the auditory system. Trends Neurosci 41:712–728.
Kulesza RJ Jr (2008) Cytoarchitecture of the human superior olivary complex: nuclei of the trapezoid body and posterior tier. Hear Res 241:52–63.
Kulesza RJ Jr, Spirou GA, Berrebi AS (2003) Physiological response properties of neurons in the superior paraolivary nucleus of the rat. J Neurophysiol 89:2299–2312.
Kulesza RJ Jr, Kadner A, Berrebi AS (2007) Distinct roles for glycine and GABA in shaping the response properties of neurons in the superior paraolivary nucleus of the rat. J Neurophysiol 97:1610–1620.
Kuwada S, Batra R (1999) Coding of sound envelopes by inhibitory rebound in neurons of the superior olivary complex in the unanesthetized rabbit. J Neurosci 19:2273–2287.
Löhrke S, Srinivasan G, Oberhofer M, Doncheva E, Friauf E (2005) Shift from depolarizing to hyperpolarizing glycine action occurs at different perinatal ages in superior olivary complex nuclei. Eur J Neurosci 22:2708–2722.
Moore BCJ (1997) An introduction to the psychology of hearing, Ed 4. San Diego, CA: Academic Press.
Morgan MJ, Thompson P (1975) Apparent motion and the Pulfrich effect. Perception 4:3–18.
Mountcastle VB, Davies PW, Berman AL (1957) Response properties of neurons of cat's somatic sensory cortex to peripheral stimuli. J Neurophysiol 20:374–407.
Oertel D, Cao XJ, Ison JR, Allen PD (2017) Cellular computations underlying detection of gaps in sounds and lateralizing sound sources. Trends Neurosci 40:613–624.
Ollo C, Schwartz IR (1979) The superior olivary complex in C57BL/6 mice. Am J Anat 155:349–373.
Penner MJ (1977) Detection of temporal gaps in noise as a measure of the decay of auditory sensation. J Acoust Soc Am 61:552–557.
Pérez-González D, Malmierca MS, Moore JM, Hernández O, Covey E (2006) Duration selective neurons in the inferior colliculus of the rat: topographic distribution and relation of duration sensitivity to other response properties. J Neurophysiol 95:823–836.
Phillips DP, Hall SE, Boehnke SE (2002) Central auditory onset responses, and temporal asymmetries in auditory perception. Hear Res 167:192–205.
Pilati N, Linley DM, Selvaskandan H, Uchitel O, Hennig MH, Kopp-Scheinpflug C, Forsythe ID (2016) Acoustic trauma slows AMPA receptor-mediated EPSCs in the auditory brainstem, reducing GluA4 subunit expression as a mechanism to rescue binaural function. J Physiol 594:3683–3703.
Pollak GD, Gittelman JX, Li N, Xie R (2011) Inhibitory projections from the ventral nucleus of the lateral lemniscus and superior paraolivary nucleus create directional selectivity of frequency modulations in the inferior colliculus: a comparison of bats with other mammals. Hear Res 273:134–144.
Pratt H, Bleich N, Mittelman N (2005) The composite N1 component to gaps in noise. Clin Neurophysiol 116:2648–2663.
Rhode WS, Oertel D, Smith PH (1983) Physiological response properties of cells labeled intracellularly with horseradish peroxidase in cat ventral cochlear nucleus. J Comp Neurol 213:448–463.
Roberts MT, Seeman SC, Golding NL (2014) The relative contributions of MNTB and LNTB neurons to inhibition in the medial superior olive assessed through single and paired recordings. Front Neural Circuits 8:49.
Saldaña E, Aparicio MA, Fuentes-Santamaría V, Berrebi AS (2009) Connections of the superior paraolivary nucleus of the rat: projections to the inferior colliculus. Neuroscience 163:372–387.
Sayegh R, Aubie B, Faure PA (2011) Duration tuning in the auditory midbrain of echolocating and non-echolocating vertebrates. J Comp Physiol A Neuroethol Sens Neural Behav Physiol Neuroethol Sens Neural Behav Physiol 197:571–583.
Schofield BR (1991) Superior paraolivary nucleus in the pigmented guinea pig: separate classes of neurons project to the inferior colliculus and the cochlear nucleus. J Comp Neurol 312:68–76.
Schofield BR (1995) Projections from the cochlear nucleus to the superior paraolivary nucleus in guinea pigs. J Comp Neurol 360:135–149.
Scholl B, Gao X, Wehr M (2010) Nonoverlapping sets of synapses drive on responses and off responses in auditory cortex. Neuron 65:412–421.
Smith AJ, Owens S, Forsythe ID (2000) Characterisation of inhibitory and excitatory postsynaptic currents of the rat medial superior olive. J Physiol 529 [Pt 3]:681–698.
Sohoglu E, Chait M (2016) Neural dynamics of change detection in crowded acoustic scenes. Neuroimage 126:164–172.
Sollini J, Chapuis GA, Clopath C, Chadderton P (2018) ON-OFF receptive fields in auditory cortex diverge during development and contribute to directional sweep selectivity. Nat Commun 9:2084.

Steinert JR, Kopp-Scheinpflug C, Baker C, Challiss RA, Mistry R, Haustein MD, Griffin SJ, Tong H, Graham BP, Forsythe ID (2008) Nitric oxide is a volume transmitter regulating postsynaptic excitability at a glutamatergic synapse. Neuron 60:642–656.

Steinert JR, Postlethwaite M, Jordan MD, Chernova T, Robinson SW, Forsythe ID (2010) NMDAR-mediated EPSCs are maintained and accelerate in time course during maturation of mouse and rat auditory brainstem in vitro. J Physiol 588:447–463.

Sun YJ, Wu GK, Liu BH, Li P, Zhou M, Xiao Z, Tao HW, Zhang LI (2010) Fine-tuning of pre-balanced excitation and inhibition during auditory cortical development. Nature 465:927–931.

Thompson AM, Thompson GC (1991) Posteroventral cochlear nucleus projections to olivocochlear neurons. J Comp Neurol 303:267–285.

Walcher J, Hassfurth B, Grothe B, Koch U (2011) Comparative posthearing development of inhibitory inputs to the lateral superior olive in gerbils and mice. J Neurophysiol 106:1443–1453.

Wehr M, Zador AM (2003) Balanced inhibition underlies tuning and sharpens spike timing in auditory cortex. Nature 426:442–446.

Yassin L, Radtke-Schuller S, Asraf H, Grothe B, Hershfinkel M, Forsythe ID, Kopp-Scheinpflug C (2014) Nitric oxide signaling modulates synaptic inhibition in the superior paraolivary nucleus (SPN) via cGMP-dependent suppression of KCC2. Front Neural Circuits 8:65.

Chapter 3

# Physiological and anatomical development of glycinergic inhibition in the mouse superior paraolivary nucleus following hearing onset

## 3.1 Author contributions

*Rajaram E, Pagella S, Grothe B, Kopp-Scheinpflug C (2020).Physiological and anatomical development of glycinergic inhibition in the mouse superior paraolivary nucleus following hearing onset. J Neurophysiol. 2020;124(2):471-483.*

The contributions of the authors Ezhilarasan Rajaram (ER), Sara Pagella (SP), Benedikt Grothe (BG), and Conny Kopp-Scheinpflug (CKS) are as follows: ER, SP and CKS performed research; ER, SP and CKS analyzed data and interpreted the results of experiments; ER, SP, BG, and CKS wrote the paper; CKS designed research. ER contributed figures 1, 2, 3, 4, 6 and 7.

*J Neurophysiol* 124: 471–483, 2020.
First published July 15, 2020; doi:10.1152/jn.00053.2020.

**RESEARCH ARTICLE** | *Sensory Processing*

# Physiological and anatomical development of glycinergic inhibition in the mouse superior paraolivary nucleus following hearing onset

**Ezhilarasan Rajaram,[1,2] Sara Pagella,[1,2] Benedikt Grothe,[1] and Conny Kopp-Scheinpflug[1]**
[1]*Department of Biology II, Division Neurobiology, Ludwig-Maximilians-University, Munich, Germany; and* [2]*Graduate School of Systemic Neurosciences, Ludwig-Maximilians-University, Munich, Germany*

Submitted 7 February 2020; accepted in final form 11 July 2020

**Rajaram E, Pagella S, Grothe B, Kopp-Scheinpflug C.** Physiological and anatomical development of glycinergic inhibition in the mouse superior paraolivary nucleus following hearing onset. *J Neurophysiol* 124: 471–483, 2020. First published July 15, 2020; doi: 10.1152/jn.00053.2020.—Neural circuits require balanced synaptic excitation and inhibition to ensure accurate neural computation. Our knowledge about the development and maturation of inhibitory synaptic inputs is less well developed than that concerning excitation. Here we describe the maturation of an inhibitory circuit within the mammalian auditory brainstem where counterintuitively, inhibition drives action potential firing of principal neurons. With the use of combined anatomical tracing and electrophysiological recordings from mice, neurons of the superior paraolivary nucleus (SPN) are shown to receive converging glycinergic input from at least four neurons of the medial nucleus of the trapezoid body (MNTB). These four axons formed 30.71 ± 2.72 (means ± SE) synaptic boutons onto each SPN neuronal soma, generating a total inhibitory conductance of 80 nS. Such strong inhibition drives the underlying postinhibitory rebound firing mechanism, which is a hallmark of SPN physiology. In contrast to inhibitory projections to the medial and lateral superior olives, the inhibitory projection to the SPN does not exhibit experience-dependent synaptic refinement following the onset of hearing. These findings emphasize that the development and function of neural circuits cannot be inferred from one synaptic target to another, even if both originate from the same neuron.

**NEW & NOTEWORTHY** Neuronal activity regulates development and maturation of neural circuits. This activity can include spontaneous burst firing or firing elicited by sensory input during early development. For example, auditory brainstem circuits involved in sound localization require acoustically evoked activity to form properly. Here we show, that an inhibitory circuit, involved in processing sound offsets, gaps, and rhythmically modulated vocal communication signals, matures before the onset of acoustically evoked activity.

3D reconstruction; auditory brain stem; development; patch clamp; synaptic inhibition

## INTRODUCTION

The function of inhibition is often described as suppressing neuronal excitation by limiting action potential firing and restricting the spread of neural activity in the temporal and spatial dimension. An additional, often neglected, function of inhibition is to drive neuronal firing via a postinhibitory rebound mechanism, even without excitatory inputs (Kopp-Scheinpflug et al. 2011b; Rajaram et al. 2019; Tadayonnejad et al. 2009). However, little is known about the development and synaptic plasticity of such inhibitory circuits, especially when this inhibition is the main drive for neuronal firing.

The medial nucleus of the trapezoid body (MNTB) is an evolutionary conserved nucleus in the mammalian auditory brainstem and represents the primary source of neuronal inhibition within the superior olivary complex (SOC) and the ventral nucleus of the lateral lemniscus (VNLL; for review, see Borst and Soria van Hoeve 2012; Kopp-Scheinpflug et al. 2011a; Kulesza and Grothe 2015). Mature MNTB neurons use glycine as their neurotransmitter and innervate, among others, neurons of the medial superior olive (MSO), the lateral superior olive (LSO), and the superior paraolivary nucleus (SPN). The MSO and LSO are binaural nuclei involved in sound localization across the horizontal plane, using interaural time and level differences, respectively. Balanced interaction between excitatory inputs from the bushy cells of the anterior ventral cochlear nucleus and fast glycinergic input from the MNTB is critical in these sound localization circuits (for review, see Grothe et al. 2010; Sanes and Friauf 2000; Tollin 2003). The SPN on the other hand is a monaural nucleus that receives predominant glycinergic inhibition and minimal excitation (Rajaram et al. 2019), both inputs originating from the contralateral ear (Felix and Magnusson 2016; Kulesza et al. 2003). Inhibition causes strong hyperpolarization in SPN neurons, which, paired with hyperpolarization-activated cyclic nucleotide gated (HCN) channels and T-type calcium channels, triggers a burst of action potentials at the end of the sound stimulus (Felix et al. 2011; Kopp-Scheinpflug et al. 2011b). This sound-offset response is believed to have implications for gap detection and sound duration encoding and processing of vocal communication sounds (for review, see Kopp-Scheinpflug et al. 2018).

The target nuclei of MNTB projections have diverse auditory processing tasks, and anatomical studies suggest that individual MNTB neurons form axon collaterals that innervate neurons in the LSO, MSO, SPN, and VNLL (Banks and Smith 1992; Kuwabara and Zook 1991; Sommer et al. 1993). This raises the question of how these diverse inhibitory projections develop and whether the presynaptic site plays a different role to the postsynaptic target in forming these neural circuits.

Pioneering studies have established the auditory brainstem as an effective model to investigate plasticity and synaptic

Correspondence: C. Kopp-Scheinpflug (cks@bio.lmu.de).

reorganization of inhibitory circuits during development (for review, see Grothe 2003; Kandler et al. 2009; Kandler and Gillespie 2005; Sanes and Friauf 2000). Glycinergic MNTB-LSO and MNTB-MSO synapses undergo the most prominent changes within the first two postnatal weeks, including a shift from depolarizing to hyperpolarizing inhibition (D/H shift), synaptic pruning, refinement of tonotopy, and acceleration of hyperpolarizing postsynaptic voltage responses. Chloride reversal potentials that are positive to the resting membrane potential are a general phenomenon during early postnatal development in the brain and allow for inhibitory circuit formation based on Hebbian plasticity rules (Ben-Ari et al. 2012). Increasing expression and activity of the chloride extruding potassium-chloride-cotransporter type 2 (KCC2) initiates the D/H shift in the auditory brainstem as early as postnatal day (P)1 in the SPN and at about P4–P9 for LSO and MSO (Balakrishnan et al. 2003; Kandler and Friauf 1995; Löhrke et al. 2005; Milenković and Rübsamen 2011). Besides the early D/H switch of inhibitory synaptic transmission, often a change from a corelease of GABA, glycine and glutamate to sole glycinergic transmission was observed (Kotak et al. 1998; Nabekura et al. 2004; Weisz et al. 2016). Both LSO and MSO neurons exhibit a significant acceleration of inhibitory postsynaptic voltage responses before hearing onset at the end of the second postnatal week (Kim and Kandler 2003; Smith et al. 2000), which continues for at least 2 wk after the onset of hearing (Magnusson et al. 2005; Pilati et al. 2016).

For the MNTB-LSO synapse, synaptic pruning during the first two postnatal weeks, reflects a reduced number of MNTB axons converging onto a given LSO cell, while the remaining synapses were strengthened (Kim and Kandler 2010). This strengthening was attributed to an increase in the quantal content of the synapse (Kim and Kandler 2010). The pruning process depends on glutamate corelease from MNTB axons, as well as patterned spontaneous activity, and resulted in a fine-tuning of tonotopic projections from MNTB to LSO (Clause et al. 2014; Noh et al. 2010). In the LSO, the developmental reorganization of inhibitory inputs takes place before hearing onset (P12–14 in rodents). MSO neurons receive similar inhibitory inputs to the LSO and exhibit analogous developmental changes (Magnusson et al. 2005) but undergo substantial spatial reorganization of inhibitory inputs much later in development. This results in spatial segregation of excitatory inputs to the dendrites and inhibitory inputs to the soma, which is characteristic for animals with low-frequency hearing (Kapfer et al. 2002), where it is suggested to improve temporal coincidence of excitation and inhibition in the MSO (Grothe 2003; Grothe et al. 2010).

Since spectral and temporal coincidence of excitation and inhibition is crucial for LSO and MSO function, the synaptic development must be coordinated between excitatory-inhibitory circuits (Couchman et al. 2010; Pilati et al. 2016; Winters and Golding 2018). The MNTB-SPN synapse offers a unique model to study developmental inhibitory plasticity, without a competing excitatory input. Differences in the development and maturation of the MNTB-SPN synapse compared with the MNTB-LSO or MNTB-MSO synapses would help to assess the contributions of the presynaptic input to this process independently and to untangle it from the contribution of experience-dependent balancing of excitation and inhibition.

We have exploited the MNTB-SPN synapse as a model to study developmental activity-dependent plasticity of inhibitory circuits that follows the natural increase in neural firing activity after the onset of hearing. Patch-clamp recordings from SPN neurons of different posthearing ages combined with the stimulation of their inhibitory inputs allowed characterization of the developmental time course of synaptic properties. Neurotracer injections into the single MNTB neurons and subsequent three-dimensional (3D) reconstructions provided information about the projection patterns between MNTB and SPN at different ages. In contrast to other inhibitory circuits in the auditory brainstem (Grothe 2003; Kandler et al. 2009; Kandler and Gillespie 2005; Sanes and Friauf 2000), inhibitory inputs to the SPN do not undergo major experience-dependent synaptic refinement following the onset of hearing.

## METHODS

All experimental procedures were reviewed and approved by the Bavarian district government (TVV AZ: 55.2-1-54-2532-38-13) and were done according to the European Communities Council Directive (2010/63/EU). C57Bl6J mice were housed in a vivarium with a normal light-dark cycle (12:12-h light-dark) and food and water ad libitum. Mice of both sexes were used for the physiological and anatomical experiments.

*In vitro electrophysiology.* P9–25 mice of either sex were briefly anesthetized with isoflurane and rapidly killed by decapitation. Coronal brainstem sections (150- to 200-$\mu$m thick) containing the SOC (Rajaram et al. 2019; Yassin et al. 2014) were cut in an ice-cold high-sucrose, low-sodium artificial cerebral spinal fluid (ACSF). Brainstem slices were maintained after slicing in normal ACSF at 37°C for 30–45 min, after which they were stored in a slice-maintenance chamber at room temperature (~22°C). Composition of the normal ACSF was as follows (in mM): 125 NaCl, 2.5 KCl, 26 $NaHCO_3$, 10 glucose, 1.25 $NaH_2PO_4$, 2 sodium pyruvate, 3 myo-inositol, 2 $CaCl_2$, 1 $MgCl_2$ 1, and 0.5 ascorbic acid pH was 7.4, bubbled with 95% $O_2$-5% $CO_2$. For the low-sodium ACSF, $CaCl_2$ and $MgCl_2$ concentrations were 0.1 and 4 mM, respectively, and NaCl was replaced by 200 mM sucrose. Experiments were conducted at 36 ± 1°C, maintained by an inline feedback temperature controller and heated stage (Warner Instruments) with the recording chamber being continuously perfused with ACSF at a rate of 1–2 ml/min. Whole cell patch-clamp recordings were made from visually identified SPN neurons using an EPC10/2 HEKA amplifier (HEKA Electronik), sampled at 50 kHz, and filtered at 10 kHz. Patch pipettes were pulled from borosilicate glass capillaries (Warner Instruments) using a DMZ Universal electrode puller (Zeitz-Instuments Vertriebs GmbH), filled with a patch solution containing the following (in mM): 126 K-gluconate, 4 KCl, 40 HEPES, 5 EGTA, 1 $MgCl_2$, 5 $Na_2$ phosphocreatine, 0.2% biocytin, and 292 mosM. HEPES at 40 mM supports a robust pH buffering of the neurons. This is particularly important in neurons receiving strong inhibitory input, which can cause an intracellular acidification (Lückermann et al. 1997). Intracellular acidification can in turn cause a pathological calcium influx though the voltage-gated calcium channel (VGCC), which is important in SPN signaling. Studies of the VGCC often use high HEPES concentrations (Cai et al. 2019; Cuttle et al. 1998; Makarenko et al. 2016; Mudado et al. 2004; Takahashi et al. 1998). pH was adjusted to 7.2 with KOH. Data were corrected for liquid junction potentials of –13.8 mV. Electrode resistance was between 2.4 and 6 MΩ. Synaptic responses were evoked by afferent fiber stimulation with concentric bipolar electrodes (FHC Inc., no. CBARC75). Voltage pulses were generated by the HEKA amplifier and postamplified by an isolated pulse stimulator (AM Systems). Inhibitory currents were recorded in ACSF containing 6,7-dinitroquinoxaline-2,3-dione (DNQX; 10 $\mu$M)

and D-2-amino-5-phosphonopentanoic acid (D-AP5; 50 $\mu$M) to block AMPA and NMDA glutamate receptors, respectively. Miniature postsynaptic inhibitory currents were recorded in the presence of 1 $\mu$M tetrodotoxin (TTX). Pharmacological compounds were obtained from Sigma-Aldrich.

*Immunohistochemistry.* Brain slices were used following single neuron biocytin injections during in vitro patch-clamp recordings. Following overnight postfixation in 4% PFA, slices were washed three times for 10 min in PBS before transferring them to a blocking solution containing 1% bovine serum albumin, 0.5% Triton X100, and 0.1% saponin in PBS. Biocytin was visualized with streptavidin conjugated to Cy3 (1:500 in blocking solution). Antibodies against the glycine transporter type 2 (GlyT2; Millipore no. 1773: 1:1,000)-stained glycinergic terminals. Tissue was then washed three times for 10 min in PBS at room temperature before incubation for 24 h at 4°C with secondary antibodies diluted in blocking solution. Then, sections were rinsed three times for 10 min in PBS and coverslipped with Vectashield mounting medium.

*Confocal microscopy and reconstruction.* Confocal optical sections were acquired with a confocal laser-scanning microscope equipped with HCX PL APO CS ×20/NA0.7 and HCX PL APO Lambda Blue ×63/NA1.4 immersion oil objectives (Leica). Fluorochromes were visualized with excitation wavelengths of 405 nm (emission filter: 410–430 nm) for amino-methylcoumarin (AMCA), 488 nm (emission filter: 510–540 nm) for Alexa 488, 561 nm (emission filter: 565–585 nm) for Cy3, and 594 nm (emission filter: 605–625 nm) for Alexa 594. For each optical section, the images were collected sequentially for the different fluorochromes. Stacks of eight-bit grayscale images were obtained with axial distances of 290 nm between optical sections and pixel sizes of 120–1520 nm depending on the selected zoom factor and objective. To improve the signal-to-noise ratio, images were averaged from three successive scans. Red, green, blue (RGB) stacks, montages of RGB optical sections, and maximum-intensity projections were assembled using the ImageJ StackGroom plugin.

Since 3D image files are generally difficult to interpret on a flat computer monitor, we used an immersive virtual reality environment (https://www.syglass.io/ IstoVisio, Inc.) that allowed us to "walk" along our traced axons and follow its turns around other structures while tracing, measuring, counting and annotating along the way. High-resolution (×63) image stacks, each containing a biocytin-filled MNTB neuron and its axonal arbor in the SPN, were imported into syGlass software. Zooming in under the control of one hand, while the other hand is guiding a tracer tool, each axon was followed up to a branch point, which was then annotated. From there, one branch was chosen randomly and traced down to its next branch point, zooming in further if needed. This process was repeated until the finest end of the axonal branch. Then, we zoomed back out to the next upstream branch point and repeated the tracing from there until eventually all branches were traced, and the full 3D arbor was created. The syGlass software then provided the number of branch points, the total length of the traced axon, and the volume calculated as a 3D convex hull.

*Experimental design and statistical analysis.* In the text, data are presented in parenthesis (median, 25/75 quartiles, or as means ± SE; test: $P$ value) unless indicated otherwise. In the figures, data are presented as medians and 25/75 quartiles in addition to individual data points. Statistical analyses of the data were performed with SigmaStat/SigmaPlot. Normality was tested by the Shapiro-Wilk test. Comparisons between different data sets were made depending on the distribution of the data using parametric tests for normally distributed data (two-tailed Student's $t$ test for comparing two groups and ANOVA for comparing three or more groups). When the normality assumption was violated, nonparametric tests (Mann-Whitney rank sum test for comparing two groups and Kruskal-Wallis ANOVA on ranks for comparing three or more groups) were used. Paired $t$ tests or Wilcoxon signed rank tests were used when two data sets were recorded from individual neurons under different conditions. Differences were considered statistically significant at $P \leq 0.05$ and presented in the figures as n.s. for nonsignificant differences. Intrinsic properties as well as postsynaptic current amplitudes and *kinetics* were analyzed using Stimfit software (Guzman et al. 2014). For data acquired with patch-clamp recording; $n$ is the number of neurons, with two to three brain slices per animal and at least three animals per group.

## RESULTS

The results of this study are based on whole cell voltage-clamp recordings from 81 SPN neurons performed at physiological temperatures of 36 ± 1°C. Additional MNTB neurons were patch clamped and filled with biocytin for subsequent histological analysis of inhibitory inputs to the SPN.

*Hearing onset does not cause changes in spontaneous vesicle release or quantal size.* Spontaneous release of glycine from presynaptic terminals was assessed by recording miniature postsynaptic inhibitory currents (mIPSCs). Developmental differences related to sound-evoked activity were analyzed for three postnatal (P) ages: immediately before hearing onset (P9–11), around hearing onset (P12–14), and well after hearing onset (P15–22). Example recordings show mISPCs of all age groups as outward currents, as expected for holding voltages of −60 mV with a low internal chloride concentration of 6 mM (Fig. 1*A*). The frequency of mIPSCs was used as an initial indicator of presynaptic strength while the amplitude of mIPSCs served as a preliminary measure of postsynaptic responsiveness.

Measurements of mIPSC frequencies in the SPN (Fig. 1*B*) did not reveal significant differences between the age groups (P9–11: 8.84 ± 1.79 Hz, $n = 8$; P12–14: 12.88 ± 1.59 Hz, $n = 9$; P15–22: 11.88 ± 2.18 Hz, $n = 7$; ANOVA: $P = 0.276$). The recordings of spontaneous events in the MNTB-SPN synapse were performed in the presence of tetrodotoxin (TTX; 1 $\mu$M) to ensure that mIPSC amplitudes were representative of single quanta and not multivesicular release in response to presynaptic action potentials. The distributions of mIPSC amplitudes were slightly skewed toward larger mIPSCs (Fig. 1*C*). Within each cell, mIPSC amplitudes varied by a factor of 6.56 ± 0.41 ($n = 24$), ranging from smallest average amplitudes of 35.76 ± 1.80 pA to the largest average amplitudes of 235.52 ± 19.63 pA. To test for the possibility that the large mIPSCs are the result of spontaneous near-synchronous multivesicular release from the same or adjacent active zones, we analyzed the time intervals between single miniature events (Fig. 1*D*). The minimum interval between two mIPSC ranged from 1.95 ms to 12.54 ms with an average of 5.52 ± 0.58 ms ($n = 24$ cells). This was too slow a time course to be caused by spontaneous multivesicular release. A similarly large range of mIPSC amplitudes based on the variability in the size of release sites has been described for other neurons in the mammalian auditory brainstem (Lim et al. 2003). Overall, amplitudes of mIPSCs did not change significantly across all the age groups tested (P9–11: 78.58 ± 8.03 pA, $n = 8$; P12–14: 102.31 ± 9.15 pA, $n = 9$; P15–22: 85.27 ± 8.88 pA, $n = 7$; ANOVA: $P = 0.151$; Fig. 1*E*).

*Evoked IPSC amplitudes are large and unaltered by hearing onset while decay times continued to accelerate.* The size of postsynaptic currents evoked by presynaptic action potentials aids the determination of synaptic strength. Pharmacologically isolated glycinergic inhibitory postsynaptic currents (IPSCs) were reliably elicited in SPN neurons by stimulating MNTB

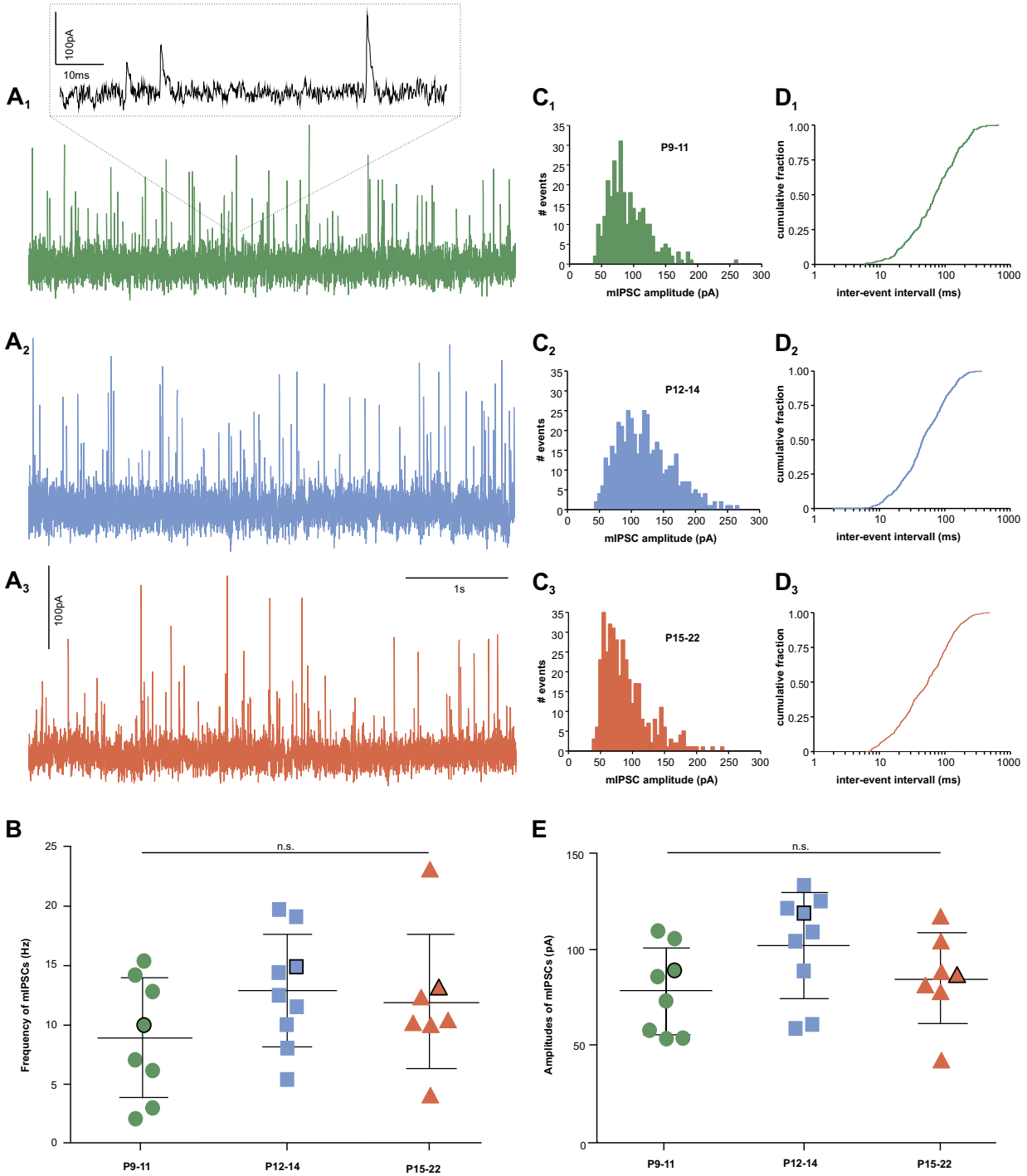


Fig. 1. Amplitude and frequency of miniature inhibitory currents (mIPSCs) in the superior paraolivary nucleus (SPN) are constant across hearing onset. *A*: example traces of mIPSCs for the prehearing onset (green, $A_1$), hearing onset (blue, $A_2$), and posthearing onset (orange, $A_3$) age groups. *B*: population data show no significant difference in the frequency of mIPSCs. Symbols with black outline represent the example cells in *A*. *C*: histograms of mIPSC amplitudes are slightly skewed, due to some occurrence of larger amplitude mIPSCs. *D*: cumulative distribution of the interevent intervals shows the minimum interval to be longer than 5–6 ms. *E*: population data show no significant difference in the amplitudes of mIPSCs. Symbols with black outline represent the example cells in *A*. P, postnatal day.

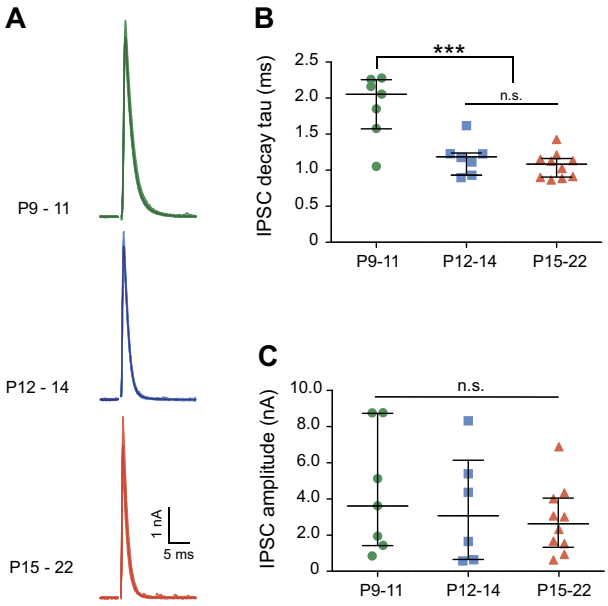


Fig. 2. Evoked inhibitory currents (IPSCs) in the superior paraolivary nucleus (SPN) are stable in amplitude but accelerate in decay time. *A*: example traces of IPSCs for the prehearing onset (green), hearing onset (blue), and posthearing onset (orange) age groups. Bold traces indicate the average of 20 individual traces. *B*: population data show a decrease in IPSC decay tau between the prehearing group [postnatal day (P)9–11] and the hearing onset group (P12–14) and no further change toward the posthearing group (P15–22). *C*: IPSC amplitudes were large and did not change across hearing onset. ***$P \leq 0.001$.

neurons at a maximum stimulus strength (100 V; Fig. 2*A*). IPSC decay time constants were obtained by fitting an exponential function to the decaying current. Decay times accelerated significantly from 1.89 ± 0.17 ms ($n = 7$) at P9–11 to 1.17 ± 0.09 ms ($n = 7$) at P12–14 with no further significant changes after that (1.06 ± 0.06 ms; $n = 10$; ANOVA followed by an all-pairwise multiple comparison Bonferroni $t$ test: P9–11 vs. P15–22: $P \leq 0.001$; P9–11 vs. P12–14: $P \leq 0.001$; P12–14 vs. 15–22: $P \geq 0.999$; Fig. 2*B*). The initial acceleration of IPSCs with the onset of hearing is in agreement with age-matched data from LSO and MSO (Fischl et al. 2012; Magnusson et al. 2005; Pilati et al. 2016; Walcher et al. 2011).

Previous studies in the MNTB-LSO synapse reported a decrease in evoked IPSC amplitudes leading up to hearing onset (P12) but no change after that (Kim and Kandler 2003; Pilati et al. 2016; Walcher et al. 2011). In contrast, peak IPSC amplitudes in the MNTB-MSO synapse continued to decrease after hearing onset (Magnusson et al. 2005). In the SPN, peak IPSC amplitudes were 4.35 ± 1.26 nA ($n = 7$) at P9–11, 3.48 ± 1.26 nA ($n = 7$) at P12–14, and 2.83 ± 0.59 nA ($n = 10$) at P15–22 and did not differ significantly between age groups (ANOVA: $P = 0.532$; Fig. 2*C*).

Multiple pre- and postsynaptic parameters determine IPSC amplitudes, including the IPSC reversal potential ($E_{IPSC}$), the number of input fibers, the number of vesicles in the readily releasable pool (RRP), the quantal amplitude, and the probability to release (Pr) such a vesicle (quantum) from the presynaptic terminal. While some presynaptic parameters (RRP, Pr) may be set by the presynaptic MNTB neuron and could therefore be similar at synapses in different target nuclei, other parameters are determined by the postsynaptic neuron ($E_{IPSC}$, mIPSC amplitudes) and thereby generate a target specificity.

The driving force of the IPSCs is governed by the difference between the resting (in our case holding) potential and the reversal potential of the IPSC, which is mostly mediated by $Cl^-$ but could also involve a flux of $HCO_3^-$ (Bormann et al. 1987; Kaila et al. 1992). SPN neurons have a hyperpolarized chloride reversal potential early during development compared with other nuclei (Löhrke et al. 2005). First, we were interested in whether IPSC amplitudes in the SPN are constant across the tested ages, or if IPSCs declined following hearing onset, as observed in the MSO (Magnusson et al. 2005). Second, if a decrease occurred, might there be compensation by an increase in driving force due to a change in the IPSC reversal potential? We estimated the IPSC reversal potential by plotting IPSC amplitudes against the holding potential at a range of different voltages between −120 mV and −60 mV (Fig. 3*A*). The reversal potential, i.e., the voltage at which there was no net synaptic current (Fig. 3*B*), was highly hyperpolarizing for all ages tested with no significant differences between groups (P9–11: −94.66 ± 1.38 mV, $n = 14$; P12–14: −96.91 ± 0.91 mV, $n = 20$; P15–22: −97.08 ± 0.99 mV, $n = 18$; ANOVA: $P = 0.249$; Fig. 3*C*).

The results show that frequency and amplitudes of mIPSCs (quantal size) and the magnitude of the evoked IPSC amplitudes were all unchanged, implying that the MNTB-SPN synapse is not affected by the sound-evoked activity which occurs following hearing onset. However, differences in syn-

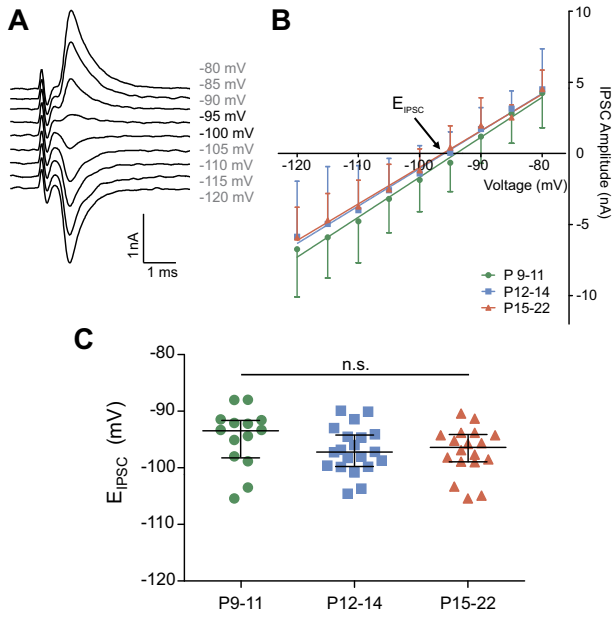


Fig. 3. superior paraolivary nucleus (SPN) neurons show strongly hyperpolarized postsynaptic inhibitory currents reversal potentials at all ages. *A*: superimposed inhibitory postsynaptic currents (IPSCs) evoked by stimulation of the medial nucleus of the trapezoid body (MNTB) over a range of holding potentials (−120 mV to −80 mV) show the 0 current potential (reversal potential, bold numbers). *B*: the mean current/voltage (*I*/*V*) relationship for the IPSCs in prehearing onset (green), hearing onset (blue) and posthearing onset mice gave a reversal potential of about −95 mV. *C*: population data show no significant difference between all age groups. $E_{IPSC}$, evoked IPSC; postnatal day.

aptic strength may be more apparent when the synapse is challenged during high-frequency stimulation. We therefore asked whether short-term plasticity induced by high-frequency stimulation changes between P9 and P22.

*Faster depression and increase in release probability occur after the onset of hearing.* The increased neuronal firing activity in the MNTB following hearing onset (Sonntag et al. 2009) is likely to affect short-term plasticity in the MNTB target nuclei. MNTB neurons firing at 100 Hz is well within their physiological firing range (Kopp-Scheinpflug et al. 2008) and caused synaptic depression in SPN neurons of all three age groups (Fig. 4, *A* and *B*). The time constant of IPSC depression became faster after hearing onset. The decay time constant was extracted by fitting an exponential function to the declining IPSC amplitudes during the 100-Hz train. Depression time constants were slowest at P9–11 (median: 7.70; 25%/75%: 3.31/10.05 ms; $n = 11$), had intermediate values at P12–14 (4.34; 3.22/5.60 ms; $n = 10$), and were fastest at P15–22 (2.89; 2.51/3.29 ms; $n = 15$; Kruskal-Wallis one-way ANOVA on ranks: P9–11 vs. P15–22: $P = 0.006$; P9–11 vs. P12–14: $P = 1.000$; P12–14 vs. 15–22: $P = 0.125$; Fig. 4*B*). The oldest age group showed the fastest depression and also the strongest. Steady-state depression (calculated as % relative to the control amplitude at 0 time) remained at a value of 45.00 ± 3.29%; ($n = 10$) at P9–11, had intermediate values at P12–14 (38.20 ± 0.27%; $n = 9$), and was reduced to the lowest values

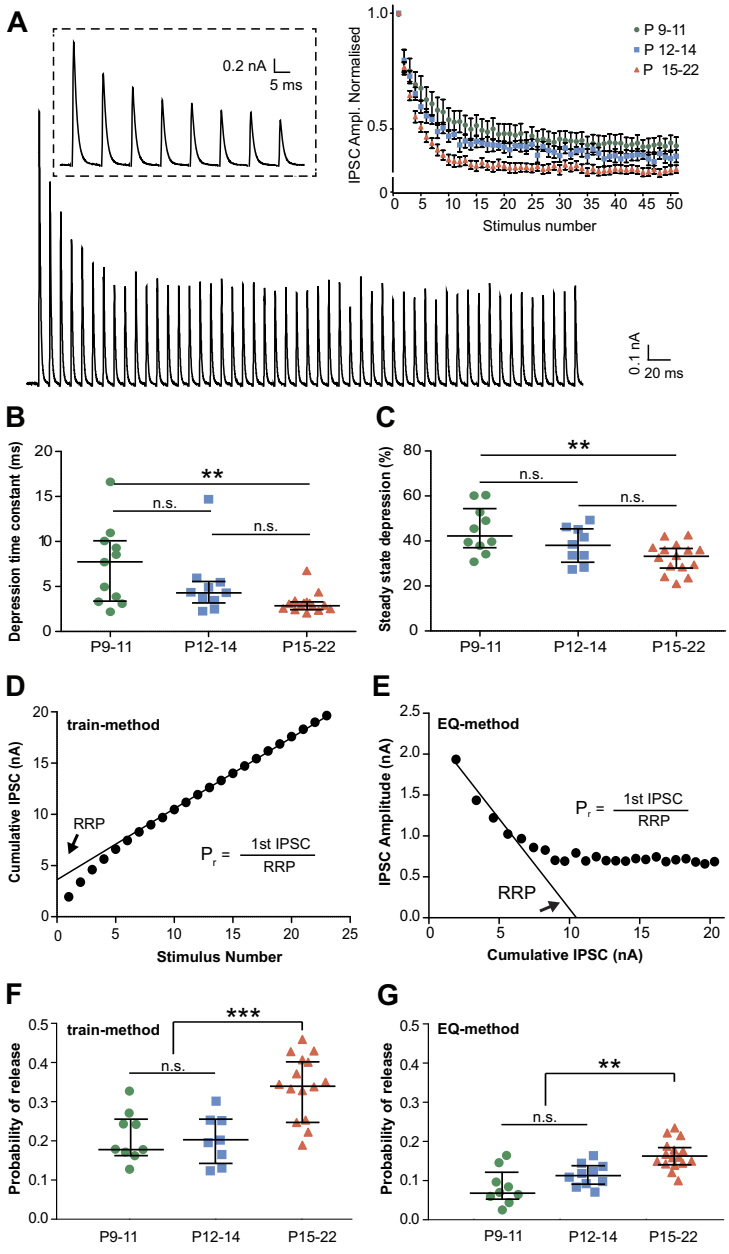


Fig. 4. Synaptic depression of inhibitory synaptic inputs to the superior paraolivary nucleus (SPN) accelerates after the onset of hearing. *A*: example of recordings in voltage-clamp from a representative synapse in SPN, 50 pulses at 100 Hz. Population data (*right top inset*) of normalized responses are shown for prehearing onset (green), hearing onset (blue), and posthearing onset (orange) mice. *B*: population data show an acceleration of the decay time constant of synaptic depression from the prehearing to the posthearing onset age group. *C*: population data show stronger steady-state depression in the oldest age group compared with the prehearing onset age group. *D*: cumulative amplitude plot of the first 25 pulses. Linear fit to the final responses is extrapolated back to the *y*-intercept. Intercept (arrow) indicate estimate of current from the readily releasable pool (RRP) of vesicles, which is then used to calculate the release probability (Pr). *E*: inhibitory postsynaptic current (IPSC) amplitudes of the first 20 responses and a linear fit to the first 4 data points. The *x*-intercept (arrow) indicate estimate of current from the readily releasable pool of vesicles, which is then used to calculate the release probability (Pr). *F* and *G*: probability of release increases significantly for the posthearing onset age group when estimated with the train method (*F*) or the EQ method (*G*). P, postnatal day. $^{**}P \leq 0.01$ and $^{***}P \leq 0.001$.

at P15–22 (32.60 ± 1.70%, $n$ = 15, ANOVA followed by Bonferroni $t$ test: P9–11 vs. P15–22: $P$ = 0.003; P9–11 vs. P12–14: $P$ = 0.247; P12–14 vs. P15–22: $P$ = 0.343; Fig. 4*C*).

The changing properties of synapses during activity are often described by fundamental characteristics such as the quantal size, the number of vesicles in the readily releasable pool (RRP), and the probability of their release (Pr). Any changes in these three parameters influences short-term depression (IPSC = RRP × Pr × quantal size). Quantal size, as shown in Fig. 1, was constant across changes in activity at hearing onset. RRP and Pr were estimated using a back extrapolation (train) method (Schneggenburger et al. 1999). A train of 50 stimuli evoked at a frequency of 100 Hz was used to achieve a steady state between the initial release of vesicles from the RRP and the replenishment occurring during the stimulus train (Couchman et al. 2010; Oline and Burger 2014; Schneggenburger et al. 1999; Thanawala and Regehr 2016). We plotted the cumulative peak IPSC amplitudes and fitted a linear function to the steady-state amplitudes, which was then back-extrapolated to the $y$-axis intercept (Fig. 4*D*, train method). The current at the $y$-intercept approximates the current that would be elicited when all vesicles were released from the RRP. Pr was then calculated from the current elicited by the RRP divided by the current elicited by the first pulse. At the MNTB-SPN synapse, Pr increased for the oldest age group from initially 0.23 ± 0.03 ($n$ = 9) at P9–11 and 0.22 ± 0.03 ($n$ = 12) at P12–14 to 0.38 ± 0.03 ($n$ = 15) at P15–22 (ANOVA followed by Bonferroni $t$ test: P9–11 vs. P12–14: $P$ = 1.000; P9–11 vs. P15–22: $P$ = 0.001; P12–14 vs. P15–22: $P \leq 0.001$; Fig. 4*F*). Since the train method allows for replenishment throughout the train, it may underestimate RRP and Pr values (Thanawala and Regehr 2016). To test whether the differences in Pr between the age groups still hold if there was no replenishment, we estimated Pr for the same data set with the EQ method. The EQ method assumes that the effects of replenishment are small and can be ignored and uses an extension of the linear fits to the first four IPSC amplitudes in the train to $x$-axis intercept as shown in Fig. 4*E* (Elmqvist and Quastel 1965; Thanawala and Regehr 2016). Pr values calculated with the EQ method were smaller compared with the train method (P9–11: 0.08 ± 0.01; P12–14: 0.11 ± 0.01; P15–22: 0.16 ± 0.01; Fig. 4*G*), but there was a similar increase in Pr with age (ANOVA followed by Bonferroni $t$ test: P9–11 vs. P15–22: $P$ = 0.001; P9–11 vs. P12–14: $P$ = 0.245; P12–14 vs. P15–22: $P$ = 0.006). Large Pr values for P15–22 age group support the faster rate of depression in this age group (Fig. 4*B*).

*Strength of the postinhibitory rebound response is maintained across hearing onset.* Faster and stronger depression of IPSCs in 100-Hz stimulus trains following hearing onset might cause differences in the postinhibitory rebound response at train offset. To test this possibility, 100-Hz synaptic stimulation was administered under current-clamp recording (Fig. 5*A*) and the reliability of generating an action potential response for each repetition of the stimulus train was measured. Neurons in each age group generated postinhibitory rebound responses containing at least one action potential with a reliability of nearly 100% (P9–11: 100 ± 0%, $n$ = 11; P12–14: 100 ± 0%, $n$ = 9; P15–22: 97.27 ± 2.72%, $n$ = 11). This reliability did not change significantly across hearing onset (ANOVA: $P$ = 0.403). A pairwise comparison of the neurons' resting membrane potential and their mean hyperpolarization achieved by the inhibitory inputs revealed that an average hyperpolarization of 15–17 mV was sufficient to trigger a synaptic postinhibitory rebound response in all age groups (P9–11: −15.05 ± 2.06 mV, $n$ = 11; P12–14: 15.78 ± 1.80 mV, $n$ = 9; P15–22: 17.03 ± 1.84 mV, $n$ = 11; ANOVA: $P$ = 0.752; Fig. 5*B*). The average number of action potentials within each synaptically evoked offset burst varied from 1 to 5.3 with only little differences between the age groups (P9–11: 2.74 ± 0.39, $n$ = 11; P12–14: 2.93 ± 0.62, $n$ = 9; P15–22: 2.31 ± 0.43, $n$ = 11; ANOVA: $P$ = 0.669; Fig. 5*C*). The latencies of the first action potential within the rebound burst were 26.78 ± 4.07 ms at P9–11 ($n$ = 11), 23.61 ± 3.12 ms ($n$ = 9) at P12–14, and 20.56 ± 3.31 ms ($n$ = 11) at P15–22 (Fig. 5*D*). Although the oldest age group had slightly briefer mean latencies, these differences were not significantly different (ANOVA: $P$ = 0.495).

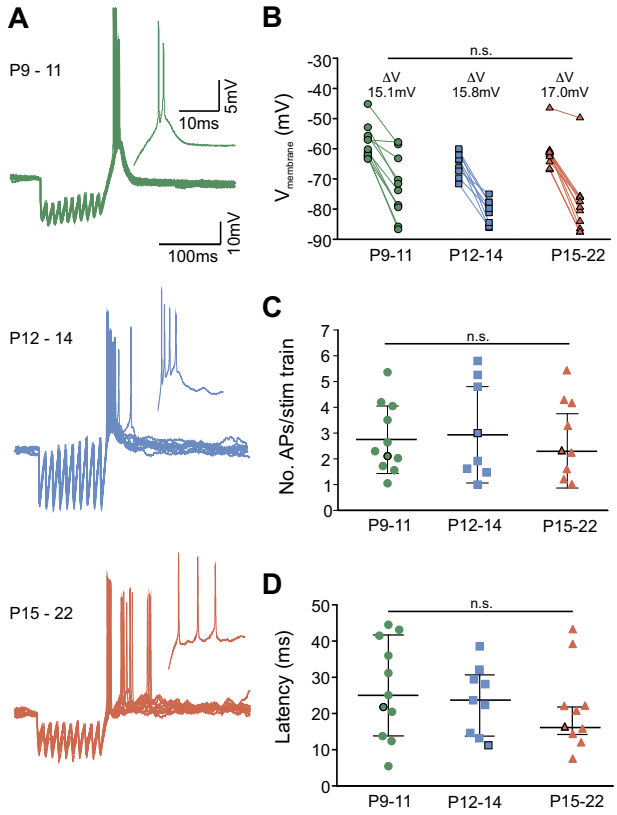


Fig. 5. Synaptically evoked postinhibitory rebound responses do not differ across the onset of hearing. *A*: example of recordings in current-clamp from representative SPN neurons of prehearing onset (green), hearing onset (blue), and posthearing onset (orange) mice. Ten stimulus trains were presented at 100 Hz, which were followed by a 100-ms period at each neuron's resting membrane potential. *Insets* show one enlarged rebound response of the respective trains. *B*: average differences between resting membrane potential and inhibitory postsynaptic current (IPSC) induced hyperpolarization were plotted for each neuron and all age groups. The differences in voltage (ΔV) were not different between the age groups. *C*: the average number of action potentials in each rebound burst was plotted for 10 repetitions of the 100-Hz stimulus for each neuron and age group. *D*: the latency between the beginning of the last stimulus artifact in the 100-Hz train and the peak of the first action potential in the rebound burst were plotted for each age group. Symbols with black outline represent the example cells in *A*. $V_{membrane}$, membrane potential; P, postnatal day; APs, action potentials.

*MNTB to SPN projections show a high convergence rate via axonal collaterals.* To establish the number of synaptic inputs to individual SPN neurons, we recorded IPSC amplitudes in response to increasing strength of electrical stimulation of MNTB axons. There were clear step-wise increments in amplitude with increasing stimulus strength (Fig. 6*A*), providing an estimate of the number of recruited axons. Objective analysis was performed by using a clustering algorithm (DBSCAN; Pedregosa et al. 2011) to estimate the number of clusters, i.e., the number of inputs (Fig. 6*B*). This conventional analysis reveals that on average SPN neurons receive inputs from 3.94 ± 0.28 MNTB neurons ($n$ = 18). No difference was observed in the number of inputs to SPN neurons between the three age groups (P9–11: 4.1 ± 0.65, $n$ = 6; P12–14: 3.67 ± 0.42, $n$ = 6; P15–22: 4.00 ± 0.45, $n$ = 6; ANOVA: $P$ = 0.789; Fig. 6*C*).

The ratio between the maximum current and the average number of inputs provides an estimate of the current evoked by a single fiber, a method that has been established to be comparable to the minimum stimulation paradigm (Couchman et al. 2010). In our data set, the average current provided by a single input fiber was 1.09 ± 0.31 nA ($n$ = 7) at P9–11, 0.87 ± 0.32 nA ($n$ = 6) at P12–14, and 0.71 ± 0.15 nA ($n$ = 10) at P15–22. The differences between age groups were not significant (ANOVA: $P$ = 0.532). The inferred average fiber conductance at P15–22 was 19.14 ± 4.03 nS.

A stimulus step size of 10 mV was chosen to compare the MNTB-SPN connectivity to its closest counterpart in the mouse auditory brainstem, the MNTB-LSO connectivity (Walcher et al. 2011). However, using step-wise increments to stimulate the afferent fibers might underestimate of the number of inputs to a SPN neuron. To test this, we applied an alternative method based on the ratio of the maximum to the minimum IPSC amplitudes for each given neuron (Kim and Kandler 2003); Fig. 6*D*). With the use of this method, our estimate of the number of inputs was much higher (P9–11: 35.76 ± 8.68, $n$ = 6; P12–14: 29.97 ± 10.66, $n$ = 6; P15–22: 26.41 ± 8.79, $n$ = 6) than the values acquired with the step protocol. However, the number of inputs acquired with this method did also not change significantly across hearing onset (Kruskal-Wallis one-way ANOVA on ranks: $P$ = 0.782).

The combined data acquired with electrophysiological recordings suggest that the inhibitory inputs to the SPN are stable in size and number across the onset of hearing, while the kinetics of single IPSCs and short-term depression continue to accelerate after hearing onset. Based on our finding that maximum inhibitory conductance (76.54 ± 16.09 nS) was elicited by activation of 4 MNTB axons and our estimate of ~26 inhibitory synaptic inputs innervating a mature SPN neuron, each MNTB axon should give rise to 6–7 synaptic boutons per SPN neuron. This suggests a strong arborization of MNTB axons within the SPN and the convergence of multiple axonal endings onto single SPN neurons. To test this hypothesis, we used anatomical measurements of the MNTB-SPN connectivity.

*Axonal length, number of branch points, and number of synaptic boutons are not different in MNTB to SPN projections between prehearing and posthearing mice.* Individual MNTB neurons (Fig. 7*A*) were injected with biocytin via the patch pipette in 200-$\mu$m-thick slices from prehearing onset (P9–11) and posthearing onset (P15–22) mice. Extensive axonal projections between MNTB and SPN could be reconstructed in three prehearing and posthearing mice (Fig. 7, *B–D*). Axons leaving the MNTB formed thick collaterals with

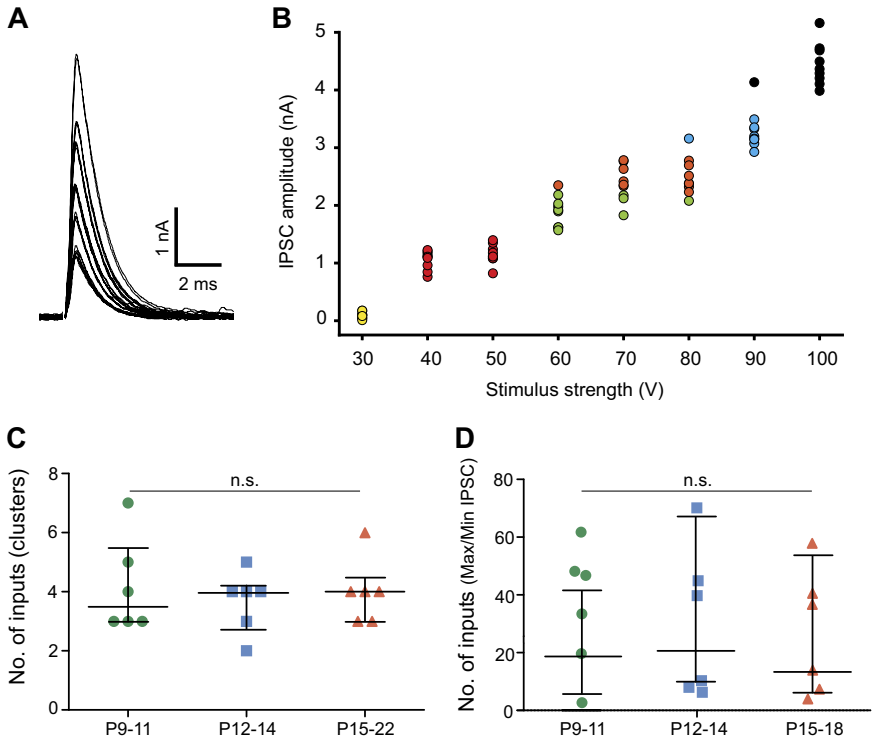


Fig. 6. Number of inhibitory inputs to superior paraolivary nucleus (SPN) neurons does not change across hearing onset. *A*: superimposed inhibitory postsynaptic currents (IPSCs) in an SPN neuron evoked by medial nucleus of the trapezoid body (MNTB) fiber stimulation at increasing stimulation intensities (30–100 V). *B*: IPSC amplitudes plotted against the stimulus number. Color-coded circles represent the number of inputs based on the clustering algorithm (Pedregosa et al. 2011). *C*: based on the clustering algorithm, the number of inputs is ~4/SPN neuron and does not vary across age groups. *D*: number of inputs calculated by dividing the maximum by the minimum current does also not vary across age groups. P, postnatal day.

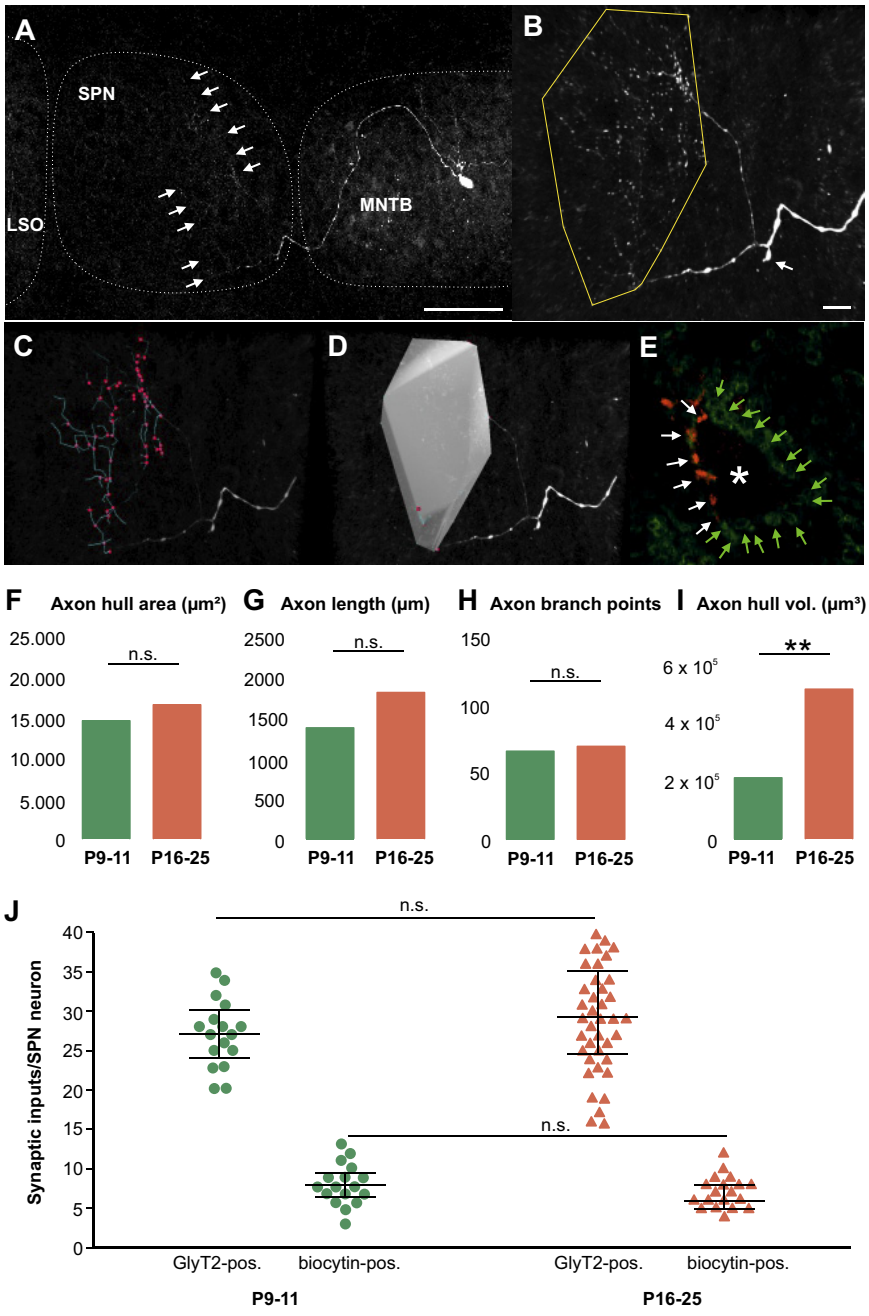


Fig. 7. Medial nucleus of the trapezoid body (MNTB) axonal arbor morphology in the superior paraolivary nucleus (SPN) also extends rostrocaudally. *A*: example of a single biocytin-labeled MNTB neuron and its projection toward the SPN. White arrows mark the extend of the arborization in the SPN. LSO, lateral superior olive. *B*: higher magnification of the tracing depicted in *A* shows the outline of the 2-dimensional (2D) convex hull analysis (yellow) and cut branch (white arrow) leading toward more rostral located targets. *C* and *D*: 3-dimensional (3D) reconstruction in syGlass allowed to label all branch points (magenta circles) and branches (turquois lines) (*C*), which formed the basis for the 3D hull analysis (*D*). *E*: single optical plane of an SPN neuron (*) showing inhibitory inputs as GlyT2-positive boutons (green arrows). The overlap with the red biocytin label (white arrows) indicate the inputs originating from 1 single MNTB neuron. *F–H*: population data show no significant differences in the 2-dimensional (2D) hull area (*F*), the overall axon length (*G*), or the number of branch points (*H*) between prehearing onset and posthearing onset mice. *I*: the volume of the axonal arbor was significantly larger in the older age group. Data in *F–I* are presented as means ± SE. *J*: population data of the number GlyT2-positive boutons and biocytin-positive boutons as exemplified in *E* were acquired from 17 neurons from 3 prehearing onset mice and from 19 neurons from 3 posthearing onset mice. The data revealed no difference between age groups. P, postnatal day. $^{**}P \leq 0.01$.

branch points either within the MNTB, within the SPN or ventral to the SPN. Here we concentrated on the endings that were traceable all the way to the SPN. However, additional collaterals carried on laterally toward the LSO or started heading ventromedial of the SPN (white arrow in Fig. 7*B*). These ventral collaterals were cut off, suggesting that they run perpendicular to the mediolateral plane of the coronal sections. No differences regarding these general projection properties were observed between the prehearing and posthearing group.

MNTB-SPN projection patterns were first analyzed in the medial-lateral extension by calculating the convex hull area in a two-dimensional (2D) maximum-intensity projection using ImageJ (Fig. 7*B*). No significant differences were found between the projection area of prehearing (13,256 ± 4,084 $\mu m^2$; $n = 3$) and posthearing (16,735 ± 3,400 $\mu m^2$; $n = 3$) mice (Fig. 7*F*; two-tailed $t$ test: $P = 0.967$). Higher resolution imaging and 3D reconstructions were employed to assess the MNTB-SPN projections in more detail using syGlass (see METHODS; Fig. 7, *C* and *D*). The total length of the axonal

arborization of an individual MNTB axon within the SPN added up to 13,82.42 ± 188.61 μm in prehearing ($n = 3$ traced axons in 3 mice) and 1,822.61 ± 202.46 μm in posthearing onset mice ($n = 3$ traced axons in 3 mice), with no significant difference between the two (two-tailed $t$ test: $P = 0.187$; Fig. 7*G*). Axons originating from single MNTB neurons formed between 50 to 92 branch points within the SPN (Fig. 7*D*) with an average of 66.00 ± 22.71 in prehearing and 69.67 ± 23.87 in posthearing onset mice. No difference was found in the number of branch points between prehearing and posthearing mice (two-tailed $t$ test: $P = 0.899$). To assess the overall target region of the 3D reconstruction, we calculated the convex hull volume (Fig. 7*D*). The volume of the axonal arborization revealed a significant increase across hearing onset from a volume of $2.13 \times 10^5$ $\mu m^3$ in prehearing mice to $5.21 \times 10^5$ $\mu m^3$ in posthearing mice (two-tailed $t$ test: $P = 0.009$; Fig. 7*I*).

Axonal varicosities were observed at the terminal branches (Fig. 7*E*) and were used together with labeling for the neuronal vesicular glycine transporter (GlyT2) to count the number of putative presynaptic boutons at individual SPN neurons (Fig. 7*E*). SPN neurons receive an average of 28.72 ± 0.84 somatic inhibitory inputs with no significant changes across hearing onset (P9–11: 27.11 ± 1.05 inputs, $n = 17$; P16–22: 29.39 ± 1.10 inputs, $n = 41$; two-tailed $t$ test: $P = 0.224$). The overlap of GlyT2-positive glycinergic inputs and biocytin-positive inputs from a single MNTB neuron was analyzed for 17 P9–11 SPN neurons (3 axonal reconstructions) and for 19 P15–22 SPN neurons (3 axonal reconstructions). These data suggest that one single MNTB neuron gives rise to only 18.9–23.5% (prehearing and posthearing, respectively) of the glycinergic input to one SPN neuron (Fig. 7, *E* and *J*) corroborating the physiologically acquired convergence ratio of 4:1 (Fig. 6, *A*–*C*).

Taken together, a single SPN neuron receives ~30 inhibitory synaptic inputs as the result of convergence from at least 4 different MNTB neurons. With respect to the increase in activity following hearing onset, no hint of tonotopic refinement was observed. Interestingly, the large axonal arborization of single MNTB neurons in mature mice, as calculated by the increased convex hull volume, spreads into the rostrocaudal direction to a much larger extend than predicted by the 2D maximum projection measures.

## DISCUSSION

The present study provides new insights into the development of inhibitory circuits. We demonstrate that purely inhibitory circuits in the auditory brainstem (MNTB-SPN) mature before the onset of sound-evoked activity, which is in contrast to neighboring auditory brainstem circuits that include competing excitatory inputs (MSO, LSO). While early functional refinement of the inhibitory inputs to the MNTB target structures is completed by P8 (Kim and Kandler 2003), experience-dependent, further refinement has been described for the inhibitory inputs to both, LSO and MSO (Couchman et al. 2010; Franzen et al. 2020; Kandler and Friauf 1995; Kapfer et al. 2002; Magnusson et al. 2005; Walcher et al. 2011). Here, we used electrophysiology and tracing techniques to show how experience-dependent plasticity is negligible in inhibitory circuits that do not need precise spectral and temporal matching of excitatory inputs. We discuss our results with respect to *1*) target-specific development of MNTB inhibition, *2*) advantage of 3D reconstruction, and *3*) different requirements of inhibition in the SPN compared with other MNTB targets.

*Target-specific development of MNTB inhibition.* The frequency of mIPSCs depends primarily on presynaptic mechanisms, while both pre- and postsynaptic factors determine the mIPSC amplitude. Comparing mIPSC frequency and amplitude of SPN neurons with data from LSO and MSO neurons may reveal target-specific differences in the development of inhibitory circuits.

Individual MNTB axons form collaterals that innervate multiple target nuclei, which was previously shown for the rat (Banks and Smith 1992; Kim and Kandler 2003; Sommer et al. 1993) and was corroborated in mouse by our present results. However, despite the common origin of presynaptic terminals in LSO, MSO, and SPN, the frequency of mISPCs is ~10-fold larger in SPN (11.88 ± 2.18) and LSO (10.2 ± 0.5; Walcher et al. 2011) compared with the age-matched MSO (Fischl et al. 2016; Magnusson et al. 2005). The low mIPSC frequency at the MNTB-MSO synapse compared with SPN and LSO is unlikely to be caused by a lower release probability, which is very similar between SPN (0.37 ± 0.03; this paper), LSO (0.3–0.4; (Krächan et al. 2017), and MSO (0.38 ± 0.04; (Couchman et al. 2010). The reduction in mIPSC frequency in the MSO happens following hearing onset (Magnusson et al. 2005), suggesting a synaptic refinement dependent on sound-evoked activity that does not seem necessary for SPN or LSO function.

Amplitudes of mIPSCs in the MNTB-LSO and MNTB-MSO synapses are not subject to change following the onset of hearing (Magnusson et al. 2005; Walcher et al. 2011). This was here corroborated for the MNTB-SPN synapse. The average conductance of spontaneous inhibitory events in SPN neurons was 2.30 ± 0.23 nS, which is comparable to data reported for LSO and MSO (Couchman et al. 2010; Walcher et al. 2011). The large range of mIPSC amplitudes within each SPN neuron (Fig. 1*B*) might be attributed to the variability between release sites at the individual neurons. Similar observations have been made at other glycinergic synapses in the auditory brainstem (Lim et al. 2003).

The maximum evoked peak inhibitory conductance in posthearing onset SPN neurons was 76.54 ± 16.09 nS ($n = 10$) and thus considerably larger than values previously reported for age matched LSO neurons but smaller compared with MSO neurons (Couchman et al. 2010; Magnusson et al. 2005; Pilati et al. 2016). Such target-specific differences in inhibitory strength can be achieved by differences in the presynaptic action potential waveform (Kawaguchi and Sakaba 2015; Vandael et al. 2015). In cerebellar stellate cells, presynaptic waveforms differ between single boutons of the same axon based on the expression levels of Kv3 currents (Rowan et al. 2016). As higher presynaptic Kv3 expression would lead to briefer presynaptic action potentials, less transmitter release, and subsequently smaller IPSCs, the smaller evoked ISPCs in the SPN in comparison to the MSO would imply a high expression of Kv3 at glycinergic terminals in the SPN and lower expression of presynaptic Kv3 for example in the MSO. TEA-sensitive Kv3 currents can be mediated by either Kv3.1 or by Kv3.3 channels, both of which are abundant in the superior olivary complex (Choudhury et al., 2020; Johnston et al. 2010). However, whether one of these channel subfamilies serves more

presynaptic or more postsynaptic functions among the MNTB target structures is not yet known.

Another important factor for limiting synaptic transmission is the number of presynaptic release sites, but the specific molecular composition necessary for the formation of release sites is not yet understood (for review, see Walter et al. 2018). The decrease in the number of release sites in the LSO and MSO collaterals associated with synaptic pruning during development (Kim and Kandler 2010; Magnusson et al. 2005) may leave the SPN with a relatively larger number of release sites and thus large inhibitory currents.

*Advantage of 3D reconstruction.* Many signal processing properties in the auditory system are described along the tonotopic axis, which extends mostly along the medial-to-lateral or the dorsal-to-ventral axis (Rübsamen 1992). Both of these axes are well defined in coronal brain sections and are commonly analyzed in 2D (Hirtz et al. 2012; Kim and Kandler 2003). However, the rostrocaudal dimensions of most auditory nuclei are similar or even larger in size than their medial-to-lateral extents (Sonntag et al. 2009). The 3D reconstruction of MNTB to SPN projections allowed us to visualize not only the tonotopic organization of inputs but also the rostrocaudal extend of inputs. In rats, cell bodies of SPN neurons and their dendritic trees were shown to extend para-sagittally (Saldaña and Berrebi 2000), but the physiological relevance of this rostrocaudal spread will have to be examined in future studies. While we were able to reconstruct a number of MNTB-SPN projections and see the synaptic arbor of the axon collaterals in the LSO within our 200-$\mu$m-thick sections, most of the ventrally directed collaterals were severed, suggesting that they follow a strong rostrocaudal gradient. These ventral collaterals might innervate the MSO, which is small in the mouse (Fischl et al. 2016), but has been successfully traced in a previous study in gerbil (Couchman et al. 2010). Performing similar tracing experiments in horizontal sections of rats or gerbils will help to identify possible rostrocaudal target-specific differences in the contribution of MNTB inhibition.

When we try and back-calculate the potential rostrocaudal dimension for the axonal arbors in the SPN from the 3D hull volume and the 2D hull area, the rostrocaudal distance seems to be very small, on the order of 10–30 $\mu$m. Such small distance would only span one to two cell layers and contradict what we saw in the syGlass virtual reality reconstruction tool. It is more likely that the 2D hull is an overestimation because some 3D information may arbitrarily contribute when the maximum projection image is created. Thus the 3D reconstruction seems advantageous even when focusing primarily on medial-to lateral dimensions.

*Different requirements of inhibition in the SPN compared with other MNTB targets.* Comparing our present data on inhibitory inputs to the SPN with previously published data on the MSO and LSO, we found two main differences: first, SPN neurons receive more inhibitory synaptic boutons compared with LSO and MSO, and second, the development of the SPN inhibitory inputs is largely complete before hearing onset.

Inhibition in the superior olivary complex operates on either a submillisecond time scale (e.g., sound localization in the LSO or MSO) or a millisecond to second time scale (e.g., encoding envelopes of vocal communication sounds in the SPN). Inhibition in the MSO and LSO complements the excitatory input in the temporal and spectral domain for sound localization (for review, see Grothe et al. 2010; Kandler et al. 2009; Tollin 2003). The developmental process of matching excitatory and inhibitory inputs in the LSO and MSO results in a low number of powerful inhibitory inputs (Couchman et al. 2010; Walcher et al. 2011). Here we show that in the SPN a higher number of inputs are maintained, with around 30 inhibitory synapses remaining at the soma. These inputs arrive from at least four different MNTB neurons, with axonal arbors spanning a large proportion of the tonotopic axis (Fig. 7*A*), consistent with SPN neurons integrating inhibition across a broad frequency range (in contrast to MSO or LSO neurons; Dehmel et al. 2002). Cross-frequency integration supports extraction of temporal information from fast fluctuations in sound envelope, which is a hallmark of the SPN physiology (Gómez-Álvarez et al. 2018; Oertel et al. 2017; Rhode and Greenberg 1994). In contrast, few but well-tuned inhibitory inputs in the LSO and MSO will facilitate the extraction of temporal fine structure necessary to localize sound sources in space.

Another target-specific property of MNTB inhibition to the SPN is its stability across the developmental critical period of hearing onset. This is consistent with changes in postsynaptic intrinsic properties and glutamatergic synaptic transmission that occur during the first postnatal week but stabilize around hearing onset (Felix and Magnusson 2016; Felix et al. 2013). This early maturation could imply that the MNTB-SPN inhibitory synaptic projection lacks sound-evoked plasticity. A second possibility is that this early maturation of the SPN inhibitory circuit contributes to developing maternal-pup vocal communication. The SPN is well equipped to encode communication calls (Gómez-Álvarez et al. 2018) and could, for example, coordinate the encoding of conspecific communication calls with the development of the pups' vocal production circuits. These ideas are currently under examination and will be part of future studies.

## ACKNOWLEDGMENTS

We thank Dr. Ian Forsythe for critical comments on an earlier version of this paper.

## GRANTS

This research was funded by the Deutsche Forschungsgemeinschaft (DFG) (SFB870 and GS-82 Graduate School of Systemic Neurosciences GSN$^{LMU}$).

## DISCLOSURES

No conflicts of interest, financial or otherwise, are declared by the authors.

## AUTHOR CONTRIBUTIONS

E.R., S.P., and C.K.-S. conceived and designed research; E.R. and S.P. performed experiments; E.R. and C.K.-S. analyzed data; E.R., S.P., B.G., and C.K.-S. interpreted results of experiments; E.R. and C.K.-S. prepared figures; E.R., S.P., B.G., and C.K.-S. edited and revised manuscript; E.R., S.P., B.G., and C.K.-S. approved final version of manuscript; C.K.-S. drafted manuscript.

## REFERENCES

**Balakrishnan V, Becker M, Löhrke S, Nothwang HG, Güresir E, Friauf E.** Expression and function of chloride transporters during development of inhibitory neurotransmission in the auditory brainstem. *J Neurosci* 23: 4134–4145, 2003. doi:10.1523/JNEUROSCI.23-10-04134.2003.

**Banks MI, Smith PH.** Intracellular recordings from neurobiotin-labeled cells in brain slices of the rat medial nucleus of the trapezoid body. *J Neurosci* 12: 2819–2837, 1992. doi:10.1523/JNEUROSCI.12-07-02819.1992.

**Ben-Ari Y, Khalilov I, Kahle KT, Cherubini E.** The GABA excitatory/inhibitory shift in brain maturation and neurological disorders. *Neuroscientist* 18: 467–486, 2012. doi:10.1177/1073858412438697.

**Bormann J, Hamill OP, Sakmann B.** Mechanism of anion permeation through channels gated by glycine and gamma-aminobutyric acid in mouse cultured spinal neurones. *J Physiol* 385: 243–286, 1987. doi:10.1113/jphysiol.1987.sp016493.

**Borst JG, Soria van Hoeve J.** The calyx of Held synapse: from model synapse to auditory relay. *Annu Rev Physiol* 74: 199–224, 2012. doi:10.1146/annurev-physiol-020911-153236.

**Cai S, Shan Z, Zhang Z, Moutal A, Khanna R.** Activity of T-type calcium channels is independent of CRMP2 in sensory neurons. *Channels (Austin)* 13: 147–152, 2019. doi:10.1080/19336950.2019.1608129.

**Choudhury N, Linley D, Richardson A, Anderson M, Robinson SW, Marra V, Ciampani V, Walter SM, Kopp-Scheinpflug C, Steinert JR, Forsythe ID.** Kv3.1 and Kv3.3 subunits differentially contribute to Kv3 channels and action potential repolarization in principal neurons of the auditory brainstem. *J Physiol* 598: 2199–2222, 2020. doi:10.1113/JP279668.

**Clause A, Kim G, Sonntag M, Weisz CJ, Vetter DE, Rűbsamen R, Kandler K.** The precise temporal pattern of prehearing spontaneous activity is necessary for tonotopic map refinement. *Neuron* 82: 822–835, 2014. doi:10.1016/j.neuron.2014.04.001.

**Couchman K, Grothe B, Felmy F.** Medial superior olivary neurons receive surprisingly few excitatory and inhibitory inputs with balanced strength and short-term dynamics. *J Neurosci* 30: 17111–17121, 2010. doi:10.1523/JNEUROSCI.1760-10.2010.

**Cuttle MF, Tsujimoto T, Forsythe ID, Takahashi T.** Facilitation of the presynaptic calcium current at an auditory synapse in rat brainstem. *J Physiol* 512: 723–729, 1998. doi:10.1111/j.1469-7793.1998.723bd.x.

**Dehmel S, Kopp-Scheinpflug C, Dörrscheidt GJ, Rübsamen R.** Electrophysiological characterization of the superior paraolivary nucleus in the Mongolian gerbil. *Hear Res* 172: 18–36, 2002. doi:10.1016/S0378-5955(02)00353-2.

**Elmqvist D, Quastel DM.** A quantitative study of end-plate potentials in isolated human muscle. *J Physiol* 178: 505–529, 1965. doi:10.1113/jphysiol.1965.sp007639.

**Felix RA 2nd, Fridberger A, Leijon S, Berrebi AS, Magnusson AK.** Sound rhythms are encoded by postinhibitory rebound spiking in the superior paraolivary nucleus. *J Neurosci* 31: 12566–12578, 2011. doi:10.1523/JNEUROSCI.2450-11.2011.

**Felix RA 2nd, Magnusson AK.** Development of excitatory synaptic transmission to the superior paraolivary and lateral superior olivary nuclei optimizes differential decoding strategies. *Neuroscience* 334: 1–12, 2016. doi:10.1016/j.neuroscience.2016.07.039.

**Felix RA 2nd, Vonderschen K, Berrebi AS, Magnusson AK.** Development of on-off spiking in superior paraolivary nucleus neurons of the mouse. *J Neurophysiol* 109: 2691–2704, 2013. doi:10.1152/jn.01041.2012.

**Fischl MJ, Burger RM, Schmidt-Pauly M, Alexandrova O, Sinclair JL, Grothe B, Forsythe ID, Kopp-Scheinpflug C.** Physiology and anatomy of neurons in the medial superior olive of the mouse. *J Neurophysiol* 116: 2676–2688, 2016. doi:10.1152/jn.00523.2016.

**Fischl MJ, Combs TD, Klug A, Grothe B, Burger RM.** Modulation of synaptic input by GABAB receptors improves coincidence detection for computation of sound location. *J Physiol* 590: 3047–3066, 2012. doi:10.1113/jphysiol.2011.226233.

**Franzen DL, Gleiss SA, Kellner CJ, Kladisios N, Felmy F.** Activity-dependent calcium signaling in neurons of the medial superior olive during late postnatal development. *J Neurosci* 40: 1689–1700, 2020. doi:10.1523/JNEUROSCI.1545-19.2020.

**Gómez-Álvarez M, Gourévitch B, Felix RA 2nd, Nyberg T, Hernández-Montiel HL, Magnusson AK.** Temporal information in tones, broadband noise, and natural vocalizations is conveyed by differential spiking responses in the superior paraolivary nucleus. *Eur J Neurosci* 48: 2030–2049, 2018. doi:10.1111/ejn.14073.

**Grothe B.** New roles for synaptic inhibition in sound localization. *Nat Rev Neurosci* 4: 540–550, 2003. doi:10.1038/nrn1136.

**Grothe B, Pecka M, McAlpine D.** Mechanisms of sound localization in mammals. *Physiol Rev* 90: 983–1012, 2010. doi:10.1152/physrev.00026.2009.

**Guzman SJ, Schlögl A, Schmidt-Hieber C.** Stimfit: quantifying electrophysiological data with Python. *Front Neuroinform* 8: 16, 2014. doi:10.3389/fninf.2014.00016.

**Hirtz JJ, Braun N, Griesemer D, Hannes C, Janz K, Löhrke S, Müller B, Friauf E.** Synaptic refinement of an inhibitory topographic map in the auditory brainstem requires functional Cav1.3 calcium channels. *J Neurosci* 32: 14602–14616, 2012. doi:10.1523/JNEUROSCI.0765-12.2012.

**Johnston J, Forsythe ID, Kopp-Scheinpflug C.** Going native: voltage-gated potassium channels controlling neuronal excitability. *J Physiol* 588: 3187–3200, 2010. doi:10.1113/jphysiol.2010.191973.

**Kaila K, Paalasmaa P, Taira T, Voipio J.** pH transients due to monosynaptic activation of GABAA receptors in rat hippocampal slices. *Neuroreport* 3: 105–108, 1992. doi:10.1097/00001756-199201000-00028.

**Kandler K, Clause A, Noh J.** Tonotopic reorganization of developing auditory brainstem circuits. *Nat Neurosci* 12: 711–717, 2009. doi:10.1038/nn.2332.

**Kandler K, Friauf E.** Development of glycinergic and glutamatergic synaptic transmission in the auditory brainstem of perinatal rats. *J Neurosci* 15: 6890–6904, 1995. doi:10.1523/JNEUROSCI.15-10-06890.1995.

**Kandler K, Gillespie DC.** Developmental refinement of inhibitory sound-localization circuits. *Trends Neurosci* 28: 290–296, 2005. doi:10.1016/j.tins.2005.04.007.

**Kapfer C, Seidl AH, Schweizer H, Grothe B.** Experience-dependent refinement of inhibitory inputs to auditory coincidence-detector neurons. *Nat Neurosci* 5: 247–253, 2002. doi:10.1038/nn810.

**Kawaguchi SY, Sakaba T.** Control of inhibitory synaptic outputs by low excitability of axon terminals revealed by direct recording. *Neuron* 85: 1273–1288, 2015. doi:10.1016/j.neuron.2015.02.013.

**Kim G, Kandler K.** Elimination and strengthening of glycinergic/GABAergic connections during tonotopic map formation. *Nat Neurosci* 6: 282–290, 2003. doi:10.1038/nn1015.

**Kim G, Kandler K.** Synaptic changes underlying the strengthening of GABA/glycinergic connections in the developing lateral superior olive. *Neuroscience* 171: 924–933, 2010. doi:10.1016/j.neuroscience.2010.09.054.

**Kopp-Scheinpflug C, Sinclair JL, Linden JF.** When sound stops: offset responses in the auditory system. *Trends Neurosci* 41: 712–728, 2018. doi:10.1016/j.tins.2018.08.009.

**Kopp-Scheinpflug C, Steinert JR, Forsythe ID.** Modulation and control of synaptic transmission across the MNTB. *Hear Res* 279: 22–31, 2011a. doi:10.1016/j.heares.2011.02.007.

**Kopp-Scheinpflug C, Tolnai S, Malmierca MS, Rübsamen R.** The medial nucleus of the trapezoid body: comparative physiology. *Neuroscience* 154: 160–170, 2008. doi:10.1016/j.neuroscience.2008.01.088.

**Kopp-Scheinpflug C, Tozer AJ, Robinson SW, Tempel BL, Hennig MH, Forsythe ID.** The sound of silence: ionic mechanisms encoding sound termination. *Neuron* 71: 911–925, 2011b. doi:10.1016/j.neuron.2011.06.028.

**Kotak VC, Korada S, Schwartz IR, Sanes DH.** A developmental shift from GABAergic to glycinergic transmission in the central auditory system. *J Neurosci* 18: 4646–4655, 1998. doi:10.1523/JNEUROSCI.18-12-04646.1998.

**Krächan EG, Fischer AU, Franke J, Friauf E.** Synaptic reliability and temporal precision are achieved via high quantal content and effective replenishment: auditory brainstem versus hippocampus. *J Physiol* 595: 839–864, 2017. doi:10.1113/JP272799.

**Kulesza RJ Jr, Grothe B.** Yes, there is a medial nucleus of the trapezoid body in humans. *Front Neuroanat* 9: 35, 2015. doi:10.3389/fnana.2015.00035.

**Kulesza RJ Jr, Spirou GA, Berrebi AS.** Physiological response properties of neurons in the superior paraolivary nucleus of the rat. *J Neurophysiol* 89: 2299–2312, 2003. doi:10.1152/jn.00547.2002.

**Kuwabara N, Zook JM.** Classification of the principal cells of the medial nucleus of the trapezoid body. *J Comp Neurol* 314: 707–720, 1991. doi:10.1002/cne.903140406.

**Lim R, Oleskevich S, Few AP, Leao RN, Walmsley B.** Glycinergic mIPSCs in mouse and rat brainstem auditory nuclei: modulation by ruthenium red and the role of calcium stores. *J Physiol* 546: 691–699, 2003. doi:10.1113/jphysiol.2002.035071.

**Löhrke S, Srinivasan G, Oberhofer M, Doncheva E, Friauf E.** Shift from depolarizing to hyperpolarizing glycine action occurs at different perinatal ages in superior olivary complex nuclei. *Eur J Neurosci* 22: 2708–2722, 2005. doi:10.1111/j.1460-9568.2005.04465.x.

**Lückermann M, Trapp S, Ballanyi K.** GABA- and glycine-mediated fall of intracellular pH in rat medullary neurons in situ. *J Neurophysiol* 77: 1844–1852, 1997. doi:10.1152/jn.1997.77.4.1844.

**Magnusson AK, Kapfer C, Grothe B, Koch U.** Maturation of glycinergic inhibition in the gerbil medial superior olive after hearing onset. *J Physiol* 568: 497–512, 2005. doi:10.1113/jphysiol.2005.094763.

**Makarenko VV, Ahmmed GU, Peng YJ, Khan SA, Nanduri J, Kumar GK, Fox AP, Prabhakar NR.** CaV3.2 T-type $Ca^{2+}$ channels mediate the augmented calcium influx in carotid body glomus cells by chronic intermittent hypoxia. *J Neurophysiol* 115: 345–354, 2016. doi:10.1152/jn.00775.2015.

**Milenković I, Rübsamen R.** Development of the chloride homeostasis in the auditory brainstem. *Physiol Res* 60, *Suppl* 1: S15–S27, 2011.

**Mudado MA, Rodrigues AL, Prado VF, Beirão PS, Cruz JS.** $Ca_V$ 3.1 and $Ca_V$ 3.3 account for T-type $Ca^{2+}$ current in GH3 cells. *Braz J Med Biol Res* 37: 929–935, 2004. doi:10.1590/S0100-879X2004000600020.

**Nabekura J, Katsurabayashi S, Kakazu Y, Shibata S, Matsubara A, Jinno S, Mizoguchi Y, Sasaki A, Ishibashi H.** Developmental switch from GABA to glycine release in single central synaptic terminals. *Nat Neurosci* 7: 17–23, 2004. doi:10.1038/nn1170.

**Noh J, Seal RP, Garver JA, Edwards RH, Kandler K.** Glutamate co-release at GABA/glycinergic synapses is crucial for the refinement of an inhibitory map. *Nat Neurosci* 13: 232–238, 2010. doi:10.1038/nn.2478.

**Oertel D, Cao XJ, Ison JR, Allen PD.** Cellular computations underlying detection of gaps in sounds and lateralizing sound sources. *Trends Neurosci* 40: 613–624, 2017. doi:10.1016/j.tins.2017.08.001.

**Oline SN, Burger RM.** Short-term synaptic depression is topographically distributed in the cochlear nucleus of the chicken. *J Neurosci* 34: 1314–1324, 2014. doi:10.1523/JNEUROSCI.3073-13.2014.

**Pedregosa F, Varoquaux G, Gramfort A, Michel V, Thirion B, Grisel O, Blondel M, Prettenhofer P, Weiss R, Dubourg V, Vanderplas J, Passos A, Cournapeau D, Brucher M, Perrot M, Duchesnay E.** Scikit-learn: machine learning in Python. *J Mach Learn Res* 12: 2825–2830, 2011.

**Pilati N, Linley DM, Selvaskandan H, Uchitel O, Hennig MH, Kopp-Scheinpflug C, Forsythe ID.** Acoustic trauma slows AMPA receptor-mediated EPSCs in the auditory brainstem, reducing GluA4 subunit expression as a mechanism to rescue binaural function. *J Physiol* 594: 3683–3703, 2016. doi:10.1113/JP271929.

**Rajaram E, Kaltenbach C, Fischl MJ, Mrowka L, Alexandrova O, Grothe B, Hennig MH, Kopp-Scheinpflug C.** Slow NMDA-mediated excitation accelerates offset-response latencies generated via a post-inhibitory rebound mechanism. *eNeuro* 6: ENEURO.0106-19.2019, 2019. doi:10.1523/ENEURO.0106-19.2019.

**Rhode WS, Greenberg S.** Encoding of amplitude modulation in the cochlear nucleus of the cat. *J Neurophysiol* 71: 1797–1825, 1994. doi:10.1152/jn.1994.71.5.1797.

**Rowan MJ, DelCanto G, Yu JJ, Kamasawa N, Christie JM.** Synapse-level determination of action potential duration by K(+) channel clustering in axons. *Neuron* 91: 370–383, 2016. doi:10.1016/j.neuron.2016.05.035.

**Rübsamen R.** Postnatal development of central auditory frequency maps. *J Comp Physiol A Neuroethol Sens Neural Behav Physiol* 170: 129–143, 1992. doi:10.1007/BF00196895.

**Saldaña E, Berrebi AS.** Anisotropic organization of the rat superior paraolivary nucleus. *Anat Embryol (Berl)* 202: 265–279, 2000. doi:10.1007/s004290000109.

**Sanes DH, Friauf E.** Development and influence of inhibition in the lateral superior olivary nucleus. *Hear Res* 147: 46–58, 2000. doi:10.1016/S0378-5955(00)00119-2.

**Schneggenburger R, Meyer AC, Neher E.** Released fraction and total size of a pool of immediately available transmitter quanta at a calyx synapse. *Neuron* 23: 399–409, 1999. doi:10.1016/S0896-6273(00)80789-8.

**Smith AJ, Owens S, Forsythe ID.** Characterisation of inhibitory and excitatory postsynaptic currents of the rat medial superior olive. *J Physiol* 529: 681–698, 2000. doi:10.1111/j.1469-7793.2000.00681.x.

**Sommer I, Lingenhöhl K, Friauf E.** Principal cells of the rat medial nucleus of the trapezoid body: an intracellular in vivo study of their physiology and morphology. *Exp Brain Res* 95: 223–239, 1993. doi:10.1007/BF00229781.

**Sonntag M, Englitz B, Kopp-Scheinpflug C, Rübsamen R.** Early postnatal development of spontaneous and acoustically evoked discharge activity of principal cells of the medial nucleus of the trapezoid body: an in vivo study in mice. *J Neurosci* 29: 9510–9520, 2009. doi:10.1523/JNEUROSCI.1377-09.2009.

**Tadayonnejad R, Mehaffey WH, Anderson D, Turner RW.** Reliability of triggering postinhibitory rebound bursts in deep cerebellar neurons. *Channels (Austin)* 3: 149–155, 2009. doi:10.4161/chan.3.3.8872.

**Takahashi T, Kajikawa Y, Tsujimoto T.** G-Protein-coupled modulation of presynaptic calcium currents and transmitter release by a GABAB receptor. *J Neurosci* 18: 3138–3146, 1998. doi:10.1523/JNEUROSCI.18-09-03138.1998.

**Thanawala MS, Regehr WG.** Determining synaptic parameters using high-frequency activation. *J Neurosci Methods* 264: 136–152, 2016. doi:10.1016/j.jneumeth.2016.02.021.

**Tollin DJ.** The lateral superior olive: a functional role in sound source localization. *Neuroscientist* 9: 127–143, 2003. doi:10.1177/1073858403252228.

**Vandael DH, Espinoza C, Jonas P.** Excitement about inhibitory presynaptic terminals. *Neuron* 85: 1149–1151, 2015. doi:10.1016/j.neuron.2015.03.006.

**Walcher J, Hassfurth B, Grothe B, Koch U.** Comparative posthearing development of inhibitory inputs to the lateral superior olive in gerbils and mice. *J Neurophysiol* 106: 1443–1453, 2011. doi:10.1152/jn.01087.2010.

**Walter AM, Böhme MA, Sigrist SJ.** Vesicle release site organization at synaptic active zones. *Neurosci Res* 127: 3–13, 2018. doi:10.1016/j.neures.2017.12.006.

**Weisz CJ, Rubio ME, Givens RS, Kandler K.** Excitation by Axon Terminal GABA Spillover in a Sound Localization Circuit. *J Neurosci* 36: 911–925, 2016. doi:10.1523/JNEUROSCI.1132-15.2016.

**Winters BD, Golding NL.** Glycinergic inhibitory plasticity in binaural neurons is cumulative and gated by developmental changes in action potential backpropagation. *Neuron* 98: 166–178.e2, 2018. doi:10.1016/j.neuron.2018.03.001.

**Yassin L, Radtke-Schuller S, Asraf H, Grothe B, Hershfinkel M, Forsythe ID, Kopp-Scheinpflug C.** Nitric oxide signaling modulates synaptic inhibition in the superior paraolivary nucleus (SPN) via cGMP-dependent suppression of KCC2. *Front Neural Circuits* 8: 65, 2014. doi:10.3389/fncir.2014.00065.

Chapter 4

# Discussion

The ability of SPN neurons to fire at the offset of sound stimulus is its characterizing feature, despite species-dependent diversity in the structure of the SPN. Along with other labs, we have demonstrated that the SPN receives major inhibition and minor excitation. In *in vivo* experiments, during a sound stimulus, when the MNTB fires, the SPN remains under inhibitory constrain and when the inhibition stops at sound offset, SPN neurons respond with rebound action potentials. Intriguingly, half the SPN neurons also fired during the sound stimulus, despite the inhibition. We refer to this response as ON-OFF response with the remaining cells displaying an OFF-only response. These two firing patterns indicate a delicate balance between excitation and inhibition, with excitation gaining a measurable impact on about half of the SPN neurons. The role of excitation in this circuit, and the difference it makes in the firing properties of SPN neurons was analyzed in Chapter 2.

The neurons with ON-OFF responses (with more excitation) had shorter offset-response latencies compared to neurons with OFF-only responses. In addition, the offset latencies were also rendered more level invariant for a wide range of supra-threshold intensities. We have shown through pharmacological experiments and computational modelling that slow NMDA-R mediated excitation

plays a crucial role in improving these two temporal features of the offset response. Presumably, the improved temporal precision has beneficial effects downstream in auditory processing. The physiological roles of offset responses are still not completely understood. Their main contributions are to sound duration encoding and gap detection. But how exactly the offset firing of the SPN impacts information processing in the inferior colliculus is not yet known. Nevertheless, the question raised by this thesis is why only half of the SPN neurons show signs of excitation when its effect seems beneficial for temporal precision of the responses. I would like to discuss it in the following contexts: 1) Are there two different types of SPN neurons? 2) Are excitation and inhibition differently regulated during development? 3) Does shifting the balance between excitation and inhibition in the SPN provide a tool to adapt offset-response latencies to the need of a specific situation, like a change in overall activity?

## 4.1 Are there two different types of neurons in SPN?

Definition of cell types within a nucleus can be based on the morphology of the cells (for e.g., basket cells, pyramidal cells, fusiform cells, stellate cells, etc.), electrophysiological characteristics of the cells (for e.g. fast-firing, burst-firing, sustained-firing, etc.) or molecular characteristics (for e.g., parvalbumin-expressing, somatostatin- expressing cells, etc.). Recent high-throughput single cell sequencing methods could provide additional insights and define molecular cell types based on the genetic make-up of cells. This however does not discount defining cell types based on their electrophysiological characteristics or connectivity, since they ultimately help to better understand information processing within a neural circuit.

The emergence of two types of neuronal temporal response patterns in the SPN could potentially be attributed to two different neuronal cell types within the SPN. Early studies have described two morphologically distinct types of cells in the SPN / DMPO of cats, bats, guinea pigs and other large mammals (Aschoff and Ostwald, 1987; Azeredo et al., 1999; Helfert et al., 1989; Morest, 1968; Nordeen et al., 1983; Willard and Martin, 1983). In guinea pigs, a more detailed study has even described up to five cell types (Brett R. Schofield, 1991). In the mouse model however, the morphological features, with almost 95% of the cells described to be large and multipolar and less

than 5% of cells showing fusiform or spindle shaped morphology, are not sufficiently distinct to warrant their categorization into distinct types (Ollo and Schwartz, 1979; Willard and Martin, 1983). However, Felix and colleagues have described three types of SPN neurons, based on *in vitro* firing properties, with one type of neuron showing bursting responses, located in the dorsolateral region of the SPN (Felix II RA et al., 2013).

If the morphologically or electrophysiologically distinct neuronal cell types occupy different regions within the SPN, differences between such cell types would manifest as a difference in the characteristic frequency, given the tonotopic nature of the SPN (Banks and Smith, 1992; Kelly et al., 1998; Saldaña et al., 2009). However, neither characteristic frequencies and thresholds nor spontaneous firing rates were significantly different between ON-OFF and OFF-only cells (Rajaram et al., 2019, Chapter 2). Our immunocytochemical investigation of the excitatory and inhibitory inputs, through vesicular glutamate and glycine transporters also did not support the notion of a heterogenous nucleus, with distinct cell types. The balance between excitation and inhibition could be tipped in favour of one more than the other at different times in order to achieve the two response modalities. The benefit of having two lines of information encoding with one line faster than the other, requires a much better understanding of SPN-IC connections and their physiological relevance. It is also necessary to consider what role the spindle shaped fusiform cells might play in the larger mammals. Do they represent one of the two subtypes with ON-OFF or OFF-only responses or do their response properties represent a completely distinct response type? This will be an important question to consider within the physiologically relevant context of the model organism by employing a combined anatomical and physiological approach. Since the balance of excitation and inhibition plays a critical role in defining the response properties of SPN neurons we studied the development of the excitatory and inhibitory inputs to the SPN around hearing onset, which has been shown to play a significant role in refining other SOC circuits (Kandler et al., 2009; Magnusson et al., 2005; Werthat et al., 2008).

## 4.2 Are excitatory and inhibitory differently regulated during development?

### 4.2.1 Development of excitation

The importance of excitation in the SPN circuit was highlighted earlier in Chapter 2. The excitatory conductance that the SPN receives is markedly weaker than the inhibitory conductance. This is in stark contrast to the levels of excitation measured in the MSO and LSO, where the excitatory and inhibitory conductances are in balance (Couchman et al., 2010; reviewed in: Grothe et al., 2010; Pilati et al., 2016). The development of excitation to the SPN has been recently investigated (Felix et al 2016, 2017). Felix et al., report developmental plasticity in the VCN derived excitation to the SPN. The excitatory inputs were observed to be pruned after hearing onset. The ratio of maximum to minimum EPSC evoked by stimulating the axons in the intermediate acoustic stria reduced from around 10 to 2 reflecting pruning in the number of fibers that innervate a given SPN cell. The maximum EPSCs however were observed to be the same through the onset of hearing. The loss of inputs seems to be compensated by an increase in the release probability. The synaptic elimination and strengthening of the remaining fibers were thus shown to be similar in SPN and LSO (Kandler et al., 2005; Kim et al., 2010). The VCN-LSO synapse convergence of 12 fibers reduced to 5 fibers after hearing onset (Felix II and Magnusson, 2016).

Our results are in line with the published data from LSO and MSO neurons and can confirm that the maximum EPSC amplitudes remain stable throughout the three age groups tested- P9-11 (before hearing onset), P12-14 (during hearing onset) and P15-22 (after hearing onset). The amplitude of the EPSCs did not change significantly between prehearing and posthearing ages. The synaptic refinement of the excitatory input seen between time periods P5-11 and P12-22, in the MNTB-to-LSO/MSO projection (ref from above) were not evident when comparing smaller time bins of P9-11, P12-14 and P15-22 around hearing onset. We observed that there is indeed an overall trend of decrease in the convergence of excitatory inputs to the SPN. The ratio of the maximum EPSC to the minimum EPSC, recorded while stimulating the axons at maximum and close to minimum strength for the three periods reflected a decreasing trend, which was not statistically significant. These results

suggest that if there is refinement, the elimination of excitatory synapses could be more pronounced at an earlier stage, before hearing onset. The synaptic elimination observed in the LSO also seems to take place before hearing onset. NMDA currents have been shown to peak in the LSO before hearing onset and believed to play an important role in inhibitory synaptic refinement (Case et al., 2011; reviewed in: Eckhard Friauf et al., 2019).

To ascertain the contribution of NMDAR to the excitation in the SPN during this time period, Felix et al., blocked NMDAR mediated current by washing in 2-amino-5-phosphonopentanoic acid (D-AP5), a NMDAR specific antagonist. The authors found that the antagonist did not affect the EPSC amplitudes, at a membrane holding potential of –60 mV and hence infer that the contribution of NMDAR in the SPN to be negligible. In that report, NMDARs could be under magnesium block at resting membrane potential and it may require sustained depolarization to remove the magnesium block. Therefore we approached these measurements in voltage-clamp mode so that we could apply such depolarization directly via the patch pipette. As a result, we were indeed able to detect NMDAR mediated EPSCs in all the three age groups tested. We measured the level of NMDA current in the SPN by holding the cell at depolarized membrane potentials of +40 mV and isolated NMDA currents in the presence of AMPAR antagonist -6,7-dinitroquinoxaline-2,3-dione (DNQX). We could also confirm histochemically, that SPN neurons express NMDARs, visualized by staining with anti-NMDA-NR2C antibodies. Electrophysiological measurement of NMDA currents showed that they were sensitive to D-AP5 and revealed the characteristic voltage-dependence causing larger currents once the membrane voltage reaches depolarized values. Given the MNTB's inhibitory control over the SPN, one could question the physiological significance of NMDA currents at more depolarized voltages. Though the excitatory conductances are smaller than the inhibitory conductances, the timing of excitation and inhibition can be different and could allow for the ON-OFF firing pattern. The initial excitation at the onset could release the magnesium block of NMDARs and hence the role of NMDARs in the SPN should not be discounted.

The NMDA currents in SPN neurons were larger in prehearing mice with values significantly decreasing during further postnatal development Decay time constants also decreased with postnatal

development. The slowly decaying EPSCs mediated by NMDARs seems to play an important role in reducing the latency of offset response in the SPN. Similar to the LSO, the NMDAR expression peaks in the SPN before hearing onset and appears to plateau after hearing onset. It is likely that increase in NMDAR expression plays a role in synaptic refinement of inhibitory inputs, as shown in the LSO. MNTB-LSO and VCN-LSO synaptic refinement coincides with prominent NMDAR activity, which decreases with time. This is corroborated in a mouse model lacking glutamate co-release from MNTB axons that result in perturbed synaptic refinement (Case et al., 2011; Noh et al., 2010).

### 4.2.2 Development of inhibition

In chapter 3, we investigated the developmental changes of the inhibitory inputs to the SPN that take place around hearing onset. Surprisingly, we did not observe any significant differences in the amplitude of the IPSCs during hearing onset. The kinetics of the IPSCs do however change significantly with age, which is similar to what has been observed in the neighboring nuclei of LSO and MSO (Magnusson et al., 2005; Pilati et al., 2016). We observed no evidence for a loss of synapses in the time period around hearing onset, as seen in the LSO. The number of inhibitory synaptic inputs to the SPN was estimated by different methods, namely the ratio of the maximum and minimum amplitude of evoked currents and clustering of the current amplitudes with increasing strength of synaptic stimulation. Both methods support that there is no synaptic elimination during posthearing development in the SPN. We also showed that neither the frequency nor the amplitude of spontaneous inhibitory synaptic events is significantly altered with the onset of hearing, suggesting that the presynaptic strength and post-synaptic responsiveness remain unaltered. It is only when the synapse is challenged with high frequency stimulation that synaptic changes become evident between the different age groups. The rate of synaptic depression increases with time, also seen as an increase in the probability of release. The probability of release of the excitatory input has also been shown to increase with age in the SPN (R. a. Felix and Magnusson, 2016). In the LSO, the loss of synaptic inputs is compensated by an increase in quantal size (G Kim and Kandler, 2010). In the SPN, the quantal size of the inhibitory inputs remained stable, reflected by the amplitudes of both the miniature IPSCs and the evoked IPSCs. Apart from the quantal size, the driving force of the IPSC, dictated by the chloride concentration, could compensate for a loss in the number of synapses. We

examined for changes in this factor, by measuring at the reversal potential of the IPSC in the different age groups. We found that the reversal potential of the IPSC was also stable during hearing onset (see Appendix).

The differences in the development of synaptic properties in the connections made by MNTB axon collaterals in the SPN, LSO and MSO suggest that there is target specific synaptic plasticity, which is determined by the postsynaptic cells. Axon collaterals that project to different nuclei can show remarkable heterogeneity. Heterogeneity within axon collaterals has been shown in axon diameter and axon thickness within the auditory brainstem (Seidl and Rubel, 2016). The differences in synaptic properties among synapses which share the same presynaptic source has also been shown in other brain regions such as the hippocampus (Sun et al., 2005, Rockland, 2018). Potential mechanisms to achieve such target specific synaptic differences include the signalling cascades activated by diffusible secreted synaptic organizers such as Wnts and Fibroblast growth factors (reviewed in Yuzaki, 2018).

## 4.3 Activity-dependent plasticity of inhibition in the SPN

In Chapter 3, we demonstrated that the increase in sound-evoked activity that accompanies the onset of hearing does not cause strong synaptic plasticity of the inhibitory inputs to the SPN.In contrast, inhibition in both the LSO and the MSO underwent plastic changes in their inhibitory input across the onset of hearing. This may suggest that inhibition in LSO and MSO is generally more plastic while it may be more stable in the SPN. However, Pilati and colleagues described an acoustic over exposure paradigm that caused changes in the excitatory input into the LSO, but not the inhibitory input, when the exposure took place well after hearing onset (Pilati et al., 2016). Does that mean that once developed, the inhibition does not undergo plastic changes at all? That study investigated a time scale of one week and more after the exposure, maybe that was too long and possible early inhibitory plasticity was missed. Therefore we used the same acoustic over exposure paradigm, but tested the mice at more immediate time points after the exposure: 0 hours, 24 hours and 48 hours. The 0 hours and the 48 hours exposure results are not yet conclusive, so that here, I will discuss some of my results from the 24 h time point.

Anesthetized mice received a single, 2 hour exposure to bandpass-filtered noise (8- 16 kHz) at 107 dB SPL. We are aware that this sound intensity is likely to cause some synaptopathy at the inner hair cell – auditory nerve synapse even after a single exposure (Kujawa  Liberman, 2009; reviewed in: Liberman  Kujawa, 2017). Therefore, we initially kept the exposure parameters equal to the study by Pilati et al for comparison, but we later added another paradigm using only 94dB SPL exposure intensity. Auditory brain stem response (ABR) recordings were performed before and after the noise exposure to assess the success of the exposure by monitoring changes in hearing threshold. After the acoustic over exposure, the animals were allowed to recover for 24 hours. Following this recovery period, I evaluated synaptic changes in the SPN using *in vitro* whole-cell patch clamp techniques.

As I described in the introduction, changes in the mini frequency typically indicate an underlying presynaptic mechanism, while changes in the mini amplitude suggest the involvement of the postsynaptic neuron. In our study, the frequency of miniature IPSC (mIPSC) events increased significantly after acoustic over exposure, compared to un-exposed control animals. The amplitude of the mIPSCs, however, did not show significant differences between the control animals and the noise exposed animals. Consequently, we investigated possible presynaptic sound-exposure induced changes in the SPN. An increase in mIPSC frequency can be caused by an increase in the number of inhibitory synaptic terminals or by changes in the presynaptic release machinery of pre-existing inhibitory terminals. Surprisingly, synaptic depression, the size of the readily releasable pool of vesicles and the probability of release of such a vesicle were unaffected by the sound over exposure (data not shown). This lack of changes in the classical presynaptic release machinery suggested that the increase in mIPSC frequency might be due to an increase in the number of synapses or the number of release sites at existing terminals.

We took two approaches to estimate the number of synaptic terminals: first, we compared the amplitude of the evoked IPSCs during maximum stimulation and found that to be significantly higher in the sound exposed animals. Additionally, we used immunohistochemical techniques to assess changes in the numbers of synaptic terminals. For most direct immunohistological comparison, we took advantage of the monaural acoustic innervation patterns of the SPN and used a unilateral noise

exposure protocol, where only one ear was exposed to the noise while the other ear served as an internal control. Synaptic changes were studied by staining for Glycine transporter 2, a pre-synaptic marker, which revealed an increase in synaptic boutons on the noise-affected side (contralateral to the exposed ear) in comparison to the control side (ipsilateral to the exposed ear). But how can new inhibitory synapses form in the mature brain, when the chloride reversal potentials are such that glycine or GABA elicit an influx of chloride and not an efflux as seen during the development of inhibitory synapses?

Early in development, GABAergic and glycinergic inputs are initially depolarizing due to the high concentration of chloride ions within the cell. This is believed to facilitate the formation of synapses through the Hebbian mechanism of "cells that fire together, wire together", in a time-dependent manner (Ben-Ari et al., 2012). Hebbian rules dictate that the presynaptic activity that leads to an action potential in the postsynaptic cell strengthens a synapse and presynaptic activity that follows an action potential in the postsynaptic weakens the synapse (Ben -Ari et al., 2012). A possible mechanism to facilitate synapse formation based on Hebbian plasticity rules is to make the postsynaptic neuron more excitable. Hence, we compared the intrinsic excitability of SPN neurons after acoustic exposure to non-exposed controls. We observed a significant increase in the input resistance and a significantly depolarized resting membrane potential in SPN neurons of exposed animals. Moreover, the ability of the SPN neurons to fire action potentials at stimulus offset was markedly higher in the noise-exposed groups. The number of action potentials fired upon the application of positive depolarizing current was also significantly higher in the noise-exposed group. While the increase in the excitability of the neurons could play an important role in the synaptogenesis, the exact contribution of increased excitability to synaptogenesis is not clear. Given the time dependent nature of Hebbian plasticity rules, it is not clear how presynaptic activity can be timed to precede postsynaptic action potentials to facilitate synaptogenesis. Other studies have however shown that acoustic over exposure leads to increased excitability in the cochlear nucleus and the inferior colliculus within a similar time frame ranging from 24 hrs to a week (Li et al., 2013; Shuang Li et al., 2015; Longenecker  Galazyuk, 2011, 2016; Vogler et al., 2011). On the other hand, acoustic over exposure has been shown to cause loss of inhibition or synaptic reorganization in the cochlear

nucleus and the inferior colliculus within a week or two (Middleton et al., 2011; Sturm et al., 2017; Wang et al., 2009b). It cannot be ruled out that within the SPN, there is an immediate loss of synapses following the noise exposure and it could be compensated for by an increase through homeostatic mechanisms. This necessitates the need for further studies at different time points and with different sound intensity levels.

## 4.4 Physiological significance of the SPN

SPN and offset firing responses have been implicated in gap detection and sound duration encoding; the physiological role of SPN however, is not well understood. Before delving into investigations studying the role of SPN neurons, the connectivity between the SPN and its main target, the IC, the nature of SPN output and the physiological significance of the target IC cell needs to be better understood. While the majority of SPN neurons fire their characteristic offset response in the mouse and the rat model (Kulesza et al., 2003, Kopp-Scheinpflug et al., 2011 and Rajaram et al., 2019), other response types such as onset, onset tonic and chopper firing have also been reported in the Gerbil and rabbit (Dehmel et al., 2002 and Behrend et al., 2002). The offset response neurons in the various models could play a role in gap detection (reviewed in Kopp-Scheinpflug et al., 2018). However, the exact pathway and the mechanism for gap detection encoding is not yet known. Systematic studies that investigate gap detection behaviour, while inactivating the SPN and other brain regions that have been shown to be involved in offset responses, could help delineate the role of SPN and the offset firing cells in gap detection. Another approach could be using transgenic mouse lines that reduce the impact of the synaptic inhibition and affect the ionic mechanisms underlying offset firing in the SPN, such as mouse lines with targeted knock down of KCC2 or HCN1 in the SPN. Disrupting the offset firing properties specifically in the SPN and then other brain regions with offset response could prove to be beneficial in understanding the role of the offset response in gap detection. The same approaches can also be used to investigate the role of offset firing in sound duration encoding. Once the role of offset firing neurons are understood, future studies can aim to then understand the role of onset, onset tonic and chopper firing cells within the SPN of other animal models.

## 4.5 Conclusion

Characterizing the inputs to SPN revealed strong synaptic inhibition and weak excitatory inputs. The excitation, while weak, still plays an important role in increasing the temporal precision of the characteristic offset response of the SPN. The presence of slow NMDAR conductance has been shown to peak before hearing onset hinting at a role in synaptic refinement during the onset of hearing as seen in other SOC nuclei. However, while the membrane kinetics and the kinetics of the synaptic currents change in the SPN with age, there is no evidence of synaptic pruning, as seen in the LSO or MSO during the time around hearing onset. Any activity-dependent plasticity induced by sound over exposure has to be carefully disentangled to whether it is within changes of normal physiology or whether it can be seen as pathophysiological changes of the auditory circuit. Here, we see evidence for an increase in the number of inhibitory synapses in the SPN after acoustic over stimulation. An increase in the intrinsic excitability of the neurons could be an important homeostatic response to facilitate the formation of inhibitory synapses. This could be a prerequisite for the formation of new inhibitory synapses in other brain regions as well. Understanding the molecular signaling pathways that underlie this increase in intrinsic excitability could pave the way for novel therapeutic targets and thus, making the SPN an ideal model to study inhibitory plasticity in the absence of competing excitation.

Appendix A

# Role of KCC2 and the reversal potential of glycinergic current

The classical approach to investigate the chloride concentration within a cell is by using the perforated patch technique (Horn and Marty, 1988). Antibiotics like gramicidin are used in the pipette solution to form pores in the cell membrane facilitating the flux of monovalent cations, but not anions, across the cell membrane. The cell is then held at different membrane potentials and synaptic currents are evoked. The potential at which there is no net synaptic current is the reversal potential of the current. In case of glycinergic currents, this becomes the reversal potential of chloride. The reversal potential can then be used to calculate the concentration of chloride within the cell. The whole cell patch clamp technique on the other hand is believed to flood the cell with the pipette solution and hence, a read out of the reversal potential of the glycinergic current in this case, is considered to be the read out of the concentration of chloride in the pipette solution.

However, we have shown earlier that this is not entirely true. The cell still influences the internal concentration of chloride ions. The internal concentration of chloride measured from the reversal potential of glycinergic currents in whole-cell patch clamp recordings of SPN neurons, with high concentration of chloride within the pipette solution were found to be significantly different

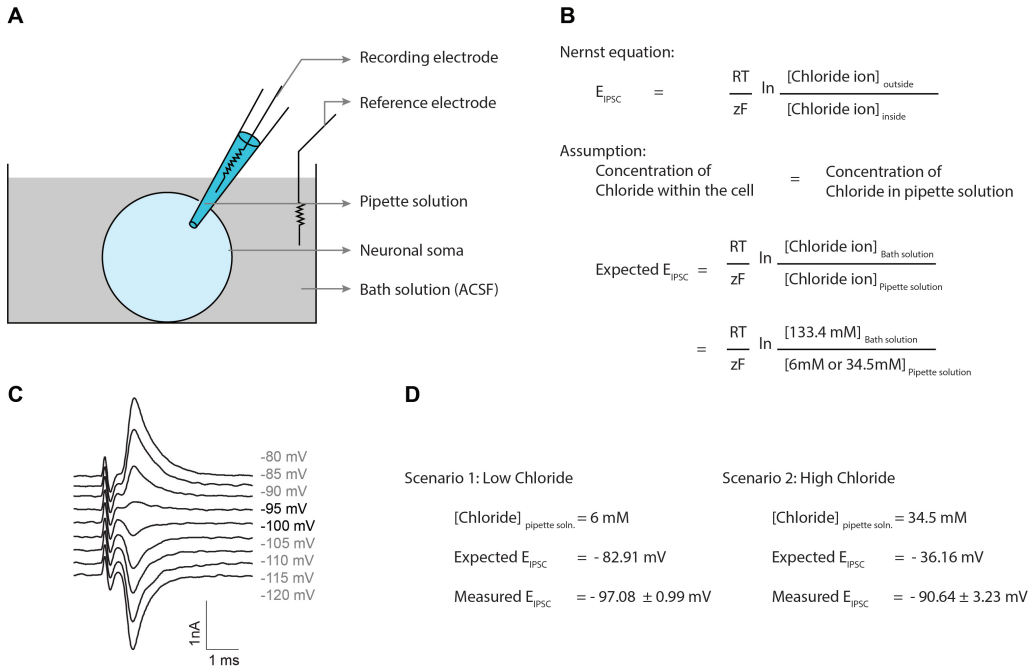


Figure A.1. Deviation of the measured reversal potential of the chloride current from the Nernst equation value. A: Schematic representation of the *in vitro* whole cell patch clamp set up that can measure the currents and potential differences between the recording electrode and the reference electrode. The bath solution is artificial cerebrospinal fluid (ACSF) B: Nernst equation to calculate the reversal potential of an ion, chloride in this case. C: Traces from a protocol that is used to estimate the reversal potential of the synaptic current (IPSC) by holding the cell in different holding potentials.D: Two different pipette solutions were used - one with low chloride concentration and another with high chloride concentration. The measured reversal potentials were more negative than the calculated values in both scenarios.

from calculated estimates using the Nernst Equation (Figure A.1). Furthermore, pharmacological blockade of the neuronal chloride transporter Potassium-Chloride Co-transporter 2 (KCC2) has been shown to shift the measurements of the reversal potential of IPSCs towards the calculated values (Kopp-Scheinpflug et al., 2011; Yassin et al., 2014). This suggests that the read out of the reversal potential of IPSCs can be used as a physiological measure of the chloride transporter activity.

An important pre-requisite for the characteristic rebound firing of the SPN cells at stimulus offset, is strongly hyperpolarizing inhibition. This is achieved through an abundance of glycinergic inputs and receptors coupled to a strong driving force for chloride. The driving force, dictated by the concentration of chloride within the cell, is set by the chloride transporters. Within the auditory

brainstem, the level of KCC2 activity is different in different nuclei. The developmental depolarization-hyperpolarization (D/H) shift of the inhibitory inputs happens at different time points in the MSO, LSO and the SPN (Löhrke et al., 2005). While this shift happens in the LSO during P4-5, and during P5-9 in the MSO, it happens as early as E18-P1 in the SPN. The estimated reversal potential of glycinergic currents is also much lower in the SPN, compared to the LSO and MSO (Yassin et al., 2014) . Together they suggest that KCC2 activity is stronger and that it gets activated earlier during development in the SPN. A rapidly declining expression and activity of a chloride importer could also account for this earlier shift and strong driving force of chloride in the SPN. It is noteworthy that the identity of the chloride importer is not yet established in the auditory brainstem. It is believed that the chloride – bicarbonate transporter (AE3) could play the role of the chloride importer in the SOC. If the strong driving force is mainly attributed to the functional levels of KCC2 is not yet clear.

However there have been studies about factors that determine the functional level of KCC2. It has been shown that the trafficking, cell surface expression and the functional activity of KCC2 are linked to neuronal activity and that its activity is linked to protein oligomerization and phosphorylation (Blaesse et al., 2006; Casula et al., 2001; Chamma et al., 2012; Fiumelli et al., 2005; Wake et al., 2007). Many sites for phosphorylation have been identified and they have been shown to be important for development and their disruption linked with pathology (Y. E. Moore et al., 2019; Pisella et al., 2019; Rinehart et al., 2009; Watanabe et al., 2019). Systematic studies of each phosphorylation site are essential to understand how the chloride transporter function is regulated. In collaboration with the Nothwang-lab, we started an investigation of the specific role of phosphorylation at KCC2- Serine-937 in the LSO and SPN. A phosphorylated version of KCC2 was created by mutating the Serine-937 to Aspartate to mimic the phosphorylated status. Additionally, a de-phosphorylated version of KCC2 was produced by replacing Serine-937 by Alanine. Transgenic mice were then created carrying either the phosphorylated version of KCC2 (KCC2-Phospho) or the de-phosphorylated version of KCC2 (KCC2-Dephospho) using the CRISPR-Cas9 system. We investigated if the phosphorylation status has an impact on KCC2 activity, by testing the reversal potential of IPSCs in LSO and SPN.

Interestingly, our analysis showed that the effect of KCC2 phosphorylation is different be-

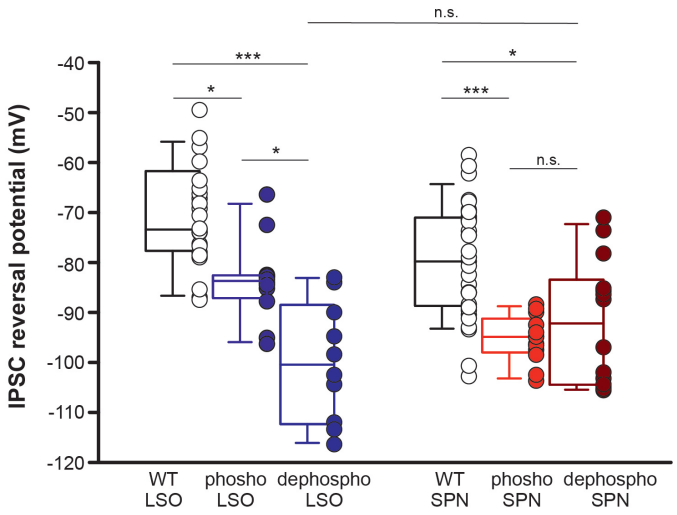


Figure A.2. Impact of KCC2 Serine 937 phosphorylation on the chloride transporter activity. Phosphorylation status plays a significant role in the LSO with the phosphorylated version of KCC2 signifcantly lowering the reversal potential of IPSC and the KCC2-dephospho with even lower reversal potential. KCC2-phospho resulted in a significantly lower reversal potential in the SPN, but the dephosphorylated version did not show a significant difference to KCC2-phospho group in the SPN.

tween SPN and LSO. In the SPN, the reversal potential of IPSC did not differ significantly between KCC2-Phopho, KCC2-dephospho and Wildtype mice (Figure A.2). This suggests that the phosphorylation status does not affect the function of KCC2. In the LSO however, there was a significant difference between KCC2-Phospho and the KCC2 WT groups. Taken together, this suggests that the phosphorylation of Serine 937 in KCC2 has an effect only in the LSO. The dephosphorylation did not significantly change the functional status of KCC2 in both the LSO and SPN, when compared to the wildtype.

A possible explanation could be that the KCC2 in the LSO can be activated by phosphorylation at S937, and the KCC2 in SPN could already be in the activated state, independent of the S937 phosphorylation. It has been shown that Serine 940 of KCC2 can be phosphorylated by the PKC pathway to activate the transporter (Lee et al., 2007). There are many more sites for phosphorylation and other post translational modifications that regulate the activity of KCC2, which warrants the need for more studies(Rinehart et al., 2009). It is noteworthy that the independence of KCC2 activity from phosphorylation status at S937, hints at tighter regulation to always keep the transporter in

an activated state and ensure strong hyperpolarization crucial for SPN neurons to produce their hallmark offset response. Higher activation level of KCC2 in SPN can also explain why even when a high concentration of chloride is used in the pipette solution to measure the reversal potential, the estimates of SPN are significantly lower than the estimates of LSO neurons (Yassin et al., 2014; figure 4.1). It is not yet clear which kinases are responsible for the phosphorylation of S937 and the differences in the phosphorylation pathways between the SPN and LSO are also not yet fully understood. Since the activity of kinases and phosphatases are also regulated by phosphorylation, pharmacologic approaches are extremely difficult.

# References


Adams, J. C. (1983). Cytology of periolivary cells and the organization of their projections in the cat. Journal of Comparative Neurology, 215(3), 275–289. 10.1002/cne.902150304

Altieri, S. C., Zhao, T., Jalabi, W., and Maricich, S. M. (2014). Development of glycinergic innervation to the murine LSO and SPN in the presence and absence of the MNTB. Frontiers in Neural Circuits, 8(September), 109. 10.3389/fncir.2014.00109

Altschuler, R. A., and Shore, S. E. (2010). Central auditory neurotransmitters (Issue June 2018). Oxford University Press. 10.1093/oxfordhb/9780199233281.013.0004

Aschoff, A., and Ostwald, J. (1987). Different origins of cochlear efferents in some bat species, rats, and guinea pigs. Journal of Comparative Neurology, 264(1), 56–72. 10.1002/cne.902640106

Azeredo, W. J., Kliment, M. L., Morley, B. J., Relkin, E., Slepecky, N. B., Sterns, A., Warr, W. B., Weekly, J. M., and Woods, C. I. (1999). Olivocochlear neurons in the chinchilla: A retrograde fluorescent labelling study. Hearing Research, 134(1–2), 57–70. 10.1016/S0378-5955(99)00069-6

Bajo, V. M., Merchán, M. A., López, D. E., and Rouiller, E. M. (1993). Neuronal morphology and efferent projections of the dorsal nucleus of the lateral lemniscus in the rat. The Journal of Comparative Neurology, 334(2), 241–262. 10.1002/cne.903340207

Banks, M. I., and Smith, P. H. (1992). Intracellular recordings from neurobiotin-labeled cells in brain slices of the rat medial nucleus of the trapezoid body. The Journal of Neuroscience: The Official Journal of the Society for Neuroscience, 12(7), 2819–2837.

Bauer, C. A., Turner, J. G., Caspary, D. M., Myers, K. S., and Brozoski, T. J. (2008). Tinnitus and inferior colliculus activity in chinchillas related to three distinct patterns of cochlear trauma. Journal of Neuroscience Research, 86(11), 2564–2578. 10.1002/jnr.21699

Behrend, O., Brand, A., Kapfer, C., and Grothe, B. (2002). Auditory response properties in the superior paraolivary nucleus of the gerbil. Journal of Neurophysiology, 87(6), 2915–2928.

Ben-Ari, Y., Woodin, M. A., Sernagor, E., Cancedda, L., Vinay, L., Rivera, C., Legendre, P., Luhmann, H. J., Bordey, A., Wenner, P., Fukuda, A., van den Pol, A. N., Gaiarsa, J.-L., and Cherubini, E. (2012). Refuting the challenges of the developmental shift of polarity of GABA actions: GABA more exciting than ever! In Frontiers in Cellular Neuroscience. 10.3389/fncel.2012.00035

Benson, C. G., and Potashner, S. J. (1990). Retrograde transport of [3H]glycine from the cochlear

nucleus to the superior olive in the guinea pig. Journal of Comparative Neurology, 296(3), 415–426. 10.1002/cne.902960307

Berger, J. I., Coomber, B., Wells, T. T., Wallace, M. N., and Palmer, A. R. (2014). Changes in the response properties of inferior colliculus neurons relating to tinnitus. Frontiers in Neurology, 5(OCT), 1–13. 10.3389/fneur.2014.00203

Beyerl, B. D. (1978). Afferent projections to the central nucleus of the inferior colliculus in the rat. Brain Research, 145(2), 209–223. 10.1016/0006-8993(78)90858-2

Bishop, A. L., and Henson, O. W. (1987). The efferent cochlear projections of the superior olivary complex in the mustached bat. Hearing Research, 31(2), 175–182. 10.1016/0378-5955(87)90124-9

Blaesse, P., Ehrhardt, S., Friauf, E., and Nothwang, H. G. (2005). Developmental pattern of three vesicular glutamate transporters in the rat superior olivary complex. Cell and Tissue Research, 320(1), 33–50. 10.1007/s00441-004-1054-8

Blaesse, P., Guillemin, I., Schindler, J., Schweizer, M., Delpire, E., Khiroug, L., Friauf, E., and Nothwang, H. G. (2006). Oligomerization of KCC2 correlates with development of inhibitory neurotransmission. Journal of Neuroscience, 26(41), 10407–10419. 10.1523/JNEUROSCI.3257-06.2006

Bonansco, C., and Fuenzalida, M. (2016). Plasticity of hippocampal excitatory-inhibitory balance: Missing the synaptic control in the epileptic brain. Neural Plasticity, 2016. 10.1155/2016/8607038

Brager, D. H., and Johnston, D. (2007). Plasticity of intrinsic excitability during long-term depression is mediated through mGluR-dependent changes in Ih in hippocampal CA1 pyramidal neurons. Journal of Neuroscience, 27(51), 13926–13937.

Brand, A., Behrend, O., Marquardt, T., McAlpine, D., and Grothe, B. (2002). Precise inhibition is essential for microsecond interaural time difference coding. Nature, 417(6888), 543–547. 10.1038/417543a

Brand, A., Urban, R., and Grothe, B. (2000). Duration Tuning in the Mouse Auditory Midbrain. Journal of Neurophysiology, 84(4), 1790–1799. 10.1152/jn.2000.84.4.1790

Brown, J. C., and Howlett, B. (1972). The olivo-cochlear tract in the rat and its bearing on the homologies of some constituent cell groups of the mammalian superior olivary complex: A thiocholine study. Cells Tissues Organs, 83(4), 505–526. 10.1159/000143889

Brown, M. C. (1993). Fiber pathways and branching patterns of biocytin-labeled olivocochlear neurons in the mouse brainstem. Journal of Comparative Neurology, 337(4), 600–613. 10.1002/cne.903370406

Brozoski, T. J., Bauer, C. A., and Caspary, D. M. (2002). Elevated fusiform cell activity in the dorsal cochlear nucleus of chinchillas with psychophysical evidence of tinnitus. The Journal of Neuroscience.: The Official Journal of the Society for Neuroscience, 22(6), 2383–2390. 10.1523/ JNEUROSCI.22-06-02383.2002

Cant, N. B., and Benson, C. G. (2006). Organization of the inferior colliculus of the gerbil (Meriones unguiculatus): Differences in distribution of projections from the cochlear nuclei and the superior olivary complex. Journal of Comparative Neurology, 495(5), 511–528. 10.1002/cne.20888

Case, D. T., Zhao, X., and Gillespie, D. C. (2011). Functional refinement in the projection from ventral cochlear nucleus to lateral superior olive precedes hearing onset in rat. PLoS ONE, 6(6). 10.1371/journal.pone.0020756

Casseday, J., Ehrlich, D., and Covey, E. (1994). Neural tuning for sound duration: role of inhibitory mechanisms in the inferior colliculus. Science, 264(5160), 847–850. 10.1126/science.8171341

Casseday, J. H., Ehrlich, D., and Covey, E. (2000). Neural Measurement of Sound Duration.: Control by Excitatory- Inhibitory Interactions in the Inferior Colliculus. 1475–1487.

Casula, S., Shmukler, B. E., Wilhelm, S., Stuart-Tilley, A. K., Su, W., Chernova, M. N., Brugnara, C., and Alper, S. L. (2001). A dominant negative mutant of the KCC1 K-Cl cotransporter: Both N- and C-terminal cytoplasmic domains are required for K-Cl cotransport activity. Journal of Biological Chemistry, 276(45), 41870–41878. 10.1074/jbc.M107155200

Chamma, I., Chevy, Q., Poncer, J. C., and Lévi, S. (2012). Role of the neuronal K-Cl co-transporter KCC2 in inhibitory and excitatory neurotransmission. In Frontiers in Cellular Neuroscience. 10.3389/fncel.2012.00005

Chang, E. F. (2003). Environmental Noise Retards Auditory Cortical Development. Science, 300(5618), 498–502. 10.1126/science.1082163

Chirila, F. V, Rowland, K. C., Thompson, J. M., and Spirou, G. A. (2007). Development of gerbil medial superior olive: Integration of temporally delayed excitation and inhibition at physiological temperature. Journal of Physiology, 584(1), 167–190. 10.1113/jphysiol.2007.137976

Citri, A., and Malenka, R. C. (2008). Synaptic plasticity: Multiple forms, functions, and mechanisms. Neuropsychopharmacology, 33(1), 18–41. 10.1038/sj.npp.1301559

Clause, A., Kim, G., Sonntag, M., Weisz, C. J. C., Vetter, D. E., Rűbsamen, R., and Kandler, K. (2014). The Precise Temporal Pattern of Prehearing Spontaneous Activity Is Necessary for Tonotopic Map Refinement. Neuron, 82(4), 822–835. 10.1016/j.neuron.2014.04.001

Coleman, J. R., and Clerici, W. J. (1987). Sources of projections to subdivisions of the inferior colliculus in the rat. Journal of Comparative Neurology, 262(2), 215–226.

Couchman, K., Grothe, B., and Felmy, F. (2010). Medial Superior Olivary Neurons Receive Surprisingly Few Excitatory and Inhibitory Inputs with Balanced Strength and Short-Term Dynamics. Journal of Neuroscience, 30(50), 17111–17121. 10.1523/JNEUROSCI. 1760-10.2010

Dehmel, S., Kopp-Scheinpflug, C., Dörrscheidt, G. J., and Rübsamen, R. (2002). Electrophysiological characterization of the superior paraolivary nucleus in the Mongolian gerbil. Hearing Research, 172(1–2), 18–36. 10.1016/S0378-5955(02)00353-2

Desai, N. S., Rutherford, L. C., and Turrigiano, G. G. (1999). Plasticity in the intrinsic excitability of cortical pyramidal neurons. Nature Neuroscience, 2(6), 515–520. 10.1038/9165

Edwards, S. B., Ginsburgh, C. L., Henkel, C. K., and Stein, B. E. (1979). Sources of subcortical projections to the superior colliculus in the cat. The Journal of Comparative Neurology, 184(2), 309–329. 10.1002/cne.901840207

Ehrlich, D., Casseday, J. H., Covey, E., Casseday, J. H., and Neural, E. C. (1997). Neural Tuning to Sound Duration in the Inferior Colliculus of the Big Brown Bat , Eptesicus fuscus. 16.

Faure, P. A., Fremouw, T., Casseday, J. H., and Covey, E. (2003). Temporal Masking Reveals Properties of Sound-Evoked Inhibition in Duration-Tuned Neurons of the Inferior Colliculus. 23(7), 3052–3065.

Felix II, R. A., Gourévitch, B., Gómez-Álvarez, M., Leijon, S. C. M., Saldaña, E., and Magnusson, A. K. (2017). Octopus Cells in the Posteroventral Cochlear Nucleus Provide the Main Excitatory Input to the Superior Paraolivary Nucleus. Frontiers in Neural Circuits, 11(May), 1–17. 10.3389/fncir.2017.00037

Felix, R. A., Fridberger, A., Leijon, S., Berrebi, A. S., and Magnusson, A. K. (2011). Sound Rhythms Are Encoded by Postinhibitory Rebound Spiking in the Superior Paraolivary Nucleus. Journal of Neuroscience, 31(35), 12566–12578. 10.1523/JNEUROSCI.2450-11.2011

Felix, R. a., and Magnusson, A. K. (2016). Development of excitatory synaptic transmission to the superior paraolivary and lateral superior olivary nuclei optimizes differential decoding strategies. Neuroscience, 334, 1–12. 10.1016/j.neuroscience.2016.07.039

Felix, R. a, Vonderschen, K., Berrebi, A. S., and Magnusson, A. K. (2013). Development of on-off spiking in superior paraolivary nucleus neurons of the mouse. Journal of Neurophysiology, 109(11), 2691–2704. 10.1152/jn.01041.2012

Felix, Richard A., Magnusson, A. K., and Berrebi, A. S. (2015). The superior paraolivary nucleus shapes temporal response properties of neurons in the inferior colliculus. Brain Structure and Function, 220(5), 2639–2652. 10.1007/s00429-014-0815-8

Fischl, M. J., Burger, R. M., Schmidt-Pauly, M., Alexandrova, O., Sinclair, J. L., Grothe, B., Forsythe, I. D., and Kopp-Scheinpflug, C. (2016). Physiology and anatomy of neurons in the medial superior olive of the mouse. Journal of Neurophysiology, 116(6), 2676–2688. 10.1152/jn.00523.2016

Fiumelli, H., Cancedda, L., and Poo, M. M. (2005). Modulation of GABAergic transmission by activity via postsynaptic Ca 2+-dependent regulation of KCC2 function. Neuron, 48(5), 773–786. 10.1016/j.neuron.2005.10.025

Friauf, E., and Ostwald, J. (1988). Divergent projections of physiologically characterized rat ventral cochlear nucleus neurons as shown by intra-axonal injection of horseradish peroxidase. Experimental Brain Research, 73(2), 263–284. 10.1007/BF00248219

Friauf, Eckhard, Krächan, E. G., and Müller, N. I. C. (2019). Lateral Superior Olive. In K. Kandler (Ed.), The Oxford Handbook of the Auditory Brainstem (Issue August, pp. 328–394). Oxford University Press. 10.1093/oxfordhb/9780190849061.013.10

Frisina, R. D., Walton, J. P., Lynch-Armour, M. A., and Byrd, J. D. (1998). Inputs to a physiologically characterized region of the inferior colliculus of the young adult CBA mouse. Hearing Research, 115(1–2), 61–81. S0378-5955(97)00176-7 [pii]

Gabriele, M. L., Brunso-Bechtold, J. K., and Henkel, C. K. (2000). Plasticity in the development of afferent patterns in the inferior colliculus of the rat after unilateral cochlear ablation. Journal of Neuroscience, 20(18), 6939–6949. 10.1523/jneurosci.20-18-06939.2000

González-Hernández, T., Mantolán-Sarmiento, B., González-González, B., and Pérez-González, H. (1996). Sources of GABAergic input to the inferior colliculus of the rat. Journal of Comparative Neurology, 372(2), 309–326.

Grothe, B., and Pecka, M. (2014). The natural history of sound localization in mammals-a story of neuronal inhibition. Frontiers in Neural Circuits, 8(OCT), 1–19. 10.3389/fncir.2014.00116

Grothe, B., Pecka, M., and McAlpine, D. (2010). Mechanisms of sound localization in mammals. Physiological Reviews, 90(3), 983–1012. 10.1152/physrev.00026.2009

Grothe, B., Schweizer, H., Pollak, G. D., Schuller, G., and Rosemann, C. (1994). Anatomy and projection patterns of the superior olivary comlex in the mexican free-tailed bat, Tadarida brasiliensis mexicana. Journal of Comparative Neurology, 343(4), 630–646. 10.1002/cne.903430412

Gu, J. W., Herrmann, B. S., Levine, R. A., and Melcher, J. R. (2012). Brainstem auditory evoked potentials suggest a role for the ventral cochlear nucleus in tinnitus. JARO - Journal of the Association for Research in Otolaryngology, 13(6), 819–833. 10.1007/s10162-012-0344-1

Guinan, J. J., Guinan, S. S., and Norris, B. E. (1972). Single auditory units in the superior olivary complex: I: Responses to sounds and classifications based on physiological properties. International Journal of Neuroscience, 4(3), 101–120. 10.3109/00207457209147165

Guinan, J. J., Norris, B. E., and Guinan, S. S. (1972). Single auditory units in the superior olivary complex: II: Locations of unit categories and tonotopic organization. International Journal of Neuroscience, 4(4), 147–166. 10.3109/00207457209164756

Heeringa, A. N., and van Dijk, P. (2014). The dissimilar time course of temporary threshold shifts and reduction of inhibition in the inferior colliculus following intense sound exposure. Hearing Research, 312, 38–47. 10.1016/j.heares.2014.03.004

Helfert, R. H., Wenthold, R. J., Altschuler, R. A., and Bonneau, J. M. (1989). GABA and glycine imunoreactivity in the guinea pig superior olivary complex. Brain Res., 501, 269–286.

Holtmaat, A., and Svoboda, K. (2009). Experience-dependent structural synaptic plasticity in the mammalian brain. Nature Reviews Neuroscience, 10(9), 647–658.

Horn, R., and Marty, A. (1988). Muscarinic activation of ionic currents measured by a new whole-cell recording method. The Journal of General Physiology, 92(2), 145–159. 10.1085/jgp.92.2.145

Jalabi, W., Kopp-Scheinpflug, C., Allen, P. D., Schiavon, E., DiGiacomo, R. R., Forsythe, I. D., and Maricich, S. M. (2013). Sound Localization Ability and Glycinergic Innervation of the Superior Olivary Complex Persist after Genetic Deletion of the Medial Nucleus of the Trapezoid Body. Journal of Neuroscience, 33(38), 15044–15049. 10.1523/JNEUROSCI.2604-13.2013

Jen, P. H.-S., and Wu, C. H. (2006). Duration selectivity organization in the inferior colliculus of the big brown bat, Eptesicus fuscus. Brain Research, 1108(1), 76–87.

Jung, S. C., and Hoffman, D. A. (2009). Biphasic somatic A-type K+ channel downregulation mediates intrinsic plasticity in hippocampal CA1 pyramidal neurons. PLoS ONE, 4(8). 10.1371/journal.pone.0006549

Kadner, a., and Berrebi, a. S. (2008). Encoding of temporal features of auditory stimuli in the medial nucleus of the trapezoid body and superior paraolivary nucleus of the rat. Neuroscience, 151(3), 868–887. 10.1016/j.neuroscience.2007.11.008

Kadner, A., Kulesza, R. J., and Berrebi, A. S. (2006). Neurons in the medial nucleus of the trapezoid body and superior paraolivary nucleus of the rat may play a role in sound duration coding. Journal of Neurophysiology, 95(3), 1499–1508. 10.1152/jn.00902.2005

Kandler, K., Clause, A., and Noh, J. (2009). Tonotopic reorganization of developing auditory brainstem circuits. Nature Neuroscience, 12(6), 711–717. 10.1038/nn.2332

Kandler, K., and Gillespie, D. C. (2005). Developmental refinement of inhibitory sound-localization circuits. In Trends in Neurosciences. 10.1016/j.tins.2005.04.007

Kapfer, C., Seidl, A. H., Schweizer, H., and Grothe, B. (2002). Experience-dependent refinement of inhibitory inputs to auditory coincidence-detector neurons. Nature Neuroscience, 5(3), 247–253. 10.1038/nn810

Kelly, J. B., Liscum, A., Van Adel, B., and Ito, M. (1998). Projections from the superior olive and lateral lemniscus to tonotopic regions of the rat's inferior colliculus. Hearing Research, 116(1–2), 43–54. 10.1016/S0378-5955(97)00195-0

Kim, G, and Kandler, K. (2010). Synaptic changes underlying the strengthening of GABA / glycinergic connections in the developing lateral superior olive. Neuroscience, 171(3), 924–933. 10.1016/j.neuroscience.2010.09.054

Kim, Gunsoo, and Kandler, K. (2003). Elimination and strengthening of glycinergic/ GABAergic connections during tonotopic map formation. Nature Neuroscience, 6(3), 282–290. 10.1038/nn1015

Kitzes, L. M., Kageyama, G. H., Semple, M. N., and Kil, J. (1995). Development of ectopic projections from the ventral cochlear nucleus to the superior olivary complex induced by neonatal ablation of the contralateral cochlea. The Journal of Comparative Neurology, 353(3), 341–363. 10.1002/cne.903530303

Kopp-Scheinpflug, Conny, Sinclair, J. L., and Linden, J. F. (2018). When Sound Stops: Offset Responses in the Auditory System. Trends in Neurosciences, 41(10), 712–728. 10.1016/j.tins.2018.08.009

Kopp-Scheinpflug, Cornelia, Tozer, A. J. B., Robinson, S. W., Tempel, B. L., Hennig, M. H., and Forsythe, I. D. (2011). The sound of silence: Ionic mechanisms encoding sound termination. Neuron, 71(5), 911–925. 10.1016/j.neuron.2011.06.028

Kudo, M., Nakamura, Y., Tokuno, H., and Kitao, Y. (1990). Auditory brainstem in the mole (Mogera): Nuclear configurations and the projections to the inferior colliculus. Journal of Comparative Neurology, 298(4), 400–412. 10.1002/cne.902980403

Kujawa, S. G., and Liberman, M. C. (2009). Adding insult to injury: Cochlear nerve degeneration after "temporary" noise-induced hearing loss. Journal of Neuroscience, 29(45), 14077–14085. 10.1523/JNEUROSCI.2845-09.2009

Kulesza, R. J., and Berrebi, A. S. (2000). Superior paraolivary nucleus of the rat is a GABAergic nucleus.

JARO - Journal of the Association for Research in Otolaryngology, 1(4), 255–269. 10.1007/s101620010054

Kulesza, R. J., Spirou, G. A., and Berrebi, A. S. (2003). Physiological Response Properties of Neurons in the Superior Paraolivary Nucleus of the Rat. Journal of Neurophysiology, 89(4), 2299–2312. 10.1152/jn.00547.2002

Kumoi, K, Saito, N., and Tanaka, C. (1987). Immunohistochemical localization of gamma-aminobutyric acid- and aspartate-containing neurons in the guinea pig vestibular nuclei. Brain Research, 416(1), 22–33. 10.1016/0378-5955(93)90121-G

Kumoi, Kazuo, Saito, N., and Tanaka, C. (1993). Immunohistochemical localization of -aminobutyric acid- and aspartate-containing neurons in the guinea pig superior olivary complex. Hearing Research, 68(2), 173–179. 10.1016/0378-5955(93)90121-G

Kuwabara, N., DiCaprio, R. a., and Zook, J. M. (1991). Afferents to the medial nucleus of the trapezoid body and their collateral projections. Journal of Comparative Neurology, 314(4), 684–706. 10.1002/cne.903140405

Kuwabara, N., and Zook, J. M. (1992). Projections to the medial superior olive from the medial and lateral nuclei of the trapezoid body in rodents and bats. Journal of Comparative Neurology, 324(4), 522–538. 10.1002/cne.903240406

Kuwabara, N., and Zook, J. M. (1999). Local collateral projections from the medial superior olive to the superior paraolivary nucleus in the gerbil. Brain Research, 846(1), 59–71. 10.1016/S0006-8993(99)01942-3

Kuwada, S., and Batra, R. (1999). Coding of sound envelopes by inhibitory rebound in neurons of the superior olivary complex in the unanesthetized rabbit. Journal of Neuroscience, 19(6), 2273–2287. 10.1523/jneurosci.19-06-02273.1999

Leao, K. E., Leao, R. N., Sun, H., Fyffe, R. E. W., and Walmsley, B. (2006). Hyperpolarization-activated currents are differentially expressed in mice brainstem auditory nuclei. 3, 849–864. 10.1113/jphysiol.2006.114702

Lee, H. H. C., Walker, J. A., Williams, J. R., Goodier, R. J., Payne, J. A., and Moss, S. J. (2007). Direct protein kinase C-dependent phosphorylation regulates the cell surface stability and activity of the potassium chloride cotransporter KCC2. Journal of Biological Chemistry, 282(41), 29777–29784. 10.1074/jbc.M705053200

Li, S., Choi, V., and Tzounopoulos, T. (2013). Pathogenic plasticity of Kv7.2/3 channel activity is essential for the induction of tinnitus. Proceedings of the National Academy of Sciences, 110(24), 9980–9985. 10.1073/pnas.1302770110

Li, Shuang, Kalappa, B. I., and Tzounopoulos, T. (2015). Noise-induced plasticity of KCNQ2/3 and HCN channels underlies vulnerability and resilience to tinnitus. ELife, 4, 1–23. 10.7554/elife.07242

Liberman, M. C., and Kujawa, S. G. (2017). Cochlear synaptopathy in acquired sensorineural hearing loss: Manifestations and mechanisms. In Hearing Research (Vol. 349, pp. 138–147). Elsevier B.V. 10.1016/j.heares.2017.01.003

Löhrke, S., Srinivasan, G., Oberhofer, M., Doncheva, E., and Friauf, E. (2005). Shift from depolarizing to hyperpolarizing glycine action occurs at different perinatal ages in superior olivary complex nuclei. European Journal of Neuroscience, 22(11), 2708–2722. 10.1111/j.1460-9568.2005.04465.

Longenecker, R. J., and Galazyuk, A. V. (2011). Development of tinnitus in CBA/CaJ mice following sound exposure. JARO - Journal of the Association for Research in Otolaryngology, 12(5), 647–658. 10.1007/s10162-011-0276-1

Longenecker, R. J., and Galazyuk, A. V. (2016). Variable Effects of Acoustic Trauma on Behavioral and Neural Correlates of Tinnitus In Individual Animals. Frontiers in Behavioral Neuroscience, 10, 207. 10.3389/fnbeh.2016.00207

Ma, W.-L. D., Hidaka, H., and May, B. J. (2006). Spontaneous activity in the inferior colliculus of CBA/J mice after manipulations that induce tinnitus. Hearing Research, 212(1–2), 9–21. 10.1016/j.heares.2005.10.003

Magnusson, A. K., Kapfer, C., Grothe, B., and Koch, U. (2005). Maturation of glycinergic inhibition in the gerbil medial superior olive after hearing onset. Journal of Physiology, 568(2), 497–512. 10.1113/jphysiol.2005.094763

Melcher, J. R., Sigalovsky, I. S., Guinan, J. J. J., and Levine, R. A. (2000). Lateralized tinnitus studied with functional magnetic resonance imaging: abnormal inferior colliculus activation. Journal of Neurophysiology, 83(2), 1058–1072. 10.1152/jn.2000.83.2.1058

Mellott, J. G., Beebe, N. L., and Schofield, B. R. (2018). GABAergic and non-GABAergic projections to the superior colliculus from the auditory brainstem. Brain Structure and Function, 223(4), 1923–1936. 10.1007/s00429-017-1599-4

Middleton, J. W., Kiritani, T., Pedersen, C., Turner, J. G., Shepherd, G. M. G., and Tzouno- poulos, T. (2011). Mice with behavioral evidence of tinnitus exhibit dorsal cochlear nucleus hyperactivity because of decreased GABAergic inhibition. Proceedings of the National Academy of Sciences of the United States of America, 108(18), 7601–7606. 10.1073/pnas.1100223108

Moore, D. R. (1988). Auditory brainstem of the ferret: Sources of projections to the inferior colliculus. Journal of Comparative Neurology, 269(3), 342–354. 10.1002/cne.902690303

Moore, J. K. (2000). Organization of the human superior olivary complex. Microscopy Research and Technique, 51(4), 403–412. 10.1002/1097-0029(20001115)51:4<403::AID-JEMT8>3.0.CO;2-Q

Moore, J. K., and Moore, R. Y. (1987). Glutamic acid decarboxylase-like immunoreactivity in brainstem auditory nuclei of the rat. Journal of Comparative Neurology, 260(2), 157–174. 10.1002/cne.902600202

Moore, Y. E., Conway, L. C., Wobst, H. J., Brandon, N. J., Deeb, T. Z., and Moss, S. J. (2019). Developmental Regulation of KCC2 Phosphorylation Has Long-Term Impacts on Cognitive Function. Frontiers in Molecular Neuroscience, 12, 173. 10.3389/fnmol.2019.00173

Morest, D. K. (1968). The collateral system of the medial nucleus of the trapezoid body of the cat, its neuronal architecture and relation to the olivo-cochlear bundle. Brain Research, 9(2), 288–311. 10.1016/0006-8993(68)90235-7

Nelson, A. B., Krispel, C. M., Sekirnjak, C., and Lac, S. Du. (2003). Long-lasting increases in intrinsic excitability triggered by inhibition. Neuron, 40(3), 609–620. 10.1016/S0896-6273(03)00641-X

Noh, J., Seal, R. P., Garver, J. A., Edwards, R. H., and Kandler, K. (2010). Glutamate co-release at GABA/glycinergic synapses is crucial for the refinement of an inhibitory map. Nature Neuroscience, 13(2), 232–238. 10.1038/nn.2478

Nordeen, K. W., Killackey, H. P., and Kitzes, L. M. (1983). Ascending auditory projections to the inferior colliculus in the adult gerbil, Meriones unguiculatus. Journal of Comparative Neurology, 214(2), 131–143. 10.1002/cne.902140203

Nothwang, H. G. (2016). Evolution of mammalian sound localization circuits: A developmental perspective. Progress in Neurobiology, 141, 1–24. 10.1016/j.pneurobio.2016.02.003

Oliver, D. L., Cant, N. B., Fay, R. R., and Popper, A. N. (2018). The Mammalian Auditory Pathways. In D. L. Oliver, N. B. Cant, R. R. Fay, and A. N. Popper (Eds.), Ear and Hearing (Vol. 65, Issue 5). Springer International Publishing. 10.1007/978-3-319-71798-2

Ollo, C., and Schwartz, I. R. (1979). The superior olivary complex in C57BL/6 mice. The American Journal of Anatomy. 10.1002/aja.1001550306

Osen, K K, Mugnaini, E., Dahl, A. L., and Christiansen, A. H. (1984). Histochemical localization of acetylcholinesterase in the cochlear and superior olivary nuclei. A reappraisal with emphasis on the cochlear granule cell system. Archives Italiennes de Biologie, 122(3), 169–212.

Osen, Kirsten Kjelsberg, and Roth, K. (1969). Histochemical localization of cholinesterases in the cochlear nuclei of the cat, with notes on the origin of acetylcholinesterase-positive afferents and the superior olive. Brain Research, 16(1), 165–185. 10.1016/0006-8993(69)90092-4

Pecka, M., Brand, A., Behrend, O., and Grothe, B. (2008). Interaural time difference processing in the mammalian medial superior olive: The role of glycinergic inhibition. Journal of Neuroscience, 28(27), 6914–6925. 10.1523/JNEUROSCI.1660-08.2008

Pérez-González, D., Malmierca, M. S., Moore, J. M., Hernández, O., and Covey, E. (2006). Duration Selective Neurons in the Inferior Colliculus of the Rat: Topographic Distribution and Relation of Duration Sensitivity to Other Response Properties. Journal of Neurophysiology, 95(2), 823–836. 10.1152/jn.00741.2005

Pilati, N., Linley, D. M., Selvaskandan, H., Uchitel, O., Hennig, M. H., Kopp-scheinpflug, C., and Forsythe, I. D. (2016). The Journal of Physiology Acoustic trauma slows AMPA receptor-mediated EPSCs in the auditory brainstem , reducing GluA4 subunit expression as a mechanism to rescue binaural function. 13, 3683–3703. 10.1113/JP271929

Pilati, N., Linley, D. M., Selvaskandan, H., Uchitel, O., Hennig, M. H., Kopp-Scheinpflug, C., and Forsythe, I. D. (2016). Acoustic trauma slows AMPAR-mediated EPSCs in the auditory brainstem, reducing GluA4 subunit expression as a mechanism to rescue binaural function. The Journal of Physiology, 13, 3683–3703. 10.1113/JP271929

Pisella, L. I., Gaiarsa, J. L., Diabira, D., Zhang, J., Khalilov, I., Duan, J. J., Kahle, K. T., and Medina, I. (2019). Impaired regulation of KCC2 phosphorylation leads to neuronal network dysfunction and

neurodevelopmental pathology. Science Signaling, 12(603). 10.1126/scisignal.aay0300

Rajaram, E., Kaltenbach, C., Fischl, M. J., Mrowka, L., Alexandrova, O., Grothe, B., Hennig, M. H., and Kopp-Scheinpflug, C. (2019). Slow NMDA-Mediated Excitation Accelerates Offset-Response Latencies Generated via a Post-Inhibitory Rebound Mechanism. Eneuro, 6(3), ENEURO.0106-19.2019. 10.1523/ENEURO.0106-19.2019

Reuss, S., Disque-Kaiser, U., De Liz, S., Ruffer, M., and Riemann, R. (1999). Immunfluorescence study of neuropeptides in identified neurons of the rat auditory superior olivary complex. Cell and Tissue Research, 297(1), 13–21. 10.1007/s004410051329

Riemann, R., and Reuss, S. (1998). Projection neurons in the superior olivary complex of the rat auditory brainstem: A double retrograde tracing study. Orl, 60(5), 278–282. 10.1159/000027610

Rinehart, J., Maksimova, Y. D., Tanis, J. E., Stone, K. L., Hodson, C. A., Zhang, J., Risinger, M., Pan, W., Wu, D., Colangelo, C. M., Forbush, B., Joiner, C. H., Gulcicek, E. E., Gallagher, P. G., and Lifton, R. P. (2009). Sites of Regulated Phosphorylation that Control K-Cl Cotransporter Activity. Cell, 138(3), 525–536. 10.1016/j.cell.2009.05.031

Roberts, R. C., and Ribak, C. E. (1987). GABAergic neurons and axon terminals in the brainstem auditory nuclei of the gerbil. Journal of Comparative Neurology, 258(2), 267–280. 10.1002/cne.902580207

Robertson, D., Cole, K. S., and Harvey, A. R. (1987). Brainstem organization of efferent projections to the guinea pig cochlea studied using the fluorescent tracers fast blue and diamidino yellow. Experimental Brain Research, 66(3), 449–457. 10.1007/BF00270677

Robertson, Donald, and Winter, I. M. (1988). Cochlear nucleus inputs to olivocochlear neurones revealed by combined anterograde and retrograde labelling in the guinea pig. Brain Research, 462(1), 47–55. 10.1016/0006-8993(88)90583-5

Roelfsema, P. R., and Holtmaat, A. (2018). Control of synaptic plasticity in deep cortical networks. Nature Reviews Neuroscience, 19(3), 166–180. 10.1038/nrn.2018.6

Saint Marie, R. L., and Baker, R. A. (1990). Neurotransmitter-specific uptake and retrograde transport of [3H]glycine from the inferior colliculus by ipsilateral projections of the superior olivary complex and nuclei of the lateral lemniscus. Brain Research, 524(2), 244–253. 10.1016/0006-8993(90)90698-B

Saldaña, E., Aparicio, M. A., Fuentes-Santamaría, V., and Berrebi, A. S. (2009). Connections of the superior paraolivary nucleus of the rat: projections to the inferior colliculus. Neuroscience, 163(1), 372–387. 10.1016/j.neuroscience.2009.06.030

Saldaña, E., and Berrebi, A. S. (2000). Anisotropic organization of the rat superior paraolivary nucleus. Anatomy and Embryology, 202(4), 265–279. 10.1007/s004290000109

Sanes, D. H., and Friauf, E. (2000). Development and influence of inhibition in the lateral superior olivary nucleus. Hearing Research, 147(1–2), 46–58. 10.1016/S0378-5955(00)00119-2

Sanes, D. H., and Siverls, V. (1991a). Development and specificity of inhibitory terminal arborizations in the central nervous system. Journal of Neurobiology, 22(8), 837–854. 10.1002/neu.480220805

Sanes, D. H., and Siverls, V. (1991b). Development and specificity of inhibitory terminal arborizations

in the central nervous system. Journal of Neurobiology, 22(8), 837–854. 10.1002/neu.480220805

Sayegh, R., Aubie, B., and Faure, P. A. (2011). Duration tuning in the auditory midbrain of echolocating and non-echolocating vertebrates. Journal of Comparative Physiology A: Neuroethology, Sensory, Neural, and Behavioral Physiology, 197(5), 571–583. 10.1007/s00359-011-0627-8

Schofield, B R, Mellott, J. G., and Motts, S. D. (2014). Subcollicular projections to the auditory thalamus and collateral projections to the inferior colliculus. Front Neuroanat, 8(July), 70. 10.3389/fnana.2014.00070

Schofield, Brett R. (1991). Superior paraolivary nucleus in the pigmented guinea pig: Separate classes of neurons project to the inferior colliculus and the cochlear nucleus. Journal of Comparative Neurology, 312(1), 68–76. 10.1002/cne.903120106

Schofield, Brett R. (1995). Projections from the cochlear nucleus to the superior paraolivary nucleus in guinea pigs. Journal of Comparative Neurology, 360(1), 135–149. 10.1002/ cne.903600110

Seidl, A. H., and Grothe, B. (2005). Development of sound localization mechanisms in the Mongolian gerbil is shaped by early acoustic experience. Journal of Neurophysiology, 94(2), 1028–1036. 10.1152/jn.01143.2004

Seki, S., and Eggermont, J. J. (2003). Changes in spontaneous firing rate and neural synchrony in cat primary auditory cortex after localized tone-induced hearing loss. Hearing Research, 180(1–2), 28–38. 10.1016/s0378-5955(03)00074-1

Shaheen, L. A., and Liberman, M. C. (2018). Cochlear synaptopathy changes sound-evoked activity without changing spontaneous discharge in the mouse inferior colliculus. Frontiers in Systems Neuroscience, 12(December), 1–19. 10.3389/fnsys.2018.00059

Shibata, S., Kakazu, Y., Okabe, A., Fukuda, A., and Nabekura, J. (2004). Experience-dependent changes in intracellular Cl- regulation in developing auditory neurons. Neuroscience Research, 48(2), 211–220. 10.1016/j.neures.2003.10.011

Shore, S. E. (2005). Multisensory integration in the dorsal cochlear nucleus: Unit responses to acoustic and trigeminal ganglion stimulation. European Journal of Neuroscience, 21(12), 3334–3348. 10.1111/j.1460-9568.2005.04142.x

Shore, Susan E., Helfert, R. H., Bledsoe, S. C., Altschuler, R. A., and Godfrey, D. A. (1991). Descending projections to the dorsal and ventral divisions of the cochlear nucleus in guinea pig. Hearing Research, 52(1), 255–268. 10.1016/0378-5955(91)90205-N

Shore, Susan E., and Wu, C. (2019). Mechanisms of Noise-Induced Tinnitus: Insights from Cellular Studies. Neuron, 103(1), 8–20. 10.1016/j.neuron.2019.05.008

Smith, A. J., Owens, S., and Forsythe, I. D. (2000). Characterisation of inhibitory and excitatory postsynaptic currents of the rat medial superior olive. Journal of Physiology, 529(3), 681–698. 10.1111/j.1469-7793.2000.00681.

Smith, P. H., Joris, P. X., Carney, L. H., and Yin, T. C. T. (1991). Projections of physiologically characterized globular bushy cell axons from the cochlear nucleus of the cat. Journal of Comparative

Neurology, 304(3), 387–407. 10.1002/cne.903040305

Sommer, I., Lingenhöhl, K., and Friauf, E. (1993). Principal cells of the rat medial nucleus of the trapezoid body: an intracellular in vivo study of their physiology and morphology. Experimental Brain Research, 95(2), 223–239. 10.1007/BF00229781

Sonntag, M., Englitz, B., Kopp-Scheinpflug, C., and Rubsamen, R. (2009). Early Postnatal Development of Spontaneous and Acoustically Evoked Discharge Activity of Principal Cells of the Medial Nucleus of the Trapezoid Body: An In Vivo Study in Mice. Journal of Neuroscience, 29(30), 9510–9520. 10.1523/JNEUROSCI.1377-09.2009

Spangler, K. M., Cant, N. B., Henkel, C. K., Farley, G. R., and Warr, W. B. (1987). Descending projections from the superior olivary complex to the cochlear nucleus of the cat. Journal of Comparative Neurology, 259(3), 452–465. 10.1002/cne.902590311

Srinivasan, G., Friauf, E., and Löhrke, S. (2004). Functional glutamatergic and glycinergic inputs to several superior olivary nuclei of the rat revealed by optical imaging. Neuroscience, 128(3), 617–634. 10.1016/j.neuroscience.2004.06.012

Stange-Marten, A., Nabel, A. L., Sinclair, J. L., Fischl, M., Alexandrova, O., Wohlfrom, H., Kopp-Scheinpflug, C., Pecka, M., and Grothe, B. (2017). Input timing for spatial processing is precisely tuned via constant synaptic delays and myelination patterns in the auditory brainstem. Proceedings of the National Academy of Sciences, 114(24), E4851–E4858. 10.1073/pnas.1702290114

Sturm, J. J., Zhang-Hooks, Y.-X., Roos, H., Nguyen, T., and Kandler, K. (2017). Noise Trauma-Induced Behavioral Gap Detection Deficits Correlate with Reorganization of Excitatory and Inhibitory Local Circuits in the Inferior Colliculus and Are Prevented by Acoustic Enrichment. The Journal of Neuroscience, 37(26), 6314–6330. 10.1523/JNEURO SCI.0602-17.2017

Thompson, A. M., and Thompson, G. C. (1991). Posteroventral cochlear nucleus projections to olivocochlear neurons. Journal of Comparative Neurology, 303(2), 267–285. 10.1002/cne.903030209

Thompson, A. M., and Thompson, G. C. (1993). Relationship of descending inferior colliculus projections to olivocochlear neurons. Journal of Comparative Neurology, 335(3), 402–412. 10.1002/cne.903350309

Tokunaga, A. (1988). Superior olivary and lateral lemniscal neurons projecting to the cochlea in the guinea pig. Neuroscience Research, 6(1), 20–30. 10.1016/ 0168-0102(88)90003-X

Toyoshima, M., Sakurai, K., Shimazaki, K., Takeda, Y., Nakamoto, M., Serizawa, S., Shimoda, Y., and Watanabe, K. (2009). Preferential localization of neural cell recognition molecule NB-2 in developing glutamatergic neurons in the rat auditory brainstem. Journal of Comparative Neurology, 513(4), 349–362. 10.1002/cne.21972

Turrigiano, G. (2012). Homeostatic synaptic plasticity: Local and global mechanisms for stabilizing neuronal function. Cold Spring Harbor Perspectives in Biology, 4(1), 1–18. 10.1101/cshperspect.a005736 Vale, C., and Sanes, D. H. (2002). The effect of bilateral deafness on excitatory and inhibitory synaptic strength in the inferior colliculus. European Journal of Neuroscience, 16(12), 2394–2404. 10.1046/j.1460-9568.2002.02302.

Vale, C., Schoorlemmer, J., and Sanes, D. H. (2003). Deafness disrupts chloride transporter function and inhibitory synaptic transmission. Journal of Neuroscience, 23(20), 7516–7524. 10.1523/jneurosci.23-20-07516.2003

Viñuela, A., Aparicio, M.-A., Berrebi, A. S., and Saldaña, E. (2011). Connections of the Superior Paraolivary Nucleus of the Rat: II. Reciprocal Connections with the Tectal Longitudinal Column. Frontiers in Neuroanatomy, 5(February), 1. 10.3389/fnana.2011.00001

Vogler, D. P., Robertson, D., and Mulders, W. H. A. M. (2011). Hyperactivity in the ventral cochlear nucleus after cochlear trauma. The Journal of Neuroscience.: The Official Journal of the Society for Neuroscience, 31(18), 6639–6645. 10.1523/JNEUROSCI.6538-10.2011

Wake, H., Watanabe, M., Moorhouse, A. J., Kanematsu, T., Horibe, S., Matsukawa, N., Asai, K., Ojika, K., Hirata, M., and Nabekura, J. (2007). Early changes in KCC2 phosphorylation in response to neuronal stress result in functional downregulation. The Journal of Neuroscience.: The Official Journal of the Society for Neuroscience, 27(7), 1642–1650. 10.1523/JNEUROSCI.3104-06.2007

Walcher, J., Hassfurth, B., Grothe, B., and Koch, U. (2011). Comparative posthearing development of inhibitory inputs to the lateral superior olive in gerbils and mice. Journal of Neurophysiology, 106(3), 1443–1453. 10.1152/jn.01087.2010

Wang, H., Brozoski, T. J., Turner, J. G., Ling, L., Parrish, J. L., Hughes, L. F., and Caspary, D. M. (2009a). Plasticity at glycinergic synapses in dorsal cochlear nucleus of rats with behavioral evidence of tinnitus. Neuroscience, 164(2), 747–759. 10.1016/j.neuroscience.200 9.08.026

Wang, H., Brozoski, T. J., Turner, J. G., Ling, L., Parrish, J. L., Hughes, L. F., and Caspary, D. M. (2009b). Plasticity at glycinergic synapses in dorsal cochlear nucleus of rats with behavioral evidence of tinnitus. Neuroscience, 164(2), 747–759. 10.1016/j.neuroscience.2009.08.026

Warr, W. B. (1975). Olivocochlear and vestibular efferent neurons of the feline brain stem: Their location, morphology and number determined by retrograde axonal transport and acetylcholinesterase histochemistry. Journal of Comparative Neurology, 161(2), 159–181. 10.1002/cne.901610203

Warr, W. B. (1995). Parallel Ascending Pathways from the Cochlear Nucleus. In W. D. B. T.-C. to S. P. Neff (Ed.), Contributions to Sensory Physiology (Vol. 7, pp. 1–38). Elsevier. 10.1016/B978-0-12-151807-3.50007-0

Watanabe, M., Zhang, J., Shahid Mansuri, M., Duan, J., Karimy, J. K., Delpire, E., Alper, S. L., Lifton, R. P., Fukuda, A., and Kahle, K. T. (2019). Developmentally regulated KCC2 phosphorylation is essential for dynamic GABA-mediated inhibition and survival. Science Signaling, 12(603). 10.1126/scisignal.aaw9315

Wenthold, R. J., Huie, D., Altshuler, R. A., and Reeks, K. A. (1987). Glycine immunoreactivity localized in the cochlear nulceus and superior olivary complex. Neuroscience, 2(3), 897–912.

Werthat, F., Alexandrova, O., Grothe, B., and Koch, U. (2008). Experience-Dependent Refinement of the Inhibitory Axons Projecting to the Medial Superior Olive. 1454–1462. 10.1002/dneu.20660

Whitley, J. M., and Henkel, C. K. (1984). Topographical organization of the inferior collicular projection and other connections of the ventral nucleus of the lateral lemniscus in the cat. The Journal of

Comparative Neurology, 229(2), 257–270. 10.1002/cne.902290210

Wigderson, E., Nelken, I., and Yarom, Y. (2016). Early multisensory integration of self and source motion in the auditory system. Proceedings of the National Academy of Sciences of the United States of America, 113(29), 8308–8313. 10.1073/pnas.1522615113

Willard, F. H., and Martin, G. F. (1983). The auditory brainstem nuclei and some of their projections to the inferior colliculus in the North American opossum. Neuroscience, 10(4), 1203–1232. 10.1016/0306-4522(83)90109-4

Willard, F. H., and Ryugo, D. K. (1983). Anatomy of the Central Auditory System. In The Auditory Psychobiology of the Mouse (pp. 201–304).

Winter, I. M., Robertson, D., and Cole, K. S. (1989). Descending projections from auditory brainstem nuclei to the cochlea and cochlear nucleus of the guinea pig. Journal of Comparative Neurology, 280(1), 143–157. 10.1002/cne.902800110

Yassin, L., Radtke-Schuller, S., Asraf, H., Grothe, B., Hershfinkel, M., Forsythe, I. D., Kopp-Scheinpflug, C., Burger, R. M., and Hurley, L. M. (2014). Nitric oxide signaling modulates synaptic inhibition in the superior paraolivary nucleus (SPN) via cGMP-dependent suppression of KCC2. 10.3389/fncir.2014.00065

Yasui, Y., Nakano, K., and Mizuno, N. (1992). Descending projections from the subparafascicular thalamic nucleus to the lower brain stem in the rat. Experimental Brain Research, 90(3), 508–518. 10.1007/BF00230933

Yin, S., Chen, Z., Yu, D., Feng, Y., and Wang, J. (2008). Local inhibition shapes duration tuning in the inferior colliculus of guinea pigs. Hearing Research, 237(1), 32–48. 10.1016/j.heares.2007.12.008

Zook, J. M., and Casseday, J. H. (1985). Projections from the cochlear nuclei in the mustache bat, Pteronotus parnellii. Journal of Comparative Neurology, 237(3), 307–324. 10.1002/cne.902370303

# Acknowledgements

Firstly, thank you Conny for taking me on as your PhD student. From the first few weeks that I spent in the level 3 meeting room till this moment, I have always felt confident to take on the various challenges that come along during a PhD, knowing that I could turn to you for support and guidance. I am truly grateful for the learnings, encouragement, patience, feedback, inspiration and your trust in me and my abilities.

Thank you Benedikt for the opportunity to be a part of your department, I enjoyed our discussions in all the lab meetings and the retreats, which were invaluable in shaping my research project. Thank you for the immense support through the GSN and the encouraging words during my TAC meetings.

Thank you Dr. Leda Dimou, Dr. Daniela Vallentin and Prof. Harald Luksch for being a valuable part of my thesis / examination committees. I would also like to thank the extended Grothe group for making this journey fun and memorable. A huge thank you to Hilde, Olga, Bea and Karin for supporting our lab work in innumerable ways. Thank you Jim and Matt for taking me on as your Padawan and showing me the ways of the force.

Thank you to the crew of fellow PhD students - Sara, Diana, Alex, Delwen, Franzi, Alisha, Ela, Ella, Marga, Gregory, Yannik, Suzan, Mihai, Shreya, Magda, Leonie, and all the other PhD and master students to walk the hallowed corridors of level 3 neurobiology labs. I will cherish the fond memories for a lifetime.

A huge thank you to my better half- Catherine for the love, support, encouragement and inspiration every step of the way. I am also very grateful for the love and support of my family- thank you Amma (Rani), Appa (Rajaram), Maran and Sowmya. Last but not least, I would like to thank my son- Leo for being cute and lifting our spirits.